12-1-2014

Identification of long term changes and evaluation of the relationships among streamflow variability and oceanic-atmospheric indices

Soumya Sagarika
University of Nevada, Las Vegas, sagarika@unlv.nevada.edu

IDENTIFICATION OF LONG-TERM CHANGES AND EVALUATION OF THE RELATIONSHIPS AMONG STREAMFLOW VARIABILITY AND OCEANIC-ATMOSPHERIC INDICES.

By

Soumya Sagarika

Bachelor in Technology in Civil Engineering
Biju Pattnaik University of Technology
2010

A thesis submitted in partial fulfillment
of the requirements for the

Master of Science in Engineering

Department of Civil and Environmental Engineering and Construction
Howard R. Hughes College of Engineering
The Graduate College

University of Nevada, Las Vegas
December 2014

UNLV
UNIVERSITY OF NEVADA LAS VEGAS

THE GRADUATE COLLEGE

We recommend the thesis prepared under our supervision by

Soumya Sagarika

entitled

Identification of Long-Term Changes and Evaluation of the Relationships among Streamflow Variability and Oceanic-Atmospheric Indices

is approved in partial fulfillment of the requirements for the degree of

Master of Science in Engineering -- Civil and Environmental Engineering

Department of Civil and Environmental Engineering & Construction

Sajjad Ahmad, Ph.D., Committee Chair

David James, Ph.D., Committee Member

Haroon Stephen, Ph.D., Committee Member

Ashok Singh, Ph.D., Graduate College Representative

Kathryn Hausbeck Korgan, Ph.D., Interim Dean of the Graduate College

December 2014

ABSTRACT

To examine the effects of climate variability on streamflow, this thesis presents a comprehensive analysis of the streamflow variability of the continental United States and its association with oceanic-atmospheric indices. First, the presence of trends with consideration of short term and long term persistence followed by shifts over the past years in the continental U.S. streamflow were analyzed by using the non-parametric tests: Mann Kendall and Pettitt. Second, the spatio-temporal relationships between seasonal streamflow variability of continental U.S. and sea surface temperatures (SST) and 500 mbar geopotential height (Z_{500}) of the Pacific and Atlantic were established using the singular valued decomposition (SVD) factorization technique. Finally, the SVD technique was used to determine the spatio-temporal relationships between western U.S. seasonal streamflow variability and indicators (SST and Z_{500}) of Pacific Ocean variability.

The results indicated that significant trends and shifts existed in the streamflow volumes in the past few decades in the continental U.S., and short term and long term persistence was evident in streamflows. Removal of the persistence characteristic removed the spurious trends, that could otherwise be misinterpreted. The 1970's were the years when major shifts took place, and most of the shift periods coincided with the phase changes of multi-decadal oscillations. A strong spatio-temporal relationship of the streamflow was established with the oceanic-atmospheric indicators and the multi-decadal oscillations (PDO, AMO) did influence these relationships. Seasonal analysis showed an improved explanation of co-variability over water-year. The lead-time approach showed that the relationships could be explained up to 9 months ahead and Z_{500}

showed improved results over SST at shorter lead-times. Several new regions apart from the well identified index regions were identified in the oceanic region to have strong relationships with seasonal streamflows. The individual basins showed unique relationships with the indicators both spatially and temporally which could be due to their unique topographical and local factors.

The contributions from this research include a better understanding of the changes in continental U.S. streamflow and the spatio-temporal relationships with oceanic-atmospheric variability that can help in better water management decisions.

EXECUTIVE SUMMARY

Identification of long-term changes and evaluation of the relationships among streamflow variability and oceanic-atmospheric indices.

By Soumya Sagarika

Dr. Sajjad Ahmad, Examination Committee Chair
Associate Professor, Civil and Environmental Engineering
University of Nevada, Las Vegas

Climate variability is a continuous phenomenon and its influence on hydrological cycle ultimately affects streamflows. In order to examine the effects of climate variability on streamflow, this thesis presents a comprehensive analysis of streamflow variability of the continental U.S., and its association with oceanic-atmospheric indices. Based on literature review, two types of changes in streamflow volumes were prioritized: the gradual change known as trend, and the abrupt change known as shift. However, methods that have been developed for analyzing these changes have not been used for continental U.S. streamflow study. Moreover hydrologic variables have the propensity to be present in clusters, which is termed as persistence. This characteristic, if not addressed, often leads to over- or underestimation of trends. Two important climate indicators identified so far are sea surface temperatures (SST) and geopotential height. The SST have been used in identifying relationships with hydroclimatic variables by considering specific regions of the oceanic-atmospheric oscillations of El Niño-Southern Oscillation (ENSO), Pacific Decadal Oscillation (PDO), Atlantic Multidecadal Oscillation (AMO), North Atlantic Oscillation (NAO), and others. 500mbar geopotential height index (Z_{500}) can

explain many complex climate mechanisms but has not been explored in relation to continental U.S. streamflow.

With this motivation, this study focused on finding the relationships of streamflow variability with oceanic-atmospheric indicators. First, the presence of trends with consideration of short term and long term persistence followed by shifts over the past years in continental U.S. streamflow were analyzed by using the non-parametric Mann Kendall and Pettitt tests. Second, the spatio-temporal relationships between seasonal streamflow variability of continental U.S. and oceanic-atmospheric indicators (SST and Z_{500}) of the Pacific and Atlantic were established using the singular valued decomposition (SVD) factorization technique. Finally, the SVD technique was used to determine the spatio-temporal relationships between western U.S. seasonal streamflow variability and indicators (SST and Z_{500}) of Pacific Ocean variability.

In order to accomplish this task, unimpaired streamflow gauges were examined for consistent and longer data periods of record. The continental U.S. study used 60 years (1951-2010) of unimpaired streamflow data of 240 streamflow gauges and the western U.S. streamflow analysis included 90 unimpaired streamflow gauges with 50 years of data (1960-2010). However, annual water-year streamflow volumes are good for long-term predictability; they often mask the big disparities that seasonal streamflow volumes show. Gridded Pacific and Atlantic SST/Z_{500} were used at different lead times with the streamflows. To distinguish the results of each major hydrologic basin the Walker test, which can measure global significance, was incorporated. Linear correlation techniques were used to determine the correlation values from the temporal expansion series obtained from SVD. All the tests were performed at a threshold significance level.

The results indicated that significant trends and shifts existed in the streamflow volumes in the past few decades in the continental U.S., and short term and long term persistence was evident in streamflows. Removal of the persistence characteristic removed spurious trends, which can be misinterpreted. The 1970s were the years when major shifts took place, and most of the shift periods coincided with the phase changes of multi-decadal oscillations. Strong spatio-temporal relationships of the streamflows were established with the oceanic-atmospheric indicators, the multi-decadal oscillations (PDO, AMO) did influence these relationships. Seasonal analysis showed improved explanation of co-variability over water-year. The lead-time approach showed that the relationships could be explained up to 9 months ahead, and Z_{500} showed improved results over SST at shorter lead-times. Several new regions apart from the well identified index regions were identified in the oceanic region to have strong relationships with seasonal streamflows. The individual basins showed unique relationships with the indicators both spatially and temporally which could be due to their unique topographical and local factors.

The contributions from this research include a better understanding of the changes in continental U.S. streamflow and the spatio-temporal relationships with oceanic-atmospheric variability. Other studies have incorporated streamflow datasets, which may not be impaired but have some minimal regularization and water-year streamflow relationships. This study was the first of its type in many aspects. First, it uses the HCDN-2009 (Hydro-Climatic Data Network) dataset in analysis, and performs both a short term and long-term persistence change analysis with the Pettit test on continental United States streamflow. Second, this study uses the Z_{500} dataset, which has not previously been, used to establish relationships with continental U.S. streamflow. Third,

this is the first study that identifies the relationships of seasonal continental streamflow with climate indicators. This study performs comparison at hydrologic region level, which is important from a water management perspective. The study aimed to provide a better understanding of the effects of climate variability on streamflows that can help in better water management decisions.

ACKNOWLEDGEMENTS

This work was supported partly by NSF under Grants IIA-1329469 and CMMI-0846952.

TABLE OF CONTENTS

LIST OF TABLES

LIST OF FIGURES

LIST OF ABBREVIATIONS

AMJ	-	April, May, June
AMJJAS	-	April, May, June, July, August, September
AMO	-	Atlantic Multidecadal Oscillation
CUSUM	-	Cumulative Sum Control Chart
ENSO	-	El Niño Southern Oscillation
ESRL	-	Earth System Research Laboratory
GAGES	-	Geospatial Attributes of Gages for Evaluating Streamflow
HCDN	-	Hydro-Climatic Data Network
HGT	-	Geopotential Height
HUC	-	Hydrologic Unit Code
IPCC	-	International Panel on Climate Change
JAS	-	July, August, September
LTP	-	Long Term Persistence
MCM	-	Million Cubic Meters
MK1	-	Mann Kendall Test
MK2	-	Mann Kendall Test with Trend Free Pre Whitening
MK3	-	Mann Kendall Test with Hurst Component
NAO	-	North Atlantic Oscillation
NCAR	-	National Centre for Atmospheric Research
NCEP	-	National Centers for Environmental Prediction
NOAA	-	National Oceanic and Atmospheric Administration
PNA	-	Pacific North American Index
NSC	-	Normalized Squared Covariance

OND	-	October, November, December
PCA	-	Principal Component Analysis
PDO	-	Pacific Decadal Oscillation
PDSI	-	Palmer Drought Severity Index
SCF	-	Squared Covariance Fraction
SOI	-	Southern Oscillation Index
SST	-	Sea Surface Temperature
Z_{500}	-	500 mbar Geopotential Height
STP	-	Short Term Persistence
SVD	-	Singular Valued Decomposition
TFPW	-	Trend Free Pre Whitening
TNI	-	Trans Niño Index
UCRB	-	Upper Colorado River Basin
USGS	-	United States Geological Society

CHAPTER 1: INTRODUCTION

1.1. Research background.

"Whiskey is for sharing and water is to fight for." This famous saying attributed to Mark Twain conveys the importance of fresh water availability to our growing needs. With the rapid increase in population and economic growth, the stress on fresh water resources has increased manifold to meet the domestic, agricultural, industrial, energy, wildlife, and recreational demands. Water managers thus face the challenge of meeting the future water demands with existing water infrastructure. Substantial anthropogenic change of earth's climate has steered the death of stationarity in hydrologic variables (Milly et al., 2008). The recent climate change as a result of increased atmospheric CO_2 and global surface temperature in the Earth's energy balance is the most unpredictable and uncontrollable factor in terms of future water management. Climate variability is a continuous slow process; minor variations directly and indirectly impact the environment (Impoinvil et al., 2007a; 2007b) and hydrological cycle. Changes in hydrological cycle can lead to extreme events such as floods and droughts (Redmond and Koch, 1991; Cayan et al., 1999; McCabe and Wolock, 2002; Huntington, 2006 Ahmad and Simonovic, 2001c; Simonovic and Ahmad, 2005). The available parameters for detecting climate variability are air temperature, air pressure, sea surface temperature, precipitation, and others. The variability in climate indicators is monitored through agencies such as the National Oceanic and Atmospheric Administration (NOAA) and continuously scrutinized by the Intergovernmental Panel on Climate Change (IPCC). Analyses on global patterns of climate trends show evidence of a warming climate, which is likely to continue into the future (Dettinger et al., 2000; Easterling et al., 2000; Milly et al 2002; Adam et al.,

2009). In the continental U.S., various studies have predicted future warming, reduced winter precipitation and snowpack accumulation in the western U.S., decreased high flows in the eastern U.S., shifting summer peak streamflow towards winter, and increases of flood and drought risks in the western United States (Dettinger and Cayan, 1995; Hamlet and Lettenmaier, 1999; Nijssen et al., 2001; Stewart et al., 2005; Hayhoe et al., 2007;). A great deal of research has tried to understand the interdependency of streamflow on climate variability; however, there is still a need to investigate these over time.

Study of the long term changes of hydroclimatic variables of the past can help in predicting the future water supply (Pagano and Garren., 2006). Streamflow is the major source of inland fresh water. With increasing human population many rivers are being heavily managed by constructing diversions to meet the different seasonal requirements. For example the water of the Colorado River is used for various purposes and is shared among seven U.S. states and Mexico as per several legal treaties, and compacts. However, to meet the states requirement, the river is highly regulated through a series of reservoirs which ensure year-round supplies of water. The effects of these diversions over the river flow are complex, and many scientific groups have tried modelling approaches to estimate the natural flow of the system. Despite these efforts, anomalies remain due to slow long-term changes. In streamflow resulting from climate change, numerous small rivers are also being diverted to meet our water requirements, these diversions further reduce unimpaired streamflows. Unimpaired streamflows can best represent long-term climate change effects, but their decreasing availability reduces our ability to study these phenomenons. For the continental U.S., the studies so far on streamflows use data that

have minimal human intervention, but are not completely unimpaired. The reliability of using them is questionable in terms of quality. Additionally there are unrealized forcing mechanisms like short-term and long-term natural variability and persistence which may influence the statistical analysis.

Some of the well-known and commonly understood climate indices like Southern Oscillation Index (SOI, El Niño and La Niña), North Atlantic Oscillation (NAO), Atlantic Multi-decadal Oscillation (AMO), SST Indices, Palmer Drought Severity Index (PDSI), Pacific Decadal Oscillation (PDO), and Atlantic Multidecadal Oscillation (AMO) have been related to streamflow in the U.S. and around the world (Walker 1925; Philander, 1990;Mantua et al 1997; Enfield et al 2001), and have also been found to have complex relationships with inland hydrology in terms of time and space (Ropelewski and Halpert, 1986; Lamb and Peppler, 1987; Redmond and Koch, 1991; Cayan and Webb, 1992; Hurrel, 1995; Trenberth, 1997; Rodo et al 1997; Kiffney et al., 2002; Gordon and Giulivi,2004; Ma, 2007; Kalra, 2012). In the U.S., these periodic oscillations have been established to have associations with hydrology such as, impacts on precipitation (Gutzler et al., 2002; Goodrich, 2004), snowpack (e.g. Aziz et al.,2010), streamflow (Barlow et al.,2001, etc), droughts(e.g. Goodrich, 2007; Nigam et al., 2011), and fires (Hessl et al., 2004). Other available climate variability information are gridded datasets of the ocean such as sea-surface temperatures, atmosphere such as geopotential height index and sea winds data, and other marine and paleoclimate data, and others (NOAA). These gridded datasets provide opportunities to explore new avenues of climate variability that are different from well-established oscillations (e.g. Grantz et al., 2005; Tootle et al., 2006; Soukop et al., 2009; Aziz et al 2010). Thus, various developments in terms of data

accumulation, development, and modeling are ongoing to understand and capture climate variability and its impacts on hydrology.

1.2. Research Motivation

A considerable amount of research has been done on long-term changes in streamflow (e.g. Kalra et al., 2014a) and its associations with climate variability (e.g. Kalra et al., 2014b). Study of the changes in streamflow using unimpaired stations can help in minimizing the effect of anthropogenic influence on land-use, flow storage, and diversions; the resulting changes can be attributed to variability and change in the climate. The changes exhibited in a hydrological time series may be gradual (trend) or abrupt (step/shift). To date, the literature has not yet adequately addressed these unrealized forcing mechanisms of short-term and long-term persistence for trend studies in continental U.S. streamflow. Trend detection can explain the long-term state of a system and its anticipated extension into the future. Abrupt changes, on the other hand, are associated with extreme hydrologic events, such as storms, floods, or droughts and can lead the streamflow towards a completely different regime (Lins and Slack, 1999). For evaluation of the impact of climate change, the distinction between trends and shifts is important. Generally, abrupt changes are unpredictable unless the causes are known. The presence of a shift in the data series might also affect the significance of the trends, which further necessitates their detection. Earlier studies on detection of shifts use a predefined shift period and test the stations for significance (Miller and Piechota, 2008; Kalra et al., 2008). This method might not be accurate when a large number of stations is considered that can have different shift periods.

Ideally, the use of different recognized indices like the ENSO, AMO, NAO, PDO, and others are used in streamflow forecasting models. These indices have a defined spatial scale (example: the Niño 3.4 region lies around 5N to 5S and 120W to 170W) and use the sea surface temperature data of that specific location. Considering these traditional indices will not incorporate any variation or shift in the spatial region of weather phenomena. Moreover some watersheds are not affected by these traditional regions of climate indices. The use of an entire gridded data set of an oceanic region will eliminate this redundancy and might be able to identify new regions could cause seasonal impacts on streamflow. Geopotential height is an index whose application in hydroclimatic modeling has been limited. It essentially affects the wind patterns, and, in response precipitation. The use of an entire gridded dataset of sea surface temperature and geopotential height could be useful in identifying relationships with the hydroclimate.

With this research motivation, this thesis uses statistical approaches in identifying the changes in the streamflow volumes of the continental U.S. and determining the spatio-temporal relationships between oceanic-atmospheric variability and streamflow. The statistical methods used to study the changes in the U.S. streamflow are the non-parametric tests, Mann Kendall and Pettitt. A factorization technique known as singular valued decomposition (SVD) is used to find the relationships between oceanic-atmospheric variability of Pacific and Atlantic and U.S. streamflow variability. The continental U.S. has a varied topography from east to west and north to south surrounded by two major oceans, i.e. the Atlantic and the Pacific, and the Gulf of Mexico. Unimpaired streamflow data is maintained by the USGS as the HCDN network, the

gauges are distributed all over the United States. The USGS has divided the U.S. into 21 major hydrologic regions depending on the major river systems. Of these, 18 hydrologic basins are present in continental United States. Comparison among the different hydrologic basins of the U.S. is an important part of this work which is achieved by using a global significance method called the Walker test. The results were evaluated at a particular significance level, typically set at $p \leq 0.10$.

1.3. Research Objectives

The objective of this research was to understand the relationships among U.S. streamflow and climate variability. In order to achieve the understanding of the patterns in the streamflow variability, the continental U.S. streamflow volumes were analyzed along with their teleconnections with the oceanic-atmospheric variability. The results are expected to improve the understanding of water-managers about the effects of climate variability on hydroclimate, and aid in planning and management of water resources. To achieve these objectives, the following questions and their corresponding hypotheses were addressed in this research.

Research Question # 1: What were the changes in the hydrology of the continental U.S. in the past years and how do they compare temporally and spatially?

Hypothesis #1: Unimpaired streamflows, which have the least anthropogenic interference, can best represent climate variability and the phase changes of the multidecadal climate indices. As streamflow data do not follow a normal distribution, using non-parametric tests will best represent streamflow variability.

Research Question # 2: How do the oceanic-atmospheric indices affect (associate with) the streamflows of the continental United States?

Hypothesis #2: The Oceanic-atmospheric indices have affected the hydrologic cycle by influencing the winds, moisture, and ultimately the precipitation. Using a lead-time methodology, the interaction between the oceanic-atmospheric indices and streamflow variability can be explored. Different basins of the continental U.S. streamflow have significant associations with the oceanic-atmospheric indices, but geography will determine the differences.

Research Question # 3: How do the oceanic-atmospheric indices play a role in affecting streamflow in adjacent basins, and can the lead time of streamflow forecasting be improved?

Hypothesis #3: Western U.S. streamflow is strongly affected by Pacific Ocean variability and depending on the precipitation of the region, the association of the oceanic-atmospheric indices and streamflow has a lagged relationship.

1.4. Research Tasks

The research is presented in a manuscript format. The current chapter is comprises of introduction and formulates the problem statement for this study. Chapter 2 is a manuscript titled, "Evaluating the effect of persistence on long-term trends and analyzing step changes in streamflows of the continental United States" that addresses Research Question #1.This chapter uses 60 years of unimpaired streamflow data from the HCDN-2009 network to analyze the persistence and changes in 240 streamflow gauges over the continental United States. Two non-parametric tests, the Mann-Kendall test with

persistence addressing variations and the Pettit test, were used. The Walker test was used to determine the global significance of the results categorized into 18 hydrologic regions. Chapter 3 is a manuscript titled, "Evaluating the influence of sea surface temperatures and geopotential height on seasonal streamflows of the continental United States" that addresses Research Question #2. This chapter uses SVD to evaluate the 1-4 month lagged spatio-temporal relationships between seasonal streamflow of the continental U.S. and Pacific and Atlantic sea-surface temperatures and 500mbar geopotential height (Z_{500}). Further, the influence of the multidecadal PDO and AMO phases on these relations is explored. Chapter 4 is a manuscript titled "Pacific Ocean SST and Z_{500} climate variability and western U.S. seasonal streamflow" that addresses Research Question #3. This chapter uses SVD to evaluate the 3-9 month lagged spatio-temporal relationships between seasonal streamflow of the western U.S. and Pacific Ocean climate variability. It also examines the effect of performing SVD on six individual basins of the western United States. Chapter 5 summarizes and concludes this thesis and provides recommendations for future research.

CHAPTER 2: EVALUATING THE EFFECT OF PERSISTENCE ON LONG-TERM TRENDS AND ANALYZING STEP CHANGES IN STREAMFLOWS OF THE CONTINENTAL UNITED STATES

Abstract

Streamflow is a very good indicator of long-term hydroclimatic changes. From a water management perspective, the identification of gradual (trend) and abrupt (shift) changes in streamflow are important for planning purposes. This study investigated the detection of comprehensive change, gradual and abrupt, in 240 unimpaired streamflow stations, categorized according to the hydrologic regions in the continental United States. The changes in streamflow volume were analyzed for water-year, autumn, winter, spring, and summer from 1951 to 2010, a 60-year period. The non-parametric Mann-Kendall test, with variations accounting for short term and long-term persistence, was used to evaluate the trends; the non-parametric change-point Pettitt test was used to evaluate the shifts. The field significance was evaluated using the Walker test. The trend results indicated increasing streamflow patterns in the majority of the eastern U.S. regions – the Upper Mississippi, Missouri, Great Lakes and Texas Gulf were field significant – and dominant decreasing streamflow trends in the Pacific Northwest region. The use of different Mann-Kendall test helped in evaluating the spatial distribution of short-term and long-term persistence and their effect on trends. The Pettitt test analysis indicated that statistically significant shifts occurred during the early 1970s and late 1980s. Similar to the trend results, the Midwest as well as the central and southern U.S. had significantly increasing shifts; the Pacific Northwest, Tennessee (winter season only), and South-Atlantic Gulf (spring season only) had decreasing shifts in streamflow. The findings may

assist water managers in better planning and management of water resources under climate variability and change.

2.1. Introduction

With the rapid increase in population, the stress on water resources has increased manifold (Qaiser et al., 2013; Shrestha et al., 2011; Ahmad and Prashar, 2010; Wu et al., 2013). Further, water managers have been concerned about the anticipated impacts of climate variability and change on water resources (Dawadi and Ahmad, 2012; Vedwan et al., 2008; Kalra and Ahmad, 2012; Dawadi and Ahmad, 2013; Zhang et al., 2014). Increased variability in streamflow due to changing climate has resulted in altering the hydrological cycle (Puri et al., 2011a; 2011b; Stephen et al., 2010; Ahmad et al., 2010; Ahmad and Simonovic 2006). In snow-fed basins, an increase in spring temperatures has led to earlier summer streamflow peaks (Arora and Boer, 2001; Voss et al., 2002; Stewart et al., 2005; Hamlet and Lettenmaier, 2007); moreover, low annual flows have increased in the northeast U.S. in the last century, and have become less extreme (Lins and Slack 1999; EPA climatic indicators, 2012).

Changes in climate variability enhance the uncertainties in the availability of fresh water for future generations (Middelkoop et al., 2001). Thus, water managers face the challenge of meeting future water demands with existing water infrastructure that may be inadequate in the future (Qaiser et al., 2011; Ahmad and Simonovic, 2001b). In addition, stress is increasing to meet environmental flow requirements and provide water for the energy needs (Shrestha et al., 2012, Venkatesan et al., 2011a; Venkatesan et al., 2011b; Melesse et al., 2011; Ahmad and Simonovic 2001a; 2005; Choubin et al., 2014).

Changes in the hydrological cycle can result from both climate variability and anthropogenic interference. These changes may be gradual (trend) or abrupt (shift). Changing hydrology may lead to under-designed or over-designed projects (Forsee and Ahmad, 2011a; 2011b; Mosquera-Machado and Ahmad, 2007; Ahmad and Simonovic 2000a), which may not meet long-term needs; thus, the traditional assumption of stationarity for hydraulic designs requires review (Milly et al., 2008). To address these issues, this study focuses on evaluating trend and step changes in streamflow while taking into account streamflow persistence, which affects long-term trends.

Study of the changes in streamflow, using unimpaired stations, helps to minimize the effect of anthropogenic influences on land use, flow storage, and diversions; the resulting change can be attributed to variability and climate change. Various studies have predicted future warming, bringing change in timings as well as increasing the quantity of monthly precipitation; reducing winter precipitation and snowpack accumulation in the western U.S.; decreases in high flows in the eastern U.S., and shifting summer peak streamflow towards winter, thus increasing the flood and drought risks in western United States (Aguado et al., 1992; Dettinger and Cayan, 1995; Hamlet and Lettenmaier, 1999; Nijssen et al., 2001; Stewart et al., 2005; Hamlet et al., 2007; Hayhoe et al., 2007). Analyses on the global pattern of climate trends concur with evidence of a warming climate (Dettinger et al., 2000; Easterling et al., 2000; Milly et al., 2002; Milly et al., 2005; Adam et al., 2009).

A great deal of research is taking place to understand the interdependency between climate variability, and streamflow (Hamlet and Lettenmaier, 1999; Kalra and Ahmad, 2011; Carrier et al., 2011; 2013; Kalra et al., 2013a and Kalra et al., 2013b).

However, there is a need to understand the changing patterns of streamflow over time, which can improve planning and operational strategies for sustainable use of available water resources (Frederick and Major, 1997; Mirchi et al., 2012; Ahmad and Simonovic, 2000b).

In the past, significant efforts have been made to study the long-term trends in streamflows over the continental United States. Several studies have shown an increase in annual moderate-to-low streamflows and a less significant increase in peak streamflows (Lettenmaier et al., 1994; Lins and Slack, 1999; McCabe and Wolock, 2002; Kalra et al., 2008). Lettenmaier et al. (1994) used monthly records of 1009 unimpaired streamflow stations in the continental U.S. for a period of 40 years (1948-1988); they found increases in streamflows from November to April that concentrated in the north-central states. Lins and Slack (1999) conducted a trend analysis on daily discharges from 395 streamflow stations of the Hydro Climatic Data Network (HCDN) for varying years, and identified decreasing trends in the Pacific Northwest and Southeast region. For the eastern United States, Small et al. (2006) indicated that increases in fall precipitation increased the low flows; on the other hand, high flows were not related statistically to trends in spring precipitation. Groisman et al. (2001) studied 385 stations from the HCDN and found increasing trends in peak streamflows in the eastern U.S. resulting from increasing precipitation; however, they found negligible change in the western United States. The differences in the results are due to the different techniques used in these studies.

Regarding regional studies on streamflow changes, in Pennsylvania, Zhu and Day (2005) found strong downward trends in the daily streamflow volume. Gebert and Krug (1996) found that annual low flows increased and flood peaks decreased in southwestern

Wisconsin, which varied from northern Wisconsin. Easterling et al., (2000) and Groisman et al. (2001) found an escalation in climate events, such as heavy precipitation, floods, and droughts, indicating abrupt climate patterns. In the 20th century, the droughts of 1930s and 1950s were identified as the most severe for large areas; the droughts of early 2000s in the western U.S. were identified as the most extreme for small areas (Andreadis et al., 2005).

So far, the documented literature has been valuable with regard to streamflow change studies. However, various unrealized forcing mechanisms, such as short-term and long-term natural variability, need to be considered while analyzing a hydrological time series. The hydro-climatic variables have a propensity to be present in clusters during certain periods of time, i.e., droughts or floods; this is termed 'scaling' or 'persistence'. Short-term persistence (STP), the most common and simple example, has been addressed in many studies using the autoregressive-1 model. The presence of long-term persistence (LTP), first identified by Hurst (1951) in a study on the Nile River, can influence considerably trends determined with independence and STP assumptions (Cohn and Lins 2005).

Long-term persistence can be postulated to exhibit the continual variability of several factors influencing climate and ultimately streamflow, such as solar forcing, volcanic activity, greenhouse gases, carryover storage of water in lakes, soil properties, and oceanic oscillations. As stated by Koutsoyiannis and Montanari (2007), the recorded data could be a small segment of a longer cycle of natural processes that, under current circumstances, are unidentified by currently available observations. Therefore, a longer observation period can provide more realistic information of the process under

investigation. Each watershed has its own characteristic hydrology, which is the basis of hydrologic spatial variability.

Vogel et al. (1998) studied the variation of persistence across the U.S., and identified larger regions with the homogenous property of persistence. The presence of LTP can significantly deviate the mean from actual trends; thus, it is essential to investigate LTP's effects on trends. Burn and Elnur (2002) analyzed trends of hydrologic and meteorological variables in Canadian catchments, using serial and cross-correlation; they observed an earlier onset of spring-melt conditions, and suggested that hydrological variables accentuate patterns existing in meteorological variables acting as input. Kalra et al. (2008) analyzed 639 unimpaired U.S. streamflow stations data for 52 years for trends with lag-1 autocorrelation; they observed decreasing streamflow trends in the Pacific Northwest and South-Atlantic Gulf, resulting from an abrupt step change followed by a gradual decreasing trend. In the analysis of streamflow in Indiana, Kumar et al. (2009) used lag-1 autocorrelation, complete autocorrelation structure, and LTP. Similarly, Ehshanzadeh et al. (2010) conducted a study identifying the STP and LTP influence on streamflow trends in Canada. Other studies have suggested that trends are influenced by the nature of streamflow statistics, annual/seasonal statistics, the time period, and take into consideration the correlation structure (Koutsoyiannis, 2003; Kumar et al., 2009).

The literature has highlighted the importance of studying long-term trends in streamflow; however, addressing the effect of LTP while identifying trends has not received prominence in studies of the continental U.S. To evaluate the impact of climate change, the distinction between trends and shifts is important. When there is a sharp increase or decrease in any hydrological variable, abrupt changes, also known as shifts,

may be associated with extreme hydrologic events, such as storms, floods (Ahmad et al., 2009; 2010a; Ahmad and Simonovic 2001d; 2004), or droughts, along with changes in ecosystems. For example, the winter of 1976-1977, in the North Pacific was extreme due to a shift in the ocean-atmosphere system (Kerr, 1992; Beamish et al., 1997; Holbrook et al., 1997; Mantua and Hare, 2002). During that period, a shift was observed in the mean sea-level temperature (Mantua and Hare, 2002). Sudden changes in the inland surface water may be result of these climate extremes.

A trend is anticipated to extend into the future, whereas the occurrence of a shift can lead the streamflow towards a completely different regime. Generally, these changes are unpredictable unless the causes are known. Previous studies on shift detection in the U.S. have been conducted by using a pre-defined known year and by comparing the means or medians in the data before and after that time (Kalra et al., 2008; Miller and Piechota, 2008). This method has limitations when a large number of stations are considered because the shift period may not coincide; hence, it is difficult to pre-define a particular shift period. The presence of a shift in the data series might affect the significance of the trends, and this necessitates its detection.

For this study, a comprehensive analysis was conducted of the long-term changes in 240 unimpaired streamflow stations over the continental United States. In an attempt to provide a better understanding of inter-relations between climate and spatial streamflow variability, the key motivation of this work was to 1) identify trends that account for STP and LTP along with shifts and 2) compare the changes among the 18 major hydrologic regions. A longer duration of data – i.e., 1951-2010 (60 years) – was taken into consideration in order to account for the effects of multi-decadal variability in climate.

Moreover, the detection of the change point was performed by identifying the shift period for each station, which can indicate major events in the particular region. In addition, any association between the occurrence of shifts and phases of climate indices, such as El Niño Southern Oscillation (ENSO) and Pacific Decadal Oscillation (PDO), was investigated.

Several other climate patterns have been shown to influence streamflow in the continental United States. A detailed analysis of the relationship between climate indices and streamflow was not within the scope of this current work. Various periods (water-year, autumn, winter, spring, and summer) were analyzed for both gradual trends and abrupt shifts so that the changes in each could be identified separately.

2.2. Study Area and Data

The hydrology of the continental U.S. varies from region to region, which makes the study of streamflow change challenging. In the western U.S., the Great Plains are semi-arid and the mountains are alpine. In the Great Basin, the climate is arid; in the Southwest, it is desert; coastal California is Mediterranean; and the coastal northwest is oceanic. In the eastern U.S., the climate varies from humid continental in the north to humid subtropical in the south.

The United States Geological Survey (USGS) divides the continental U.S. into 18 regions. Further, each region is divided into sub-regions, accounting units, and cataloging units, denoted with a unique hydrologic unit code (HUC) consisting of two to eight digits based on the four levels of classification. The USGS online database (http://www.usgs.gov/) makes streamflow data readily available.704 stations within the

continental U.S. were verified from the USGS Hydro-Climatic Data Network 2009 (HCDN-2009) (Lins F. Harry, 2012). The HCDN-2009 dataset is a revision of 1) the USGS original HCDN network (Slack et al., 1992) and 2) the streamflow stations within the dataset area subset of the revised Geospatial Attributes of Gages for Evaluating Streamflow, version II (GAGES) dataset (Falcone et al 2010). Only stations having continuous streamflow data from 1951 to 2010 water-years (Oct 1950 to Sept 2010) were considered for long-term analysis, which narrowed the total stations. From the HCDN-2009 network, only 252 stations had continuous data from 1951 to 2010. To avoid spatial bias in the results, only one station on a particular stream within each HUC was considered; this reduced the number of stations to 240. Stations with missing data could be considered by filling the gaps, using imputation methods (Gill et al., 2007); however, the results were more likely to be compromised, and these methods were avoided.

Reducing the temporal period would have increased the number of stations; however, the need for a longer streamflow record resulted in the elimination of the stations. Taking into consideration the water-year (the previous year October to the current year September) facilitated the comparison for seasonal changes, i.e., autumn (Oct-Dec), winter (Jan-Mar), spring (Apr-Jun), and summer (Jul-Sept). For the analysis, the data was averaged for the water-year and the four seasons.

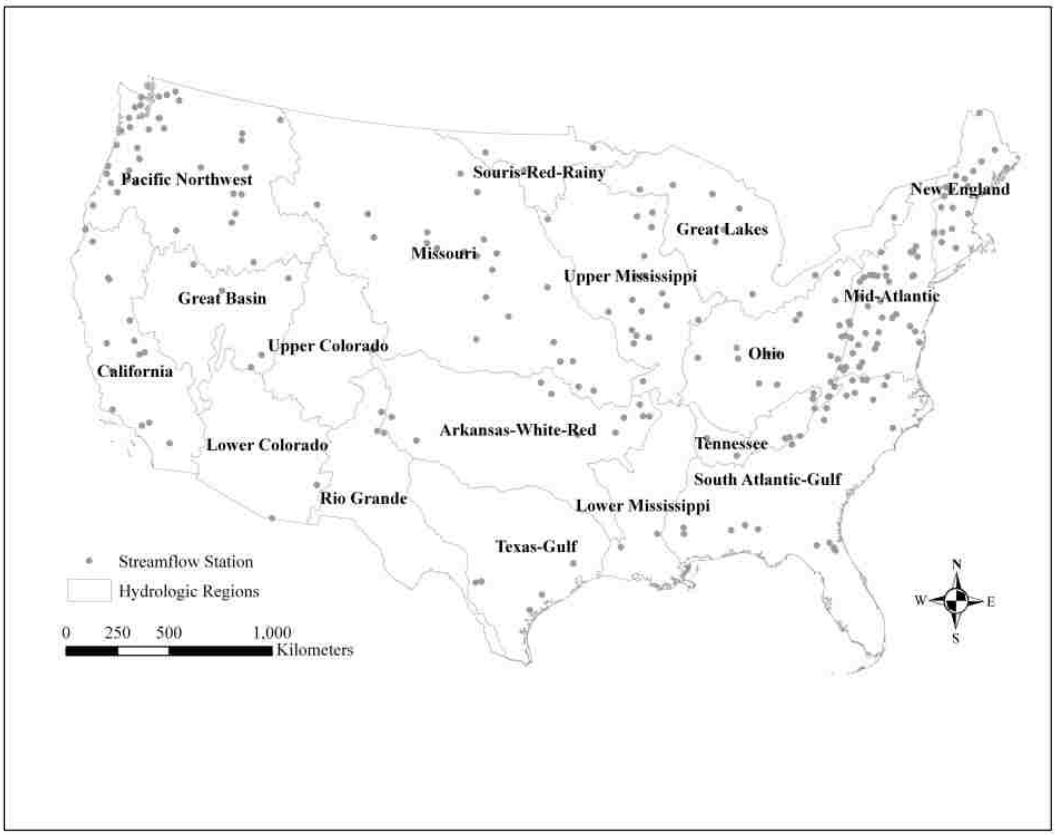

Figure 2.1: Map of continental U.S. showing the spatial distribution of the 240 unimpaired streamflow stations over 18 hydrologic regions.

In the spatial distribution of the streamflow stations shown in Figure 2.1 (a list of stations is provided in Table 2.1), it can be seen that the eastern U.S. has streamflow stations that have been maintained for a considerably longer duration than in other regions. Regions as the Mid-Atlantic (2) and Pacific Northwest (17) have more than 30 stations, whereas the Upper Colorado (14) has no unimpaired station with 60 years of data. The regional comparison of trends and abrupt shifts may be influenced by this disparity; however, the overall nature of trends can be inferred.

The other dataset used in the analysis consists of climate indices, i.e., ENSO and PDO. ENSO is the natural coupled cycle in the ocean-atmospheric system over the

tropical Pacific. It operates on a timescale of two to seven years as a warm phase (El Niño, positive index) and a cool phase (La Niña, negative index). The PDO is an index of the decadal-scale variability in sea-surface temperature (SST) in the North Pacific Ocean (McCabe and Dettinger, 2002). Similar to ENSO, PDO has two phases, warm and cold. Several studies have indicated two full phases of PDO in the past century, with a periodicity of 25 to 50 years (Mantua and Hare, 2002; Tootle et al., 2005). For the current study, the coupled relationship between PDO and ENSO has been used to verify the shift periods. The El Niño, La Niña, and neutral ENSO years have been obtained for PDO warm and cold phases, and checked for possible patterns in streamflow shifts (http://www.atmos.washington.edu/~mantua/TABLES2.html)

2.3. Method

Four statistical tests were used to evaluate the characteristics of changes in streamflow. The properties of hydrologic variables facilitate non-parametric tests better than parametric tests (Helsel and Hirch, 1992; Yue and Pilon, 2004). While many statistical tests have been used for streamflow trend analysis, the non-parametric Mann-Kendall tests have received wide acceptance due to their independency from the distribution of data and robustness against outliers (Lins and Slack 1999; Zhu and Day, 2005; Burn, 2008; Kumar et al., 2009; Villarini et al., 2009; Villarini and Smith, 2010). Villarini et al. (2009) compared five methods for change-point detection, i.e., the Pettitt, CUSUM, Guan, Rodionov, and Bayesian methods. They concluded that the non-parametric Pettitt test has better accuracy than the other tests in identifying change points. Using Walker's test (Wilks, 2006), field significance was evaluated to assess if the trend and shifts result in each region are globally significant. Further, the shifts in streamflow

were checked against the phases (warm and cold) of ENSO and PDO climate indices for any possible pattern. The basis for this analysis was to see if there was a pattern in streamflow shifts that coincided with the phase change of climate indices.

A brief description of the Mann-Kendall tests, abstracted from Yue et al. (2002) and Hamed (2008); the Pettitt (1979) test; and Walker's test, abstracted from Wilks (2006), is presented in this section. For a more detailed description, the readers are referred to the sources of these tests (Mann, 1945; Kendall, 1975; Hamed and Rao, 1998; Koutsoyiannis, 2003; Hamed, 2008; Pettitt, 1979, Wilks, 2006).

2.3.1. Trend Test

Statistically significant trend detection in temporal and spatially correlated streamflow using the Mann-Kendall test was studied by Yue and Wang (2002), Yue et al. (2002), and Khaliq et al. (2009). Use of scaling hypothesis to detect the Hurst component was developed by Koutsoyiannis (2003).The rank-based non-parametric Mann-Kendall test (Mann, 1945; Kendall, 1975) is robust against data containing outliers and non-linear trends (Helsel and Hirsch, 1992; Onoz et al., 2003) and doesn't assume serial interdependency or a probability distribution of data. The power of the test is compared against other tests in various investigations (Onoz et al., 2003; Yue et al., 2002; Yue and Pilon, 2004). To detect trends, this study used the independent Mann-Kendall test, represented as MK1; the modified Mann-Kendall test for STP (lag-1 autocorrelation) by Trend Free Pre-Whitening (TFPW), represented as MK2; and the modified Mann-Kendall test for LTP with scaling hypothesis, represented as MK3.

2.3.1.1. Independent Mann-Kendall test (MK1)

For a series $x_1, x_2, x_3, \ldots x_n$, the Mann-Kendall test statistic (S) is given by Equation 2.1.

$$S = \sum_{i=1}^{n-1} \sum_{j=i+1}^{n} sgn(x_j - x_i), \tag{2.1}$$

where the x_i represents the sequential data values, n is the length of the data set, and

$$sgn(\theta) = \begin{cases} 1 & \theta > 0 \\ 0 & \theta = 0 \\ -1 & \theta < 0 \end{cases} \tag{2.2}$$

Assuming the data is serially independent and identically distributed:

$$E(S) = 0 \tag{2.3}$$

$$var(S) = \frac{n(n-1)(2n+5) - \sum_{i=1}^{n} t_i i(i-1)(2i+5)}{18} \tag{2.4}$$

where $E(S)$ is the mean, $var(S)$is the variance of S, and t_i is the number of ties of extent i. The Mann-Kendall standardized test statistic Z is given by:

$$Z = \begin{cases} \frac{S-1}{\sqrt{V(S)}} & for\ S > 0 \\ 0 & for\ S = 0 \\ \frac{S+1}{\sqrt{V(S)}} & for\ S < 0 \end{cases} \tag{2.5}$$

The sign of S gives the direction of the trend; that is, a negative sign indicates a decreasing trend, and vice versa. The value of Z gives the significance level of rejecting the null hypothesis.

2.3.1.2. Mann-Kendall with lag-1 Autocorrelation for STP (MK2)

It has been established that the existence of serial correlation can lead to the rejection of the null hypothesis due to inflation of the variance (Hamed and Rao, 1998; Yue et al., 2002). Thus, the serial correlation was removed by 1) pre-whitening of the series by assuming lag-1 autocorrelation; and 2) de-trending the series before removing

the lag-1 autocorrelation, also known as trend free pre-whitening (TFPW) (Yue et al., 2002). The lag-1 autocorrelation coefficient (r_1) is computed from Equation 2.6:

$$r_1 = \frac{1}{n-1}\sum_{i=1}^{n-1}[x_i - E(x_i)][x_{i+1} - E(x_i)] / \frac{1}{n}\sum_{i=1}^{n}(x_i - E(x_i))^2, \quad (2.6)$$

where $E(x_i) = \frac{1}{n}\sum_{t=1}^{n} x_i$ (2.7)

and the confidence interval is:

$$\frac{-1-1.645\sqrt{n-2}}{n-1} \leq r_1 \leq \frac{-1+1.645\sqrt{n-2}}{n-1}. \quad (2.8)$$

If the lag-1 serial correlation computed from Equation 2.6 lies between the confidence interval given by Equation 2.8, the sample data is assumed to be serially independent at $p \leq 0.10$. Pre-whitening was applied on data that were found to be serially dependent. The magnitude of trend is computed using Equation 2.9 (Thiel, 1950, Sen, 1968).

Thiel-Sen approach (TSA) slope $b = median\left(\frac{x_j - x_l}{j-l}\right) \forall\ l < j$ (2.9)

The de-trended series is obtained from Equation 2.10 by removing the trend.

$$x_i' = x_i - (b \times i) \quad (2.10)$$

The serial correlation is removed from the de-trended series by using Equation 2.11.

$$y_i' = x_i' - r_1 \times x_{i-1}' \quad (2.11)$$

After removal of serial correlation the trend is added back to the series, using Equation 2.12.

$$y_i = y_i' + (b \times i) \quad (2.12)$$

The S and Z statistics are calculated again for the new series.

2.3.1.3. Mann-Kendall with the Hurst Component for Long-Term Persistence (MK3)

The presence of long-term persistence, or the Hurst phenomenon (Hurst, 1951), might lead to an underestimation of the serial correlation of the data and an over-estimation of the significance of the Mann-Kendall test. To detect the trend under LTP, the method proposed by Hamed (2008) was adopted. The presence of LTP usually is determined by evaluating the Hurst component *H*, which ranges between 0 and 1. The equivalent normal variates of the de-trended time series (Equation 2.10), is given by Equation 2.13:

$$Z_t = \varphi^{-1}\left(\frac{R_t}{n+1}\right), \tag{2.13}$$

where R_t is the rank of the de-trended series x_i' , n is the number of observations, and $\varphi^{-1}()$ is the inverse standard normal distribution function.

The autocorrelation function at lag l for any scale is given by Koutsoyiannis (2003) as Equation 2.14:

$$\rho_l = \frac{1}{2}(|l+1|^{2H} - 2|l|^{2H} + |l-1|^{2H}), \tag{2.14}$$

and the correlation matrix for a given scaling coefficient H is given by Equation 2.15.

$$C_n(H) = \left[\rho_{|j-i|}\right], i = 1{:}\,n, j = 1{:}\,n \tag{2.15}$$

The scaling coefficient (H) is estimated using Equation 2.16. The significance of the *H* was tested using mean (μ_H) and variance (σ_H) values from Equations 2.17 and 2.18.

$$\log L(H) = -\frac{1}{2}\log|C_n(H)| - \frac{z^T[C_n(H)]^{-1}z}{2y_o} \tag{2.16}$$

$$\mu_H = 0.5 - 2.874n^{-0.9067} \tag{2.17}$$

$$\sigma_H = 0.77654n^{-0.5} - 0.0062 \tag{2.18}$$

If H is found to be significant, $p \leq 0.10$, the variance of S is calculated from Equation 2.19.

$$V(S)^{H'} = \sum_{i<j} \sum_{k<l} \frac{2}{\pi} \sin^{-1}\left(\frac{\rho|j-l|-\rho|i-l|-\rho|j-k|+\rho|i-k|}{\sqrt{(2-2\rho|i-j|)(2-2\rho|k-l|)}}\right), \quad (2.19)$$

where ρ is calculated from Equation 2.14.

The variance is corrected for bias in Equation 2.20 by multiplying with the factor B from Equation 2.21, where:

$$V(S)^{H} = V(S)^{H'} \times B \quad (2.20)$$

$$B = a_0 + a_1 H + a_2 H^2 + a_3 H^3 + a_4 H^4 \, . \quad (2.21)$$

The value a_k is explained in Appendix I. The modified test statistic is calculated further, using Equation 2.5.

Stations with significant lag-1 autocorrelations and Hurst coefficients (H) were analyzed with the MK2 test and MK3 test, respectively.

2.3.2. Change point test

The non-parametric Pettitt test (Pettitt, 1979) is used to detect abrupt shifts. It is least sensitive to outliers, and skewed distribution makes it most suitable for the analysis of streamflow data. This test can discern the anomaly in the mean (median) when the shift period is unclear. It uses a version of Mann-Whitney statistics for delivering the significance of probabilities by testing two samples from the same population.

Adopted from Pettitt (1979), let T be the length of the time series and τ be the year of the shift. Presuming the time series as two samples $X_1 \ldots X_t$ and $X_{\tau+1} \ldots X_T$, an index V_τ is defined from Equation 2.22:

$$V_\tau = \sum_{j=1}^{T} sgn(X_\tau - X_j) \text{ for any } \tau \quad (2.22)$$

where $sgn(x)$ is same as for Equation 2.2.

A further index, U_τ, is defined by Equation 2.23:

$$U_\tau = \sum_{i=1}^{\tau} \sum_{j=1}^{T} sgn(X_i - X_j) \quad (2.23)$$

In presence of a change point, the graph between $|U_\tau|$ and τ increases up to the change point and then decreases; in the absence of a change point, the graph would continually increase. The most significant change point τ is established at the point where the value of $|U_\tau|$ is maximum, given as K_T (Equation 2.24).

$$K_T = \max_{1 \le t \le T} |U_\tau| \quad (2.24)$$

The probability of a shift in a year where $|U_\tau|$ is the maximum, is estimated by:

$$p = 1 - \exp\left(\frac{-6K_T^2}{T^3 + T^2}\right) \quad (2.25)$$

The probabilities of $p \le 0.10$ are considered, and the direction of the change is evaluated, contingent upon the minimum or maximum value of U_τ extracted by K_T. The minimum value indicates negative change, and a maximum value indicates a positive change.

2.3.3. Walker's test

Field significance was evaluated to assess if the results in each region were globally significant. Walker's test considers the magnitude of the *p* value of each of the *K* individual (local) trend tests to determine if the global null hypothesis – that *all K* local null hypotheses are true – can be rejected at a global significance level.

If all the *K* of the local null hypotheses were true, then each of the respective test statistics represent random draws from their null distributions, whatever those distributions may be. If those local null distributions are continuous, and if the results of the local tests are independent of each other, the resulting *K p* values will be a random

sample from the uniform distribution, $f(u) = 1, 0 \leq u \leq 1$. If some of the local null hypotheses were false, their p values tend to be smaller than would be expected from this uniform distribution.

Let $p_{(1)}$ be the smallest of the K local p values. The probability distribution for the sampling distribution for the smallest p value from K independent tests, all of whose null hypotheses are true, is given by:

$$f[p_{(1)}] = \frac{\Gamma(K+1)}{\Gamma(1)\Gamma(K)} p_{(1)}^{0}[1 - p_{(1)}]^{K-1}, 0 \leq p_{(1)} \leq 1, \quad (2.26a)$$

$$f[p_{(1)}] = K[1 - p_{(1)}]^{K-1} \quad (2.26b)$$

For field significance to be present, $p_{(1)}$ must be no larger than some critical value p_{Walker}, corresponding to the global test level α_{global}. That is, if the smallest p value is small enough, it can be concluded with high confidence that the collection of K local p values did not result from independent draws from a uniform distribution. The critical value for this global test can be obtained by:

$$\alpha_{global} = K \int_{0}^{pWalker} [1 - p_{(1)}]^{K-1} dp_{(1)} \quad (2.27a)$$

$$= 1 - (1 - p_{Walker})^{K}, \quad (2.27b)$$

Thus,

$$p_{Walker} = 1 - (1 - \alpha_{global})^{1/K} . \quad (2.28)$$

This indicates that a global null hypothesis may be rejected at the α_{global} level if the smallest of K independent local p values is less than or equal to p_{Walker}.

Using the above described statistical tests, changes (gradual and abrupt) were evaluated for the water-year, autumn, winter, spring, and summer at a 90% confidence level ($p \leq 0.10$) for 240 unimpaired streamflow stations in the continental United States. All the computations were performed using Matlab 2013a version.

2.4. Results

Trend and step changes were evaluated for the streamflow stations with and without considering the effect of lag-1 autocorrelation and LTP for water-year and four seasons at a significance level of $p \leq 0.10$, as shown in Figures. 2.2 through 2.7. In these figures, the upward-pointing blue triangles represent a significant increasing trend or step change, and the downward-pointing red triangles represent a significant decreasing trend or step change for the various streamflow stations. In Figures. 2.2 and 2.4, the magnitude of the trend, computed using Sen's slope and shown in color on the maps, represents the change in the runoff volume in million cubic meters, (MCM)/ year. In Figures. 2.4 and 2.5, the lag-1 autocorrelation is shown by blue circles, LTP by red pentagons, and green squares represent stations with both Lag-1 autocorrelation and LTP. In Figure. 2.6, triangles in yellow, green, and pink show the step changes coinciding with the PDO, El Niño, or La Niña years, respectively. In Figures. 2.6 and 2.7, regions with a beige shade imply field-significant regions having a step change.

In Figures. 2.8 and 2.9, the bar graphs depict the number of stations showing shifts. An upward direction indicates increasing shifts, and a downward direction indicates decreasing shifts.

2.4.1. Trends under MK1 Test

Long-term trends in the water-year, autumn, winter, spring, and summer for the 18 regions at $p \leq 0.10$ are shown in Figures. 2.2 and 2.3. The spatial distribution of trends under MK1 tests in the water-year suggests the monthly mean streamflow has increased in most of the central east and northeast part of U.S. and decreased in the northwest part and as the southeast (Figure 2.2a). The magnitude of the trend, as expressed by Sen's

slope, shows a maximum of a 9.9 MCM/yr increase and a 1.2 MCM/yr decrease in the streamflow volumes over a 60-year period (Figure. 2.2). All 240 streamflow stations showed

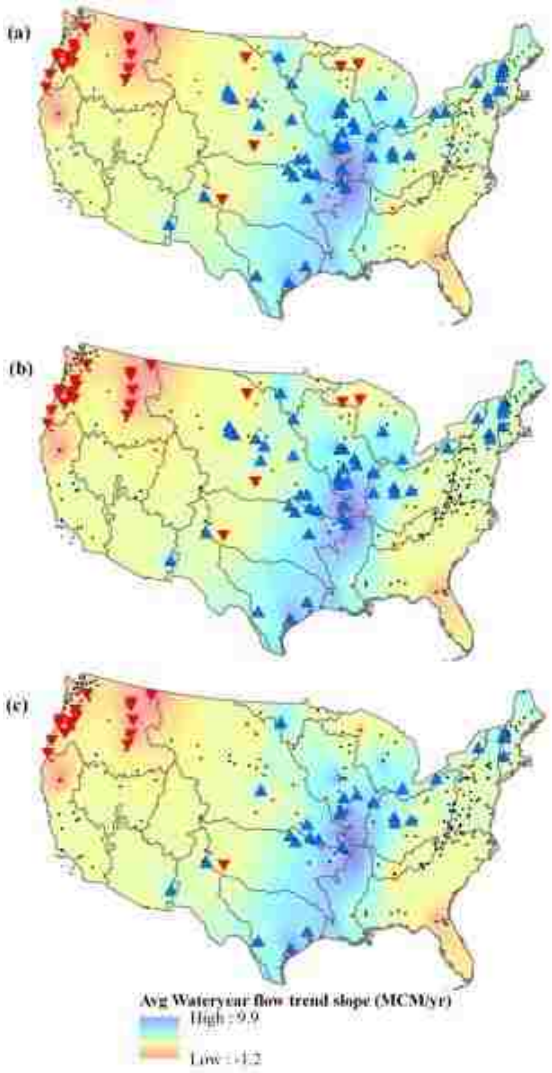

Figure 2.2: Map showing water-year trends using (a) MK1, (b) MK2, and (c) MK3 tests at p≤ 0.10. Upward-pointing triangles indicate significant increasing trends, and downward pointing triangles indicate significant decreasing trends. Dots indicate stations with no trends. The trend slope shows the magnitude of the change in MCM/year.

trend tendencies; however, in the water-year, only 50 stations had increasing trends that were statistically significant and 23 stations had decreasing trends that were statistically

significant (Table 2.1). Regions that showed significant increasing trends in the water-year were the Great Lakes (4), Ohio (5), Upper Mississippi (7), Souris-Red-Rainy (9), Missouri (10), Texas-Gulf (12), and Rio Grande (13).

During autumn (Figure 2.3a), the spatial distribution of trends showed a slight variation from the water-year trends. New England (1), Lower Mississippi (8), and Lower Colorado (15) showed an increase in the number of stations having significantly increasing trends, compared to the water-year, and were field-significant (Figure 2.3a). Trends in Ohio (5) were not field-significant in autumn, and the number of stations showing significant decreasing trends in Pacific Northwest (17) decreased. Other regions had trends similar to the water-year. A total of 236 stations showed trend tendencies, out of which 57 stations had significantly increasing trends and 10 stations had significantly decreasing trends (Table 2.1). The maximum increase in autumn streamflows was 10.9 MCM/yr, and the maximum decrease was 21.2 MCM/yr (Figure 2.3). Overall, there was an increase in the percentage of increasing trends compared to decreasing trends over continental United States.

The winter season trends (Figure 2.3a) showed decreasing streamflow trends in Ohio and Tennessee and more stations with significant increasing trends in New England (1), the Great Lakes (4), Arkansas-White Red (11), the Great Basin (16), and California (18). Trends in Arkansas-White Red were field-significant as compared to the water-year and autumn. However, in Ohio (5), the Lower Mississippi (8), and the Lower Colorado (15), trends were not field-significant. As shown in Table 2.1, 239 stations showed trend tendencies, out of which 52 stations had significantly increasing trends and 12 stations

had significantly decreasing trends. The maximum increase in winter flows was 14.8 MCM/yr and the maximum decrease was 34.1 MCM/yr (Figure 2.3).

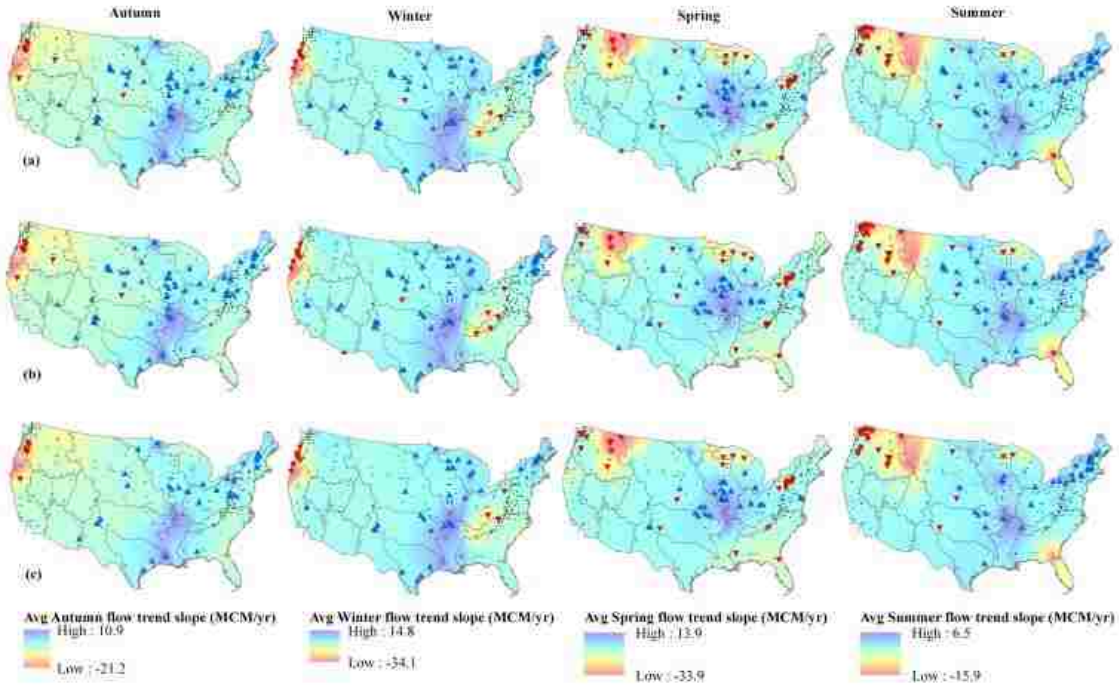

Figure 2.3: Map showing seasonal trends using (a) MK1, (b) MK2, and (c) MK3 tests. Results are reported for autumn, winter, spring, and summer at $p \leq 0.10$. Upward-pointing triangles indicate significant increasing trends, and downward-pointing triangles indicate significant decreasing trends. Dots indicate stations with no trends. The trend slope shows the magnitude of the change in MCM/year in each season.

The spring season had more stations with decreasing trends compared to the water-year, autumn, and the winter seasons (Figure 2.3a). Mostly, the trends were limited to areas of the Midwest, South-Atlantic-Gulf (3), and Pacific Northwest (17) regions. New England (1), Mid-Atlantic (2), Great Lakes (4), Arkansas–White-Red (11), and Texas-Gulf (12) had reductions in the number of stations with increasing trends, compared to autumn and winter (Table 2.1). Stations in the Mid Atlantic (2), South Atlantic-Gulf (3), and Ohio (5) showed significant decreasing trends as compared to autumn and winter seasons. Taken as a whole, in the spring, 239 stations showed trend

tendencies, out of which 35 stations had significantly increasing trends and 30 stations had significantly decreasing trends (Table 2.1). The maximum increase in spring flows was 13.9 MCM/yr and the maximum decrease was 33.9 MCM/yr (Figure 2.3).

The summer season had regions with increasing trends as well as decreasing trends (Figure 2.3a). The regions of New England (1), Mid-Atlantic (2), Great Lakes (4), and Tennessee (6) had significant increasing trends as compared to other seasons. Pacific Northwest (17) had an increase in stations showing decreasing trends compared to other seasons (Table 2.1). On the whole, 237 stations showed trend tendencies, out of which 43 stations had significantly increasing trends and 28 stations had significantly decreasing trends (Table 2.1) during the summer. The maximum increase in summer flows was 6.5 MCM/yr and the maximum decrease was 15.9 MCM/yr.

2.4.2. The Effect of Short-Term and Long-Term Persistence

The stations whose coefficient values for lag-1 autocorrelation were not in the range of $-0.23 \leq r\_1 \leq 0.198$ were significantly correlated at $p \leq 0.10$. Likewise, stations with H values that were not in the range of $0.50 \leq H \leq 0.58$ were significantly correlated at $p \leq 0.10$. Figure 2.4 and 2.5 show the spatial distribution of stations with lag-1 autocorrelation and LTP in the water-year, autumn, winter, spring, and summer seasons. In the Midwest and eastern United States, the water-year (Figure 2.4) had more stations with significant correlation for lag-1 autocorrelation and LTP. New England (1), Great Lakes (4), and Ohio (5) had more stations with lag-1 autocorrelation than LTP during the water-year.

Table 2.1. Results of the Three Mann Kendall (MK) Tests Reported at the Station Level for Each Hydrologic Region for the Water-Year, Autumn, Winter, Spring, and Summer

Hydrologic Region No.	Hydrologic Region Name	Number of Unimpaired Stations	Number of Stations with Trends															
			Water Year			Autumn			Winter			Spring			Summer		
			MK1 +/-	MK2 +/-	MK3 +/-	MK1 +/-	MK2 +/-	MK3 +/-	MK1 +/-	MK2 +/-	MK3 +/-	MK1 +/-	MK 2+/-	MK3 +/-	MK1 +/-	MK2 +/-	MK3 +/-
1	New England	18	4/0	4/0	3/0	**5/0**	**5/0**	**5/0**	**9/0**	**9/0**	**4/0**	0/0	0/0	0/0	**10/0**	**10/0**	**9/0**
2	Mid-Atlantic	39	3/0	2/0	0/0	5/0	5/0	2/0	1/0	1/0	0/0	2/7	2/7	2/7	6/0	6/0	6/0
3	South Atlantic-Gulf	21	0/0	0/0	0/0	1/0	1/0	1/0	0/0	0/0	0/0	0/2	0/3	0/2	1/1	1/1	0/0
4	Great Lakes	10	**4/2**	**3/2**	**3/0**	**3/0**	**3/0**	**2/0**	**7/0**	**7/0**	**7/0**	**2/3**	**2/4**	**2/3**	**5/2**	5/2	**4/2**
5	Ohio	21	**5/0**	**5/0**	3/0	6/0	6/0	6/0	0/2	0/2	0/2	5/1	5/1	4/1	2/0	2/0	2/0
6	Tennessee	8	0/0	0/0	0/0	0/0	**0/0**	0	0/2	**0/3**	0/1	0/2	0/2	0/1	**1/0**	**1/0**	**1/0**
7	Upper Mississippi	19	**13/0**	**12/0**	**5/0**	**12/0**	**13/0**	4/0	**5/0**	**5/0**	**4/0**	12/1	11/1	10/1	5/0	**6/0**	2/0
8	Lower Mississippi	2	0/0	0/0	0/0	**1/0**	**1/0**	**1/0**	0/0	0/0	0/0	0/0	0/0	0/0	0/0	0/0	0/0
9	Souris-Red-Rainy	3	**1/0**	**1/0**	1/0	**2/0**	**2/0**	2/0	**2/0**	**2/0**	**2/0**	**1/0**	**1/0**	0/0	**1/0**	**1/0**	0/0
10	Missouri	22	**10/2**	**11/2**	4/0	**8/1**	**7/1**	2/0	**7/1**	**7/1**	1/0	**8/2**	**8/2**	**5/1**	**6/2**	**7/2**	2/2
11	Arkansas-White-Red	11	5/1	5/1	3/1	6/0	6/0	1/0	**8/0**	**8/0**	**8/0**	**2/1**	**2/1**	**2/1**	**5/1**	**6/1**	**4/1**
12	Texas-Gulf	5	**3/0**	**3/0**	**3/0**	**3/0**	**3/0**	**2/0**	**5/0**	**5/0**	**4/0**	0/0	**0/0**	0/0	**1/0**	**1/0**	**1/0**
13	Rio Grande	3	**1/0**	**1/0**	**1/0**	**3/0**	**3/0**	**2/0**	**3/0**	**3/0**	**2/0**	2/0	2/0	2/0	0/0	0/0	0/0
14	Upper Colorado	-	-	-	-	-	-	-	-	-	-	-	-	-	-	-	-
15	Lower Colorado	2	1/0	1/0	1/0	**1/0**	**1/0**	**1/0**	1/0	1/0	0/0	**1/0**	**1/0**	0/0	0/0	0/0	0/0
16	Great Basin	5	0/0	0/0	0/0	1/0	1/0	0	**2/0**	**2/0**	0/0	0/0	0/0	0/0	0/0	0/0	0/0
17	Pacific Northwest	37	0/17	0/17	0/16	0/7	0/7	0/6	0/6	0/6	0/6	0/11	0/11	0/11	**0/22**	**0/22**	**0/19**
18	California	14	0/1	0/1	0/1	0/2	0/2	0/1	2/1	2/1	1/1	0/0	0/0	0/0	0/0	0/0	0/0
	Total	240	50/23	48/23	27/18	57/10	57/10	31/7	52/12	52/13	33/10	35/30	34/32	27/28	43/28	46/28	31/24

MK1, MK2, MK3: Corresponding MK test.
+ : Total number of stations showing increasing trends .
- : Total number of stations showing decreasing trends.
Entries in bold indicate results that are field significant at $p \leq 0.10$.

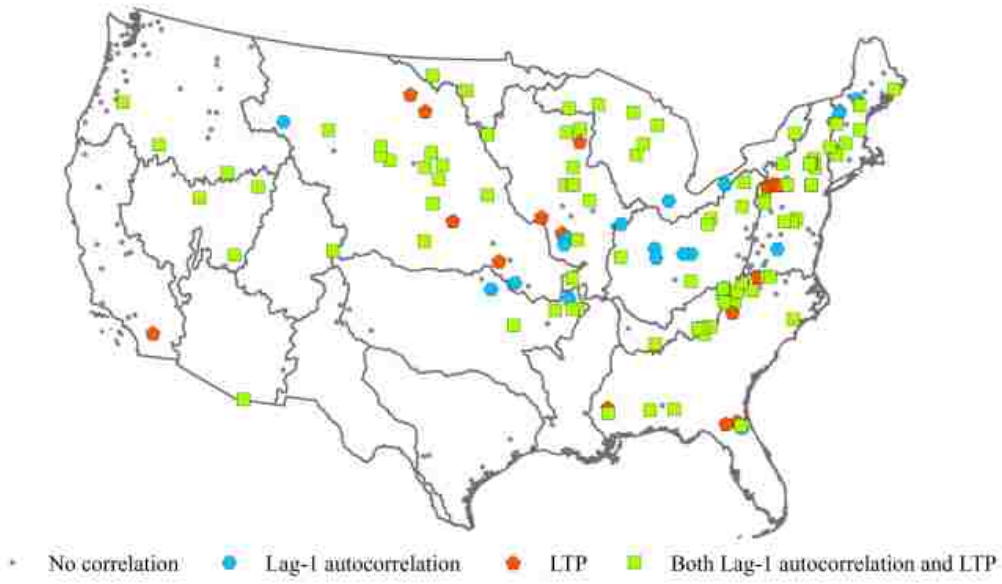

Figure 2.4: Map showing the spatial distribution of persistence in the water-years at $p \leq 0.10$.

Table 2.2 summarizes the results of lag-1 autocorrelation and LTP. In the water-year, 106 stations showed lag-1 autocorrelation and 106 showed LTP at $p \leq 0.10$. A total of 89 stations showed both lag-1 autocorrelation and LTP. The Mid Atlantic (2), South-Atlantic Gulf (3), and Missouri (10) showed a higher number of stations with LTP than with lag-1 autocorrelation. Seasonally, autumn had the highest persistence compared to the remaining three seasons, with 50 stations showing lag-1 autocorrelation and 73 stations showing LTP. However, New England (1) had higher persistence in winter and summer seasons, Mid-Atlantic (2) had higher persistence in summer seasons, and South Atlantic-Gulf had the least persistence in autumn compared to other seasons. The Great Lakes (4) had the highest persistence in summer, Ohio (5) had the highest persistence in spring, and Tennessee (6) had the highest persistence in winter.

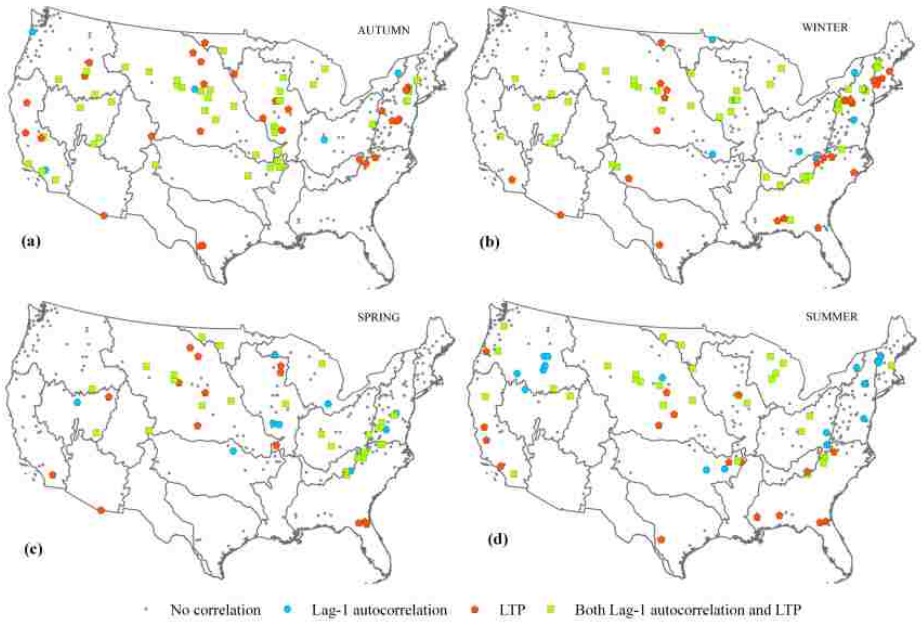

Figure 2.5: Map showing the spatial distribution of persistence in a) autumn, b) winter, c) spring, and d) summer at $p \leq 0.10$.

The stations with significant correlation at p≤ 0.10 in lag-1 autocorrelation and LTP were tested for trends (Table 2.2). In the water-year, out of the 106 stations with significant lag-1 autocorrelation, 38 stations showed trends under the MK2 test. Out of 106 stations showing significant LTP, three stations had significant trends under the MK3 test. In autumn, out of the 50 stations with significant lag-1 autocorrelation, 26 stations showed trends; out of the 75 stations with significant LTP, three stations showed trends under the MK3 test. Similarly, in winter, out of 49 stations with lag-1 autocorrelation, 21 showed trends; out of 69 stations with LTP, three stations showed trends. In spring, out of the 35 stations with significant lag-1 autocorrelation, 15 stations showed trends; out of the 40 stations with significant LTP, only two stations showed trends under the MK3 test. In summer, out of 46 stations with significant lag-1 autocorrelation, 25 stations showed trends in the MK2 test; out of 46 stations showing LTP, only two stations showed trends under the MK3 test.

Table 2.2. Summary of Stations with lag-1 Autocorrelation and Long-Term Persistence (LTP) and Stations that Showed Trends under the MK2 and MK3 Tests in 18 regions for the Water-Year, Autumn, Winter, Spring, and Summer at $p \leq 0.10$

Hydrologic Region No	Hydrologic Region Name	Water-year		Autumn		Winter		Spring		Summer	
		lag-1/ Trend	LTP/ Trend	lag-1 /Trend	LTP/ Trend	lag-1/ Trend	LTP/ Trend	lag-1/ Trend	LTP/ Trend	lag-1/ Trend	LTP/ Trend
1	New England	8/2	6/0	0/0	0/0	2/2	6/0	0/0	0/0	3/3	1/0
2	Mid-Atlantic	15/2	18/0	4/2	12/0	7/0	13/0	5/0	3/0	3/1	0/0
3	South Atlantic-Gulf	11/0	15/0	0/0	2/0	3/0	8/0	4/1	7/0	3/0	8/0
4	Great Lakes	10/5	8/1	3/2	2/0	4/2	3/1	3/3	1/0	5/2	4/0
5	Ohio	13/5	9/0	2/1	1/0	1/1	1/0	5/1	5/0	4/0	2/0
6	Tennessee	7/0	7/0	0/0	1/0	6/3	6/0	3/2	2/0	0/0	1/0
7	Upper Mississippi	13/9	13/0	8/6	13/0	7/1	6/0	3/2	4/0	3/3	4/0
8	Lower Mississippi	0/0	0/0	0/0	0/0	0/0	0/0	0/0	0/0	0/0	0/0
9	Souris-Red-Rainy	2/1	2/1	1/1	2/1	1/1	1/0	2/1	2/0	2/1	2/0
10	Missouri	13/9	15/1	13/7	16/2	9/6	12/1	5/4	10/2	8/6	10/2
11	Arkansas-White-Red	7/4	5/0	5/4	6/0	1/1	2/1	2/1	1/0	3/2	3/0
12	Texas-Gulf	0/0	0/0	0/0	2/0	0/0	1/0	0/0	0/0	0/0	1/0
13	Rio Grande	0/0	0/0	1/1	1/0	1/1	1/0	0/0	0/0	0/0	0/0
14	Upper Colorado	-	-	-	-	-	-	-	-	-	-
15	Lower Colorado	1/0	1/0	0/0	1/0	0/0	1/0	0/0	1/0	0/0	0/0
16	Great Basin	3/0	3/0	4/1	4/0	4/2	4/0	2/0	2/0	2/0	1/0
17	Pacific Northwest	3/1	3/0	4/1	5/0	2/0	2/0	1/0	1/0	8/7	4/0
18	California	0/0	1/0	5/0	7/0	1/1	2/0	0/0	1/0	2/0	5/0
	Total	106/38	106/3	50/26	75/3	49/21	69/3	35/15	40/2	46/25	46/2

2.4.3. Comparison of MK1 with MK2 and MK3 Tests

Table 2.1 summarizes the MK1, MK2 and MK3 test results. Figure 2.2 and 2.3 give the spatial distribution of trends for the hydrologic regions for the water-year, autumn, winter, spring, and summer for the three MK tests. The MK2 test results are similar to MK1 test results for the water-year and the four seasons.

There was a reduction in stations having significant trends under MK3 tests in the Mid-Atlantic (2), Ohio (5), Upper Mississippi (7), and Missouri (10) in the water-year (Table 2.2, Figure 2.2). The MK3 results showed a greater number of stations with trends in the spring and summer, compared to fall and winter. In total:27 stations showed significantly increasing trends and 18 stations showed significantly decreasing trends in

the water-year (Table 2.1); 31 stations showed significantly increasing trends and 7 stations showed significantly decreasing trends in autumn; 33 stations showed significantly increasing trends and 10 stations showed significantly decreasing trends in winter. In spring, 27 stations showed significantly increasing trends and 28 stations showed significantly decreasing trends. In summer, 31 stations showed significantly increasing trends and 24 stations showed significantly decreasing trends under the MK3 test (Table 2.1).

2.4.4. Change Point Test

Significant change points or shifts in the water-year, autumn, winter, spring, and summer in the various hydrologic regions are summarized in Table 2.3. Figure 2.6 and 2.7 show the spatial profile of step changes in the water-years and the four seasons for PDO warm, PDO cold, and ENSO years (i.e. El Niño and La Niña).

In the water-year, the Great Lakes (4), Upper Mississippi (7), Lower Mississippi (8), Souris-Red-Rainy (9), Texas-Gulf (12) and Rio Grande (13) showed significant step changes in more than 60% of the stations (Figure 2.6a, Table 2.3). Increasing shifts were seen in New England (1), the Mid-Atlantic (2), the South Atlantic-Gulf (3), Great Lakes (4), Ohio (5), Upper Mississippi (7), Lower Mississippi (8), Souris-Red-Rainy (9), Missouri (10), Arkansas-White-Red (11), the Texas-Gulf (12), Rio Grande (13), and Lower Colorado (15). Decreasing shifts were seen in the Great Lakes (4), Missouri (10), Arkansas-White-Red (11), the Great Basin (16), and the Pacific Northwest (17). However, Lower Mississippi (8), Souris-Red-Rainy (9), Missouri (10), Arkansas-White-Red (11), Texas-Gulf (12), Rio Grande (13), and Lower Colorado (15) had field significant shifts in the water-year.

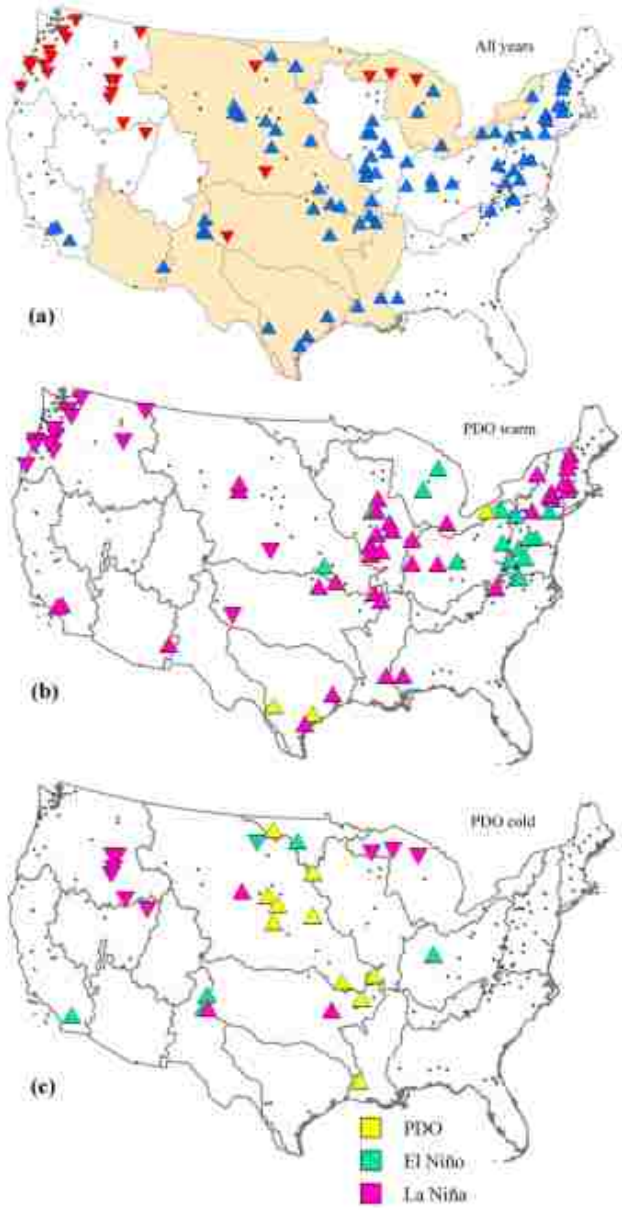

Figure 2.6: Map showing stations with shifts in the a) water-year, b) PDO warm years and c) PDO cold years at $p \leq 0.10$. Upward-pointing blue triangles represent an increasing step change, and downward-pointing red triangles represent a decreasing step change for the various streamflow stations. Triangles in yellow, green, and pink show the step changes coinciding with the PDO, El Niño, or La Niña years, respectively. The regions with color show field significance.

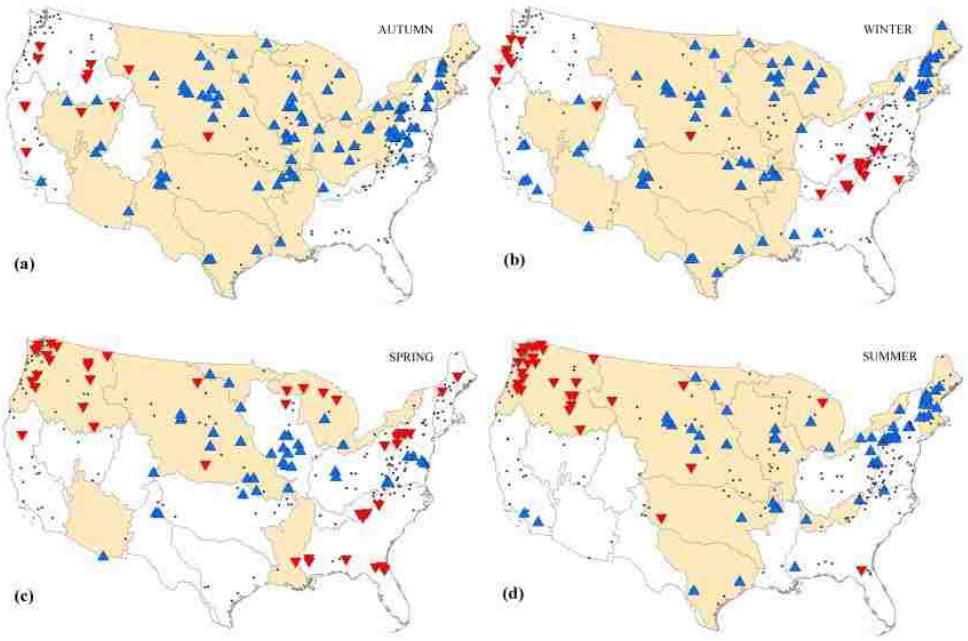

Figure 2.7: Map showing stations having shifts in the a) autumn, b) winter, c) spring, and d) summer at $p \leq 0.10$. Upward-pointing blue triangles represent an increasing step change, and downward-pointing red triangles represent a decreasing step change for the various streamflow stations. The regions with color show field significance.

Figure 2.6 (b-c) shows the occurrence of abrupt shifts in relation to inter-annual (ENSO) and multi-decadal (PDO) climate patterns. The results indicate that the decreasing streamflow shift years in the Pacific Northwest (17) region coincided with the La Niña years during PDO phases (both warm and cold). The years in which increasing streamflow shift occurred in the Upper Mississippi (7) and New England (1) regions coincided with La Niña years, and increasing streamflow shift for the Mid-Atlantic (2) region coincided with El Niño years during the PDO warm phase. Streamflow shifts years (increase or decrease) in the Great Lakes (3) region coincided with both PDO and ENSO phases. In contrast, the majority of stations in the Missouri (10) region had increasing streamflow shifts that were not related to an ENSO phase change, and only

coincided with the PDO cold phase. Additionally, stations in other hydrologic regions had shifts that coincided with both ENSO and PDO phases simultaneously.

Table 2.3. Results of the Pettitt Test, Reporting a Shift for the Water-Year, Autumn, Winter, Spring, and Summer at $p \leq 0.10$

Hydrologic Region No	Hydrologic Region Name	Stations showing shifts				
		Water-Year	Autumn	Winter	Spring	Summer
		+/-	+/-	+/-	+/-	+/-
1	New England	5/0	**4/0**	**12/0**	0/2	**10/0**
2	Mid-Atlantic	12/0	15/0	4/2	6/7	12/0
3	South Atlantic-Gulf	3/0	1/0	2/3	0/9	2/1
4	Great Lakes	**5/3**	**5/0**	**7/0**	**2/4**	**5/1**
5	Ohio	7/0	**11/0**	0/3	2/1	4/0
6	Tennessee	0/0	1/0	0/6	0/3	**2/0**
7	Upper Mississippi	13/0	**15/0**	**6/0**	12/1	**5/0**
8	Lower Mississippi	**2/0**	**1/0**	**1/0**	**0/1**	0/0
9	Souris-Red-Rainy	**2/0**	**2/0**	**3/0**	**2/0**	**2/0**
10	Missouri	**10/2**	**13/2**	**11/1**	**8/2**	**7/3**
11	Arkansas-White-Red	**5/1**	**8/0**	**8/0**	2/0	**4/1**
12	Texas-Gulf	**4/0**	**3/0**	**4/0**	0/0	**2/0**
13	Rio Grande	**3/0**	**3/0**	**3/0**	2/0	0/0
14	Upper Colorado	-	-	-	-	-
15	Lower Colorado	**1/0**	**1/0**	**1/0**	**1/0**	0/0
16	Great Basin	0/1	**3/2**	**2/1**	0/0	0/0
17	Pacific Northwest	0/19	1/5	1/7	**0/18**	**0/26**
18	California	3/0	1/3	5/1	0/1	2/0
	Total	75/26	88/12	70/24	37/49	57/32

+ : Number of stations showing increasing shifts.
- : Number of stations showing decreasing shifts.
Entries in bold indicate results that are field significant at $p \leq 0.10$.

In autumn, a greater number of stations had significant shifts than during the water-year or other seasons (Table 2.3). The Great Lakes (4), Souris-Red-Rainy (9), and Missouri (10) had field significant shifts in all the seasons; on the other hand, New England (1), Upper Mississippi (7), Arkansas-White-Red (11), and Texas-Gulf (12) had field-significant shifts in all seasons except spring. Ohio (5) had field significance in

autumn, Tennessee (6) had field-significant shifts in winter, and the Lower Mississippi (8) and Lower Colorado (15) had field significant shifts in all seasons except winter. The Rio Grande (13) and Great Basin (16) had field-significant shifts in autumn and winter, and the Pacific Northwest (17) had field significant shifts in spring and summer.

Figure 2.8 and 2.9 show the different periods in which stations had shifts, beginning from 1950 to 2010 for the water-year, autumn, winter, spring, and summer. The shifts start after 1963, and show increasing and decreasing phases that continued

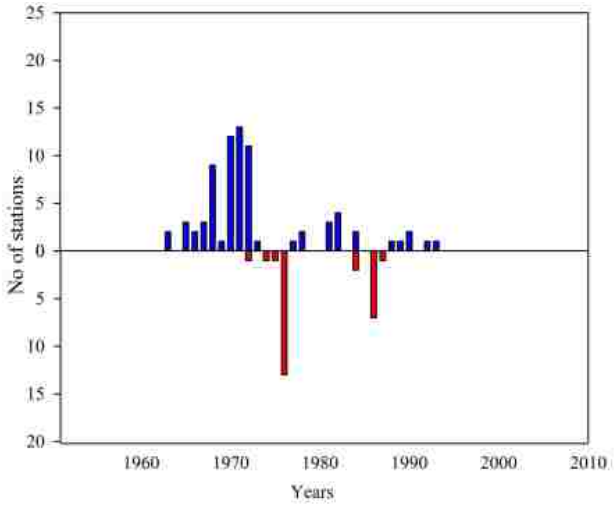

Figure 2.8: Increasing and decreasing shifts at $p \leq 0.10$ over a 60-year period during the water-year. The upward-pointing blue bars show increasing shifts, and downward-pointing red bars show decreasing shifts

until 2002. A total of 101 stations showed shifts in the water-year at $p \leq 0.10$, out of which 75 were increasing and 26 decreasing. Water-years from 1963 to 1973 mostly had increasing shifts in 57 stations, with the period from 1970 to1972 having 36 stations with increasing shifts (Figure 2.8). The period from 1974 to 1976 showed decreasing shifts in 15 stations; out of which 13 were in the water-year 1976. The period from 1977 to 1978 showed increasing shifts in 3 stations, and the period from 1981 to 1984 showed increasing shifts in 9 stations and decreasing shifts in 2 stations. The period from 1986 to

1987 showed decreasing shifts in 8 stations, and the period from 1988 to1993 showed increasing shifts in 6 stations.

Autumn had a total of 100 stations that showed shifts at $p \leq 0.10$, out of which 88 were increasing and 12 decreasing. Shifts in autumn started earlier than the water-year (Figure 2.9a). One station in the Texas-Gulf showed increasing shifts starting early in 1957. The period from 1963 to 1974 showed increasing shifts in 61 stations. Two stations had decreasing shifts from 1974 to 1976. The period from 1977 to 1985 showed 16 stations with increasing shifts, and the period from 1985 to 1987 showed 10 stations with decreasing shifts. The period from 1991 to 1993 showed 6 stations with increasing shifts, and 2002 showed 4 stations with increasing shifts.

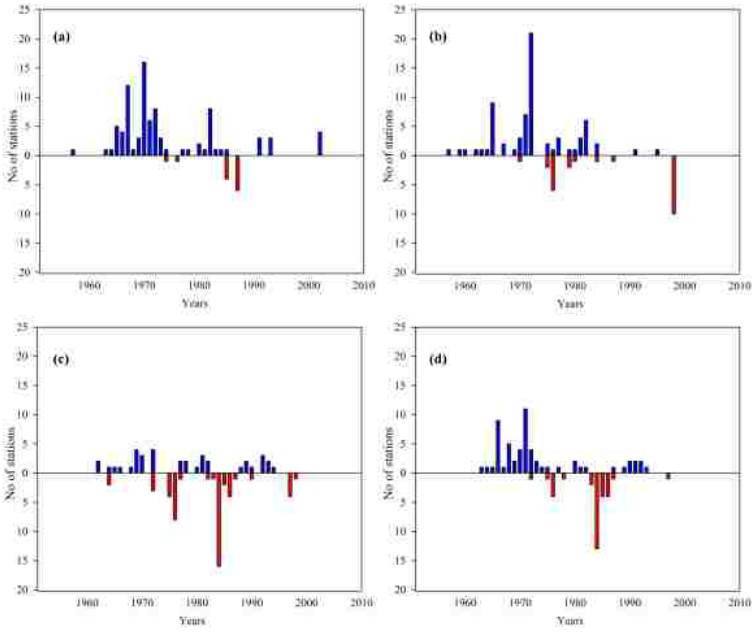

Figure 2.9: Increasing and decreasing shifts at $p \leq 0.10$ over a 60-year period in a) autumn, b) winter, c) spring, and d) summer. Upward-pointing blue bars show increasing shifts, and downward-pointing red bars show decreasing shifts.

Winter had a total of 94 stations that showed shifts at $p \leq 0.10$, out of which 70 were increasing and 24 decreasing. Shifts in winter started in 1957 (Figure 2.9b). One station showed increasing shifts starting early in the 1957, and 2 stations showed increasing shifts from 1959 to 1960. The period from 1962 to 1972 showed increasing shifts in 46 stations, and 1 station had a decreasing shift in 1970. The period from 1975 to 1977 showed 6 stations with increasing shifts, and the period from 1975 to 1976 showed 8 stations with decreasing shifts. The period from 1979 to 1982 showed 11 stations with increasing shifts, and 1998 showed 10 stations with decreasing shifts

Spring had a total of 86 stations with shifts at $p \leq 0.10$, out of which 37 stations had increasing shifts and 49 stations had decreasing shifts. The period from 1964 to 1972 had 15 stations with increasing shifts (Figure 2.9c). The period from 1975 to 1977 had 13 stations with decreasing shifts, and the period from 1977 to 1982 had increasing shifts in 10 stations. The period from 1988 to1987 had decreasing shifts in 25 stations; the period from 1988 to1994 had increasing shifts in 10 stations; and a later period, 1997 to 1998, had decreasing shifts in 5 stations.

Summer had a total of 89 stations with shifts at $p \leq 0.10$, out of which 57 stations had increasing shifts and 32 stations had decreasing shifts. The period from 1963 to 1975 had 43 stations with increasing shifts (Figure 2.9d). The period from 1975 to 1976 had 5 stations with decreasing shifts, and the period from 1980 to 1982 had increasing shifts in 4 stations. The period from 1983 to1987 had decreasing shifts in 24 stations; the period from 1989 to 1993 had increasing shifts in 8 stations.

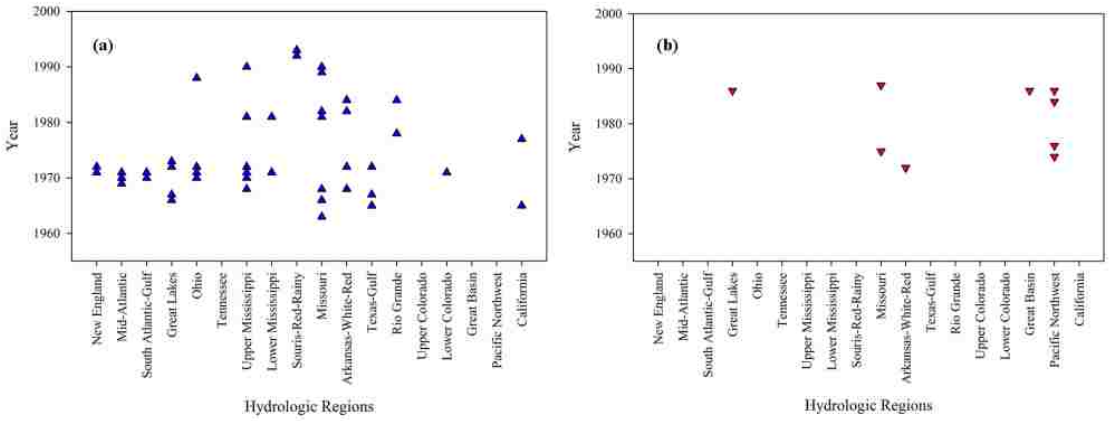

Figure 2.10: Periods showing several hydrologic regions with a) increasing and b) decreasing shifts in the water-year.

Figures 2.10a and 2.10b show time periods in which several hydrologic regions showed both increasing and decreasing shifts. The period from 1970 to 1973 showed increasing shifts in most of the Midwest regions. The Upper Mississippi (7), Missouri (10), and Arkansas-White-Red (11) showed a greater number of distributed shift periods, indicating a higher association to natural changes and climate variability than for other regions. Souris-Red-Rainy (9) shows increasing shifts only after 1990. Missouri (10) and Pacific Northwest (17) showed a high number of stations with decreasing shifts in the period from 1975 to 1977 and the period from 1984 to 1987.

2.5. Discussion

Based on the results, it is evident that significant long-term changes have occurred in the streamflow quantity across the United States. Analyses based on the water-year suggest that there is an observed increase in streamflow across most of the southern regions (Texas-Gulf and Arkansas-White-Red) and eastern regions (Upper Mississippi, Missouri, Ohio, New England), and significant decreases in the Pacific Northwest region. These observations are consistent with those from previous studies (Lins and Slack,

1999; Kalra et al., 2008). In autumn and winter, approximately 80% of the statistically significant trends were increasing. Spring showed a mix of both increases and decreases; in summer, approximately 60% of the significant trends were increasing.

The higher number of stations with significant increasing trends occurred in autumn and winter in the Midwest region, which may be attributed to an increase in fall and winter precipitation (Groisman et al., 2001; Small et al., 2006; Martino et al., 2013). A similar percentage of spring and summer flow stations experienced trends; however, a greater number of stations showed decreasing trends compared to autumn and winter, which is in agreement with previous studies (Stewart et al., 2005; Miller and Piechota, 2008). The spring season showed the least increases in trends and the greatest decreases, indicating drier conditions.

The magnitude calculated from the Sen's slope revealed the effect of non-significant trends (Bawden et al., 2013). Regions with larger flow increases or decreases are observed where trends were not significant and vice versa (Figure 2.3). The slope for the seasonal streamflow trend showed that the decreases in volume were much higher than the increases; however, they varied spatially for all the seasons.

The regional assessments of trends indicated that, spatially, trends varied based on seasons, topography, climate, and other factors. Some areas are snow-dominant, while others are rainfall-dominant; this accounts for distinct variations in seasonal streamflow peaks. The Upper Mississippi (7) region had the highest percentage of stations with significant trends, approximately 84% of the stations in the MK1 test (Table 2.2). A concentration of increasing trends was found in the Midwest regions, and decreasing

trends in the Pacific Northwest (17) and South-Atlantic Gulf (3) (Table 2.2). Even after accounting for lag-1 autocorrelation and LTP, Souris-Red-Rainy (9) showed significant trends for MK2 and MK3 tests during the water-year as well as autumn and winter.

The quantitative and spatial distributions of the trends varied for the different seasons (Figure 2.2, Table 2.2). Spatially, the decreases in streamflows were prevalent in spring and summer, whereas higher decreases were observed along the Pacific Northwest coast (17) in autumn and winter. Increases in streamflow were prevalent in winter, with Sen's slope values of 14.8MCM/year, indicating an emerging winter season that is wetter except in the Pacific Northwest (17), South-Atlantic Gulf (3), southern parts of Missouri (10), and northern parts of Arkansas-White-Red (11). This suggests a fluctuation in peak streamflow timings, as evident in previous studies (Dettinger and Cayan, 1995; Groisman et al., 2001; Burn and Elnur, 2002; Hamlet et al., 2005; Regonda et al., 2005; Hamlet et al., 2007).

Statistically, correlations can conceal crucial information in sample data, which may lead to a more moderate hypothesis test. In other words, trend detection analysis may lead to misleading results when serial correlation, if it exists, is ignored (Khaliq et al. 2008). Moreover, some of the patterns observed in a hydrologic series could be explained better by accounting for long-term persistence (e.g., Koutsoyiannis, 2002, 2003, 2006; Koutsoyiannis and Montanari, 2007). The trend tests that do not consider LTP greatly overstate the statistical significance of the observed trends when LTP is present (Cohn and Lins, 2005). Khaliq et al. (2008) found that some evidence of LTP led to a reduction in the number of trends detected under a random data assumption. Similarly, in this current study, the number of stations with trends identified under independent postulation

was more than that accounted for after LTP; further, negligible departures were seen after TFPW (Figure 2.2, 2.3, Table 2.1). The persistence characteristic was more prevalent in the autumn and winter seasons than in spring and summer. The use of the three MK tests helped to differentiate the trends that existed under the assumption of serial independence.

Overall, taking into consideration only the lag-1 autocorrelation (for MK2) was not sufficient to remove all significant serial correlations in the data series. For example, the water-years in which the Missouri (10), Ohio (5), and Souris-Red-Rainy (9) showed field-significant increasing trends under MK1 and MK2 tests (Table 2.1) did not show field-significant trends under MK3 tests. In addition, the introduction of variations to the Mann-Kendall test helped in evaluating the persistence characteristics. Variations in correlations of different U.S. regions with climate indices (Tootle and Piechota, 2006) and the serial structure of the time series for PDO indices conforming to a stochastic process with LTP (Khaliq and Gachon, 2010) might explain the varying reduction in the number of stations due to TFPW and LTP.

The change point test indicated that more than 40% of the stations experienced an abrupt shift in water-year volumes. Most of those shifts were increasing, and were observed in more stations than for trends. For seasonal variation, the step change results agreed with trend results. Most of the increasing step changes were seen in autumn and winter; most of the decreasing step changes occurred in spring. The 1970s to the 1990s had the largest number of abrupt changes in the water-year data. The greatest number of increasing shifts occurred in 1972, whereas the majority of decreasing shifts occurred around 1986. Seasonally, a greater number of stations with significant increasing shifts

occurred in autumn and winter, with similar periods as the water-year; however, spring and summer had a higher number of significant decreasing shifts from 1983 to 1987.

The trend and shift results indicated increases in the streamflow volumes for most of the U.S. except for Tennessee (6) during the winter and the Pacific Northwest (17) and South-Atlantic Gulf (3) during spring. All the regions had a greater number of shifts than trends (Table 2.1, Table 2.3) In the past, responses of streamflow to distinct climate indices have been studied in various works, for example, Dettinger and Cayan (1995), McCabe and Dettinger (2002), Stewart et al. (2005), Hodgkins and Dudley (2006), Hamlet and Lettenmaier (2007), and others. The step changes could be associated with the phase changes in various climatic indices. For example, the majority of the water-year step changes (increases or decreases) coincided with the PDO (warm) years and ENSO phase changes (El Niño and La Niña).

It is well established that ENSO affects the atmospheric anomalies over the low- and mid-latitudes at both regional and global scales (Ropelewski and Halpert, 1986; Redmond and Koch, 1991; Kahya and Dracup, 1993). In the past, coupling of ENSO with PDO has served as an important indicator of climate variability. Hidalgo and Dracup (2003) identified significant correlations between warm season precipitation and El Niño in the Upper Colorado River Basin (UCRB) from June to November; they observed shifts in the mean of UCRB precipitation and streamflow coincident to shifts in PDO phases. Analysis of the influence of PDO and ENSO on precipitation and temperature by Hamlet and Lettenmaier (2007) showed increased flood risk in the transient basins along the coast of Washington, Oregon, and California. McCabe et al. (2007) indicated that decadal to multi-decadal variability in sea surface temperatures (SST) was associated with

fluctuations in streamflow for the UCRB. Praskievic and Chang (2009) studied winter precipitation intensity and ENSO/PDO variability in the Willamette Valley of Oregon; they found that the ENSO phase and precipitation intensity was negative in November and positive in April, and the relation between PDO and intensity was negative and strongest in January and March.

In addition to ENSO and PDO, such climate indices as the Atlantic Multi-decadal Oscillation, North Atlantic Oscillation, sea surface temperature, and geopotential height have been studied individually or in conjunction with ENSO or PDO; they have been shown to be hydrologically connected within the United States. Even so, the regional variation of shift periods is indicative of the spatial variation of the influence of climate indices. It is interesting to see that shifts in streamflow volume start early in some regions and late in others (Figure 2.10); this needs further study regarding the response of different regions to climate variability. The findings of the step change analysis in relation to climate indices were purely statistical and informative in nature. Analysis using large-scale climate models and evaluation of the individual and coupled effects of other teleconnections is recommended in order to draw definitive conclusions.

Villarini et al., (2009) showed that neglecting a change point could result in obtaining a significant trend even when no significant trend was detected before or after the change point. Previously, if a station had both a trend and a step change, then the change was attributed to the step change (McCabe and Wolock, 2002; Kalra et al., 2008; Ehsanzadeh et al., 2011), indicating that the former followed the latter and not vice versa. Analysis of the influence of abrupt shifts on gradual trends was not covered in this study; however, further research on this aspect should be done to assess the occurrences of

shifts, whether they follow a spatial pattern that coincides with the trends or are regionalized due to a changing climate. Although, the discussion of results may have been influenced due to the non-uniform distribution of stations – i.e., densely located stations in the western and eastern regions and a sparse distribution in the central regions of the U.S. – the overall temporal and spatial pattern of streamflow changes (trend and shift) still can be analyzed.

Identifying abrupt shifts is even more important from a climate-change perspective. Changes due to climate are assumed part of long-term periodicity, also known as multi-decadal variability. Often, gradual trends are attributed to global warming or interactions of the system, whereas shifts are attributed to periodic variability. The interpretation of a gradual trend is that the trend is likely to continue into the future; on the other hand, the interpretation of a step change is that the climate system has shifted to a new regime that will likely remain relatively constant until a new shift or step change occurs (McCabe and Wolock, 2002). Decadal scale fluctuations are crucial, due to their capacity to influence water supplies, biota, and such high-frequency events as floods and droughts (Hare and Mantua, 2000). According to Koutsoyiannis (2006), the length of the analysis period between a dependent variable and its predictor can influence understanding their relationship. The result of this statistical analysis can potentially vary with a change in the length of the time series considered. Knowledge of seasonal variations in streamflow are important from the perspective of regional water management (Ghumman et al., 2014) in order to regularize the flows and maintain adequate levels in reservoirs for dry and wet spells.

2.6. Conclusions

In this study, a comprehensive change analysis was performed on the streamflows across the continental U.S. for 240 stations for 60 years (1951-2010). Analysis was performed using non-parametric statistical tests, accounting for STP and LTP, for the water-year and the four seasons (autumn, winter, spring, and summer). The nature of the change varied from a monotonic gradual trend to an abrupt shift. Overall, the following conclusions can be drawn from the statistical analysis.

Most of the southern (Texas-Gulf and Arkansas-White-Red) and eastern U.S. (Upper Mississippi, Missouri, Ohio, New England) is becoming wetter; streamflow is decreasing during winter in Tennessee, and during spring in the southeastern U.S. In autumn and winter, approximately 80% of the statistically significant trends are increasing. Spring shows a mix of both increases and decreases, whereas summer shows that approximately 60% of the significant trends are increasing.

The three MK tests helped to differentiate the trends that existed under the assumption of serial independence. A larger number of stations with trends were identified under the independent postulation than those accounted for after LTP; and negligible departures were seen after TFPW.

From 1951 to 2010, analysis of seasonal streamflow showed that the decreases in volumes were much higher than the increases, but varied spatially for all seasons.

The change point test indicated more than 40% of the stations experienced an abrupt shift in the water-year streamflows, the majority of which were increasing in

nature. All hydrologic regions had a higher number of stations having shifts rather than trends; however, patterns for the water-year and seasonal shifts were similar to trends.

Increasing shifts occurred more around 1970 to 1973, and decreasing shifts occurred around 1976. The spatial variation of the shift periods could be indicative of the spatial variation of the influence of climate indices. Moreover, variations in seasonal shift periods were observed.

The spatial and temporal variability of persistence helps interpretation of understand the peculiarities in the nature of streams. The assessment of shifts on a regional basis shows recognizably distinct periods for increasing and decreasing shifts in various regions. The number of stations showing shifts at a particular time could be indicative of the severity of a particular climate event. The relationship of shifts with the climate indices phases shows a pronounced effect during coupled phases compared to their individual phase changes. The greater number of shifts compared to trends – as well as their spatial and seasonal variability – highlights the importance of local characteristics in influencing variability; this requires further investigation.

The spatial variability of trends and step changes indicate that adjacent basins behave similarly. Moreover, this variability provides an improved realization of the probable implications of climate variability on U.S. water resources. Unavailability of longer runoff records is one of the limitations in understanding relationships between long-term memory, short-term memory, and trends, which can be possibly addressed by considering reconstructed streamflows. The underlying physical dynamics that govern the relationship between climate signals and hydrology are not determined in this study, but

the results open a possible scope for further investigations that are regionally focused, as well as for attribution analysis of observed trends.

Appendix I.

Bias Correction

$$a_0 = \frac{1.0024n - 2.5681}{n + 18.6693}$$

$$a_1 = \frac{-2.2510n + 157.2075}{n + 9.2245}$$

$$a_2 = \frac{15.3402n - 188.6140}{n + 5.8917}$$

$$a_3 = \frac{-31.4258n + 549.8599}{n - 1.1040}$$

$$a_4 = \frac{20.7988n - 419.0402}{n - 1.9248}$$

CHAPTER 3: EVALUATING THE INFLUENCE OF SEA SURFACE TEMPERATURES AND GEOPOTENTIAL HEIGHT ON SEASONAL STREAMFLOWS OF THE CONTINENTAL UNITED STATES

Abstract

This study evaluates the influences of two indicators of climate variability – sea surface temperatures (SST) and 500-mbar geopotential height (Z_{500}) – on spring-summer streamflows of the continental United States. Singular Value Decomposition is used to evaluate the spatio-temporal association between the SST/$Z_{500,}$ and the continental U.S. streamflow. An approach using a one-to-four month lag of streamflow showed the dominant variability modes of winter and fall SST and Z_{500}. Regions of highly correlated SST and Z_{500} were identified that did not have the bias of conservative index regions. Better seasonal variability in streamflow was represented by Z_{500}, compared to SST. Interdecadal-temporal evaluation of the phases of the Pacific Decadal Oscillation and Atlantic Multidecadal Oscillation showed variations in SST regions influencing streamflows and 2) weakening of teleconnections. The El Niño Southern Oscillation region 3.4, 3 as well as regions in the central and north tropical Pacific Ocean had strong associations with U.S. streamflow.

3.1. Introduction

Changes in climate variability have led to an increasing interest in improving forecasting techniques for various components of the hydrologic cycle, especially streamflow. The Fifth Assessment Report of the Intergovernmental Panel on Climate Change (IPCC, 2014) focused on three major elements of climate change: physical aspects, impacts and adaptation, and mitigation of climate change. Understanding the

effects of climate variability on spatial and temporal characteristics of streamflow is of special interest for sustainable management of water resource (Venkatesan et al., 2011a; 2011b; Shrestha et al., 2011; 2012; Qaiser et al., 2011; 2013;Dawadi and Ahmad, 2012; 2013; Wu et al., 2013) Out of numerous available climate indicators, land surface, air temperature, sea-surface temperature(SST), sea level, specific humidity, snow cover, sea-ice extent, glacier mass, stratospheric temperatures and pressure, and precipitation commonly have been used to study changes in the hydrologic cycle.

Understanding the relationship between climate indices and streamflow is important to improve streamflow estimates (Kalra et al., 2013a) and forecast extreme events (Mosquera-Machado and Ahmad, 2007; Stephen et al., 2010; Forsee and Ahmad, 2011a; 2011b; Puri et al., 2011a; 2011b). The relationship between climate variability and streamflow is known to be highly complex and non-linear, in both time and space. Hydrologists and climatologists have used various climate indices and their teleconnections to study the impacts on precipitation and streamflow. In particular, studies have evaluated oceanic– atmospheric variability and hydrological response of the continental United States in terms of streamflow, precipitation, and snowpack (Cayan and Peterson, 1989; Cayan and Webb, 1992; Kahya and Dracup, 1993; Gershunov, 1998; Cayan et al., 1999; Enfield et al., 2001; McCabe and Dettinger, 2002; Rogers and Coleman, 2003; Tootle et al., 2005; Hunter et al., 2006; Kalra and Ahmad, 2012; Kalra et al., 2013b).

Variability studies of climate indices – including Pacific Decadal Oscillation (PDO), El Niño Southern Oscillation (ENSO), Atlantic Multi-decadal Oscillation (AMO), Pacific North American Index (PNA), North Atlantic Oscillation (NAO), Niño

Regions 3 and 3.4 SST Indices, Trans-Niño Index (TNI), and Palmer Drought Severity Indices as well as such hydrologic variables as temperature, precipitation, and streamflow – have shown significant correlations (Folland et al., 1986; Kahya and Dracup, 1993; Cayan, 1996; Piechota and Dracup, 1999; Dettinger et al., 2000b; Barlow et al., 2001; Hidalgo and Dracup, 2003; Tootle et al., 2005; Singhrattna et al., 2005; Hunter et al., 2006; Hamlet and Lettenmaier, 2007; Burn, 2008; Kalra and Ahmad, 2009; Kalra and Ahmad, 2011). The correlations have led to the use of climatic variables in predicting long lead-time streamflow (Tootle and Piechota 2004; Grantz et al., 2005; Pagano and Garen, 2006; Tootle et al., 2007; Soukup et al., 2009). Analysis of global patterns of climate trends show an evidence of warming climate (Dettinger et al., 2000a; Easterling et al., 2000; Milly et al., 2002; Milly et al., 2005; Adam et al., 2009), which is expected to continue in the future.

Spatial variation of teleconnections of hydrologic variables and climate indices is important for regional water management. Numerous studies have identified the correlation between oceanic indices and regional hydrology (Chiew et al., 1994; Dettinger et al., 2000b; Barlow et al., 2001; Neal et al., 2002; Uvo, 2003; Koczot and Dettinger, 2003; McCabe et al., 2004; Gobena and Gan, 2006; Chandimala and Zubair, 2007; Zhang et al., 2010; Kalra et al., 2013b). A consistent pattern has been observed during the phases of ENSO; that is, the El Niño phase has been linked with the Southwest U.S. getting wetter, whereas the Northwest gets drier, with opposite changes during the La Niña phase (Redmond and Koch, 1991; Kahya and Dracup, 1994; Livezey et al., 1997). Coastal central California experiences an escalation in the number of extreme streamflow days during El Niño, and streamflow responses to ENSO are amplified over

temperature and precipitation (Cayan et al., 1999). Significant correlations between warm-season precipitation and the El Niño index in the Upper Colorado River Basin and high-elevation areas with ENSO activity from June to November have been observed, along with shifts in mean precipitation and streamflow, coincident to shifts in PDO (Hidalgo and Dracup, 2003). Analysis on the influence of PDO and ENSO on climate variability by Hamlet and Lettenmaier (2007) showed increased flood risk in the transient basins along the coasts of Washington, Oregon, and California. Praskievic and Chang (2009) indicated that the ENSO phase and winter-precipitation intensity was negative in November and positive in April; the association of PDO and winter precipitation was negative and more profound in January and March in the Willamette Valley of Oregon.

Due to the proximity to the Pacific Ocean, the western part of North America is influenced the most by long-term and short-term fluctuations in the Pacific Ocean. Association of the phases of traditional climate indices, such as positive and negative PDO and AMO, have been associated with streamflow variations. Coupled effects among oceanic phenomena – for example, the AMO influencing the La Niña effects in the southeast U.S. and the NAO influencing the La Niña effects in the Midwest – have been accounted for by Tootle et al. (2005). In addition, phases of PDO and AMO are recognized to have significant and varied associations with the U.S. streamflows.

The Pacific Ocean SST, during the negative PDO phase, has been affiliated with the streamflows of the eastern and western United States. During the positive PDO phase, these SSTs have been associated with the streamflow in the regions of Upper Colorado and Mid Atlantic (Tootle and Piechota, 2006). Similarly, the SST of the Atlantic Ocean has been associated with the streamflow in the Mid-Atlantic and central U.S. regions

during the negative phase of AMO, and with the streamflow of the Upper Mississippi, northwest U.S., and peninsular Florida during the positive phase. Out of the available climate indices, SST has been used successfully for forecasting because it eliminates any bias towards a particular spatial index (Tootle and Piechota, 2006; Soukup et al., 2009). In addition to SST, different mechanisms at particular air-pressure zones can significantly influence the effects of oceanic-atmospheric climate variability.

Geopotential height (HGT) is defined as the height above mean sea level of a particular pressure level. Study of the 500-mbar geopotential height (Z_{500}) show the Z_{500} index values to be identified with significant climate variability (Blackmon, 1976; Blackmon et al., 1977). The Z_{500} has been found to be associated with precipitation over Greece (Xoplaki et al., 2000), Europe (Casty et al., 2007), eastern U.S., (Serreze et al., 1998), and southeast U.S. (Chen et al., 2014). When used as a predictor in streamflow forecasting models, the Z_{500} has shown a substantially improved skill (Grantz et al., 2005). The Z_{500} has mostly shown to improve the short-lead time (3 month) forecasts in comparison to SST (Soukup et al., 2009; Aziz et al., 2011).

Various studies have used Singular Valued Decomposition (SVD) to evaluate the relationships of SST and the Z_{500} with hydrological variability (Uvo et al., 1998; Enfield and Alfaro, 2000; Giannini et al., 2000; Wang and Ting, 2000; Rajagopalan et al., 2000; Rodriguez-Fonseca and de Castro, 2002; Martin et al., 2004; Shabbar and Skinner, 2004; Tootle and Piechota, 2006; Tootle et al., 2008; Aziz et al., 2010; Soukup et al., 2009; Aziz et al., 2011). While principal components analysis (PCA) is very common for this type of analysis, SVD has the advantage of being able to establish the similarities between two spatio-temporal fields by evaluating the cross-covariance matrix. In

contrast, PCA evaluates only one spatial–temporal field. Additionally, the use of SVD on gridded SST, Z_{500} and streamflow eliminates the limitations associated with using pre-defined regions, e.g., AMO of climate indices and the resultant streamflow responses to their variability.

Previous efforts by Tootle and Piechota (2006) identified the relationship between Pacific and Atlantic SSTs and 639 unimpaired streamflow stations in the continental U.S. They based the selection of stations from Wallis et al. (1991), and gages were analyzed through 1988. These gages were based on whether substantial regulation was noted in the data reports of the United States Geological Survey (USGS). The gages of the Hydro-Climatic Data Network (HCDN) (Slack and Landwehr, 1992) are measured by USGS, which take into consideration more than just regulations for their unimpaired status. Further, the USGS has updated its network of unimpaired gages. The latest network – called the Geospatial Attributes of Gages for Evaluating Streamflow, Version II (GAGES-II) (HCDN, 2009) – is based on several additional factors, including quantitative GIS-based coverages such as land use as well as local USGS input. A new dataset includes an additional 20 years of streamflow, which provides knowledge of recent watershed conditions and changes since the last dataset was developed in 1988. Moreover, in studies similar to this one, there is a preference to use as many sites as possible. However, many of the sites are spatially correlated, being on the same stream or in the same 8-digit hydrologic unit. These additional sites do not add extra information, and may contribute to misleading spatial correlation in a region when two or more sites show a statistically significant relationship but are measuring the same thing. The relationships developed between the oceanic-atmospheric regions and significant

hydrologic regions should be obtained by calculating the global/field significance as opposed to local relationships at gages within a region. It has been observed that Z_{500} has an immediate effect on precipitation, and should be included as an important indicator when developing relationships for streamflow climate variability. HGT has been used in developing relationships and forecasting models at local scale but its influence on the whole of U.S. streamflow might provide new insights.

This current study evaluates the spatio-temporal relationships between two climate indicators and continental U.S. streamflow for long-term variability. Using SVD analysis on 60 years (1951-2010) of fall and winter Pacific and Atlantic SST and Z_{500} -- with 240 unimpaired spring-summer streamflow stations of continental U.S. categorized into 18 hydrologic regions – this study attempted to establish one-to-four month lagged relationships between climate and streamflow variability. This study improves upon the works of Tootle and Piechota (2006) by incorporating the most recent data and an additional important climate variability indicator, i.e., Z_{500}.

3.2. Data

The dataset used comprises monthly streamflow and SST and Z_{500} index for Pacific and Atlantic Ocean. A brief description of the data and their sources is provided as follows:

3.2.1. Streamflow Data

Streamflow data used in this study was derived from Sagarika et al. (2014), a compilation of 240 unimpaired stations from the Hydro-Climatic Data Network 2009 (HCDN-2009) maintained by the USGS (Lins, 2009).This dataset is a revision to the

USGS's original HCDN network (Slack and Landwehr, 1992). The new stations are a subset of the GAGES II dataset (Falcone, 2011). The USGS divided the continental U.S.

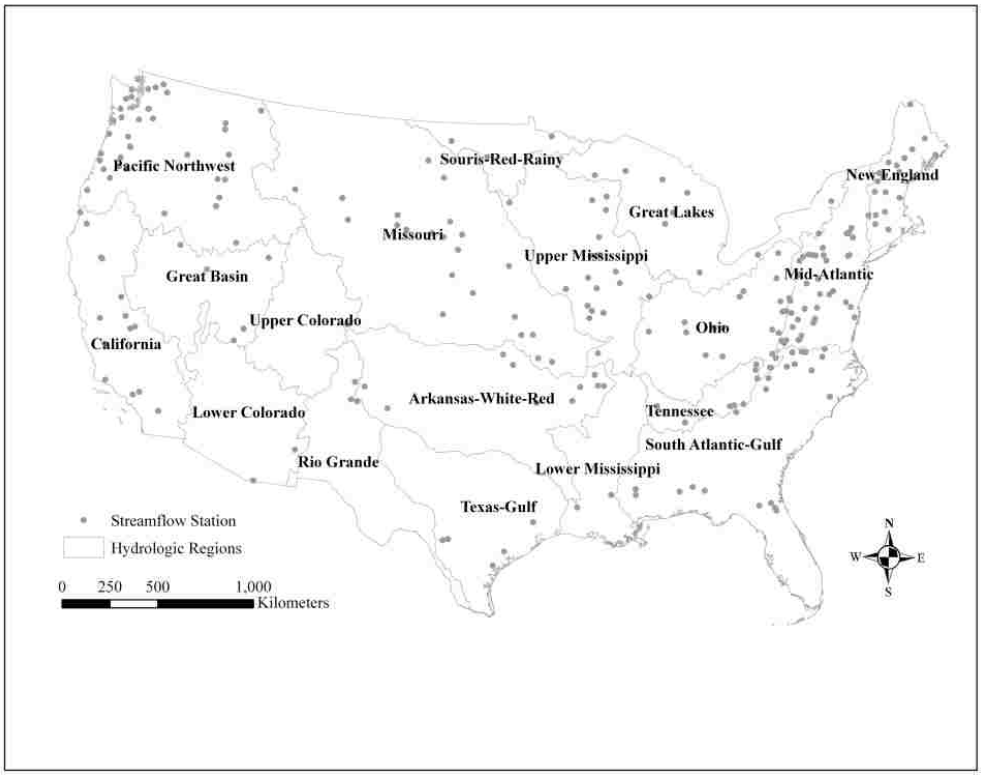

Figure 3.1: Map showing the distribution of 240 streamflow stations across the continental United States and the 18 hydrologic regions.

into 18 major basins, or regions; each region is divided into sub-regions, denoted with a unique Hydrologic Unit Code (HUC). Each region has its own typical characteristic topography. The 240 stations were grouped into the 18 hydrologic regions. Average monthly streamflow data for all the stations were obtained from the USGS online database (http://www.usgs.gov/). Flows for spring- summer (March to August), spring (March to May), and summer (June to August) were averaged for 60 years (1951 to 2010). For a given time frame, no stations were present in Upper Colorado region. The distribution of the stations is illustrated in Figure 3.1 and Table 3.1.

Table 3.1: Number of Unimpaired Stations per each Hydrologic Region in the Continental United States

Hydrologic Region No	Hydrologic Region Name	Number of Unimpaired Stations
1	New England	18
2	Mid-Atlantic	39
3	South Atlantic-Gulf	21
4	Great Lakes	10
5	Ohio	21
6	Tennessee	8
7	Upper Mississippi	19
8	Lower Mississippi	2
9	Souris-Red-Rainy	3
10	Missouri	22
11	Arkansas-White-Red	11
12	Texas-Gulf	5
13	Rio Grande	3
14	Upper Colorado	-
15	Lower Colorado	2
16	Great Basin	5
17	Pacific Northwest	37
18	California	14

3.2.2. Sea Surface Temperature (SST)

The monthly SST data used in this study was obtained from the NOAA ESRL Physical Sciences Division (http://www.esrl.noaa.gov/psd/data/gridded/data.noaa.ersst/sst.mnmean.nc). The oceanic SST data consisted of average monthly values for a 2˚ X 2˚ grid cell (Smith and Reynolds, 2004). In this study, the region used for Pacific Ocean SST was 100E to 80W and 30S to 70N; for the Atlantic Ocean SST, the region used was between 80W to 20W and 30S to 70N. This composed a gridded set of 3432 SST cells in the Pacific Ocean and 1149 cells in the Atlantic Ocean.

The SST monthly data was averaged for 60 years for fall (September to November from 1950 to 2009) and winter (December to February from 1950 to 2009). The interdecadal PDO and multidecadal AMO have periodicity of 25 to 50 years for their respective phases i.e., warm (positive) and cold (negative). The periods used in McCabe et al. (2004) and Tootle and Piechota (2006) were adopted to demarcate PDO and AMO phase years for the SST data. Based on Mantua (2004), PDO warm phase was from 1977 and continued until the end of the study period (2009), whereas AMO warm phase was from 1995 to year 2009. Thus, the PDO had a cold phase from 1950 to 1976 and a warm phase from 1977 to 2009. AMO had a warm phase from 1950 to 1963, a cold phase from 1964 to 1994, and then went back to a warm phase from 1995 to 2009. The warm and cold phases of the PDO and AMO were considered for separate periods, and analysis was conducted on the SST and streamflow values of particular phases.

3.2.3. 500-mbar Geopotential Height Index (Z_{500})

The monthly Z_{500} index data available from the NOAA Physical Sciences Center (http://www.esrl.noaa.gov/psd/data/gridded) was used. The dataset is a product of the NCEP/NCAR Reanalysis (Kalnay et al., 1996), which was a 40-year project. The Z_{500} data are available in 2.5˚ X 2.5˚ degree grid cells. The region used for gridded data of the Pacific Ocean Z_{500} was from 100E to 80 W and 70N to 30S; the region used for data of the Atlantic Ocean Z_{500} was from 80W to 20W and 70N to 30S. The Pacific region involved 2988 grid cells and the Atlantic region involved 1025 grid cells.

3.3. Method

3.3.1. Singular Valued Decomposition

For finding the spatial-temporal relationships between two fields, SVD has emerged as a suitable tool. This paper provides a brief description of this method; for a more detailed discussion, readers are referred to Bretherton et al. (1992) and Strang (1998). SVD is a factorization of a matrix that results in three matrices (i.e., $M = USV^T$). The orthogonal matrices, U and V, consist of the generated singular vectors commonly referred to as left and right matrices. The center diagonal matrix, S, consists of non-zero singular values of the original matrix. In general, the first three modes (i.e., the first three diagonal elements in S) must explain a significant portion of the variance for SVD in order to be statistically applicable (Newman and Sardeshmukh, 1995). Due to issues related to statistical inference, caution must be observed when making assertions about the cause of the relationships based on the results of SVD, as is required when using most statistical tools. In order to apply SVD, the matrices of standardized anomalies for the variables should be generated. The temporal resolution and size must match among all matrices in order to apply SVD; however, the spatial characteristics do not need to be similar. Cross-covariance matrices are found among the matrices, and are decomposed using SVD. A square covariance fraction (SCF), or percentage, is calculated by taking the square of each singular value and dividing it by the sum of all the squared singular values. The SCF value, which indicates how much variability can be explained by the model used, has been found to explain variability better than other models (Bretherton et al., 1992). The generated singular values – when squared and divided by the count of one variable data point times the count of a second variable data point – gives the normalized

square covariance (NSC) (Wallace et al., 1992; Bretherton et al., 1992). Similar to the SCF, the NSC value is a comparative measurement of the decomposition by SVD, with a lower value explaining a better fit. The column vectors contained in the left and right matrices are projected onto the original standardized anomaly matrices and the original standardized anomaly matrices, respectively. The i^{th} projected vector is the temporal expansion series for the i^{th} mode. Only the modes that correspond to a SCF of 10% or greater are retained. Finally, the temporal expansion series are correlated with the original standardized anomalies of variables, in order to find the relationship between the two fields.

3.3.2. Statistical Approach

SVD is used to evaluate the spatio-temporal relationships between Pacific and Atlantic SST and Z_{500}, and the continental U.S. streamflow. Before applying SVD, monthly SST and Z_{500} values were averaged for fall (September to November from 1950 to 2009) and winter (December to February from 1950 to 2009). The monthly streamflows were summed for spring-summer (March to August), spring (March-May), and summer (June to August) from 1951 to 2010. This provides a one-to-four month lag in evaluating the influence of Pacific and Atlantic SST/Z_{500} on the seasonal streamflow.

SVD was used to decompose the winter Pacific and Atlantic SST and Z_{500} with spring-summer, spring, and summer streamflows, followed by SVD decomposition of fall Pacific and Atlantic SST and Z_{500} with spring-summer, spring, and summer streamflows. Heterogeneous correlation values were used to generate heterogeneous correlation maps, which are used to analyze the significant regions at $p \leq 0.10$. The SST Pacific and Atlantic SST data for PDO and AMO cold and warm phases were averaged separately for

their corresponding years, for example, PDO cold fall, from 1950 to 1976 (September to November) and winter from 1977 to 2009 (December to February). The streamflows for PDO cold analysis were spring-summer, spring, and summer averages from 1951 to 1977, maintaining the same one-to-four month lag. SVD was performed on the PDO (AMO) cold and warm years with the Pacific (Atlantic) SST and streamflows, and the temporal expansion series were obtained.

Finally, field significance of the significant correlated regions was calculated using the Walker Test, which assesses whether the results are globally significant. The individual stations in a region might be significant; however, for a regional comparison to occur, the field significance test is important to determine whether the corresponding correlations provided by the SVD analysis are significant or not for the whole region. This helps in a comparison of the interconnections of the regions. The Walker test, extracted from Wilks (2006), takes the p values of the stations derived from the SVD analysis. The test considers the p-value of each of the K significance tests in order to reject the global null hypothesis that all local null hypotheses are true. Please refer Wilks (2006) for detailed description on the Walker test. Using the Walker test in this study, changes were evaluated at a confidence level ($p \leq 0.10$) for 240 unimpaired streamflow stations in the continental United States.

Presence of trends in data can often lead to biased results while detecting temporal variability. Time series that assume stationarity are generally preprocessed by some type of detrending technique before further analysis. The impacts of trends on time series can be computed by the fraction of variance of the original series to the variance of the fitted trend line as shown in equation 3.1.

$$R^2 = 1 - \frac{v\,(y)}{v\,(x)} \qquad (3.1)$$

where v(y) is the variance of the original time series, and v(x) is the variance of the residuals from the fitted trend line.

The values of R^2 range from 0 to 1, 0 for no trend and 1 explaining the variability by a pure trend. A least-squares-fit is used to remove the trend from the time series. This approach is well documented and has been used in numerous studies (Haan, 1977; Owens, 1978). Using this approach, trends were first removed from the streamflow data and then SVD was applied to evaluate the relationship of detrended SST and Z_{500} with detrended streamflow data. All the computations were performed using Matlab 2013a which has inbuilt SVD function. SVD, within Matlab, is implemented through geometric mechanism quantified through QR < 75 for convergence and identification of singular eigenvectors.

3.4. Results

This section describes the SVD results for SST and Z_{500}. Section 3.4.1 describes the SVD results of the SST with continental U.S. streamflow followed by section 3.4.2 describing the Z_{500} and streamflow results. Section 3.4.3 describes the results for PDO phases with streamflow and section 3.4.4 presents the AMO phase relationship with the U.S. streamflow. Finally section 3.4.5 presents the SVD results on the detrended datasets.

The SST and Z_{500} heterogeneous correlation maps for winter variability (Figures 3.2 to 3.10), depicting significant correlated regions at $p \leq 0.10$, are presented to identify the spatio-temporal relationships for the first mode. The highlighted regions in the figures represent where the correlations are field significant. This approach was used for all

heterogeneous correlation maps. The positive/negative correlated regions of SST have direct correlations with the positive/negative streamflow regions such that increases (decreases) in streamflow relates with increases (decreases) in SST/Z_{500}, and vice versa.

3.4.1. Streamflow and Oceanic Sea Surface Temperature

3.4.1.1. Pacific Ocean SST and U.S. Streamflows

Figure 3.2 depicts the heterogeneous correlation maps displaying significant regions of the Pacific Ocean winter SST; Figure 3.2a depicts spring-summer, Figure 3.2b depicts spring, and Figure 3.2c depicts summer streamflows for the first mode of SVD. The Pacific Ocean variability resulted in SCFs of 52.9%, 56.9%, and 45.6%, respectively, and NSC values of 2.7%, 3.0%, and 2.5%, respectively, for spring-summer, spring, and summer season streamflows (Table 3.2). Similarly, the second mode resulted in SCFs of 17.1%, 18.1%, and 20.3%, respectively. Out of 3432 cells, 2390 cells (70%) correlated significantly with spring-summer streamflows at $p \leq 0.10$. Approximately 69% and 67% of the Pacific SST grid cells correlated significantly with spring and summer streamflows at $p \leq 0.10$.

Two dominant significant regions, representing winter SST variability in the Pacific Ocean, were identified for spring-summer (Figure 3.2a). The first SST region was identified with positive (+) signals closer to the Asian and Australian continents; it showed direct correlations with the Pacific Northwest (17) and opposite correlations with California (18), Texas-Gulf (12), and South-Atlantic Gulf (3). The second SST region was identified near the equator (90W to 150W), and was more widespread with negative (-) signals, indicating opposite correlations with the Pacific Northwest(17) and direct correlations with California (18), Texas-Gulf (12), and South-Atlantic Gulf (3). The

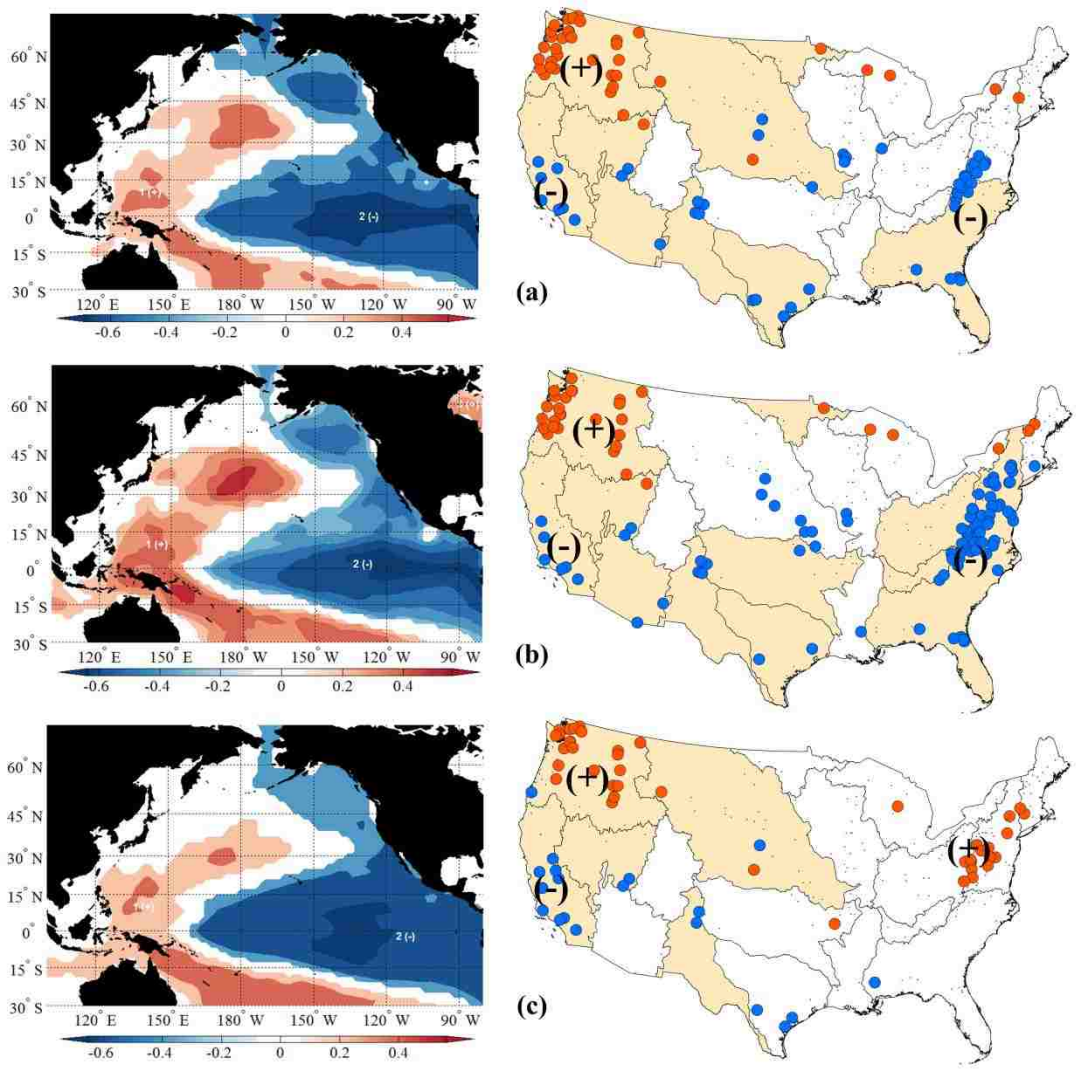

Figure 3.2. Heterogeneous correlation figures (first mode) for Pacific winter (Dec-Feb) SST and (a) spring-summer (Mar-Aug) streamflow, (b) spring (Mar-May) streamflow, and (c) summer (Jun-Aug) streamflow generated through SVD. Significant (>90%) grid regions approximated as positive (negative) are represented as red (blue) colors. Significant (>90%) positive (negative) streamflow stations are represented by red (blue) circles. Colored regions in continental U.S. show field significance.

significant SST for spring streamflows were similar to that for the spring-summer seasons; however, the region influencing summer streamflows were more concentrated near the equator and highly correlated along 120W to 150W. As shown in Figure 3.2, significant streamflow regions identified with higher correlations with the Pacific SST were South Atlantic Gulf (3), Souris-Red Rainy (9), Missouri (10), Texas-Gulf (12), Rio

Grande (13), the Lower Colorado (15), the Great Basin (16), the Pacific Northwest (17), and California (18). The spring season showed significant correlation with the Mid-Atlantic (2), Ohio (5), and Tennessee (6); however, the summer season showed field-significant correlations mostly in the western United States.

Table 3.2 presents the summary using fall climate variability and streamflows. SVD analysis of the Pacific Ocean fall SST and the spring-summer, spring, and summer streamflows for the first mode of SVD resulted in NSC values of 2.9%, 3.2%, and 2.6%. 56.2%, 59.9%, and 46% of the variance was explained in the first mode for spring-summer, spring, and summer, respectively. Similarly, the second mode explained 13.8%, 13.6%, and 18.9% of the variance, respectively (Table 3.2). Regarding the Pacific SST grid cells, 67%, 63%, and 67% correlated significantly with the streamflow at $p \leq 0.10$ for the three seasons. The seasonal spatial variation of the significant SST regions and significant streamflow regions showed patterns similar to the winter Pacific SST.

3.4.1.2. Atlantic Ocean SST and U.S. Streamflows

Significantly correlated regions with the U.S. spring-summer streamflow were identified in the Atlantic winter SST region, as shown in the heterogeneous correlation maps in Figure 3.3 for the first mode of SVD for spring-summer, spring, and summer streamflows. The SVD on the Atlantic winter SST and continental U.S. streamflow resulted in SCF of 36.9%, 41.7%, and 31%, respectively, for the first mode and a NSC value of 2.2%, 2.2%, and 2.04%, respectively, for the three streamflow seasons (Table 3.2). Out of 1149 SST grid cells, 561 cells (49%), 485 (42%), and 835 (73%) of the Atlantic SST grid cells were found to be correlated significantly with the streamflow at $p \leq 0.10$ in the three seasons. The second mode resulted in SCF of 25.1%, 21.6%, and

21.5% for the three seasons. Parts of Atlantic Ocean SST near Europe showed significant correlation with the streamflows. The spring season had stronger correlation with the northern Atlantic Ocean, whereas the summer streamflows had stronger correlation

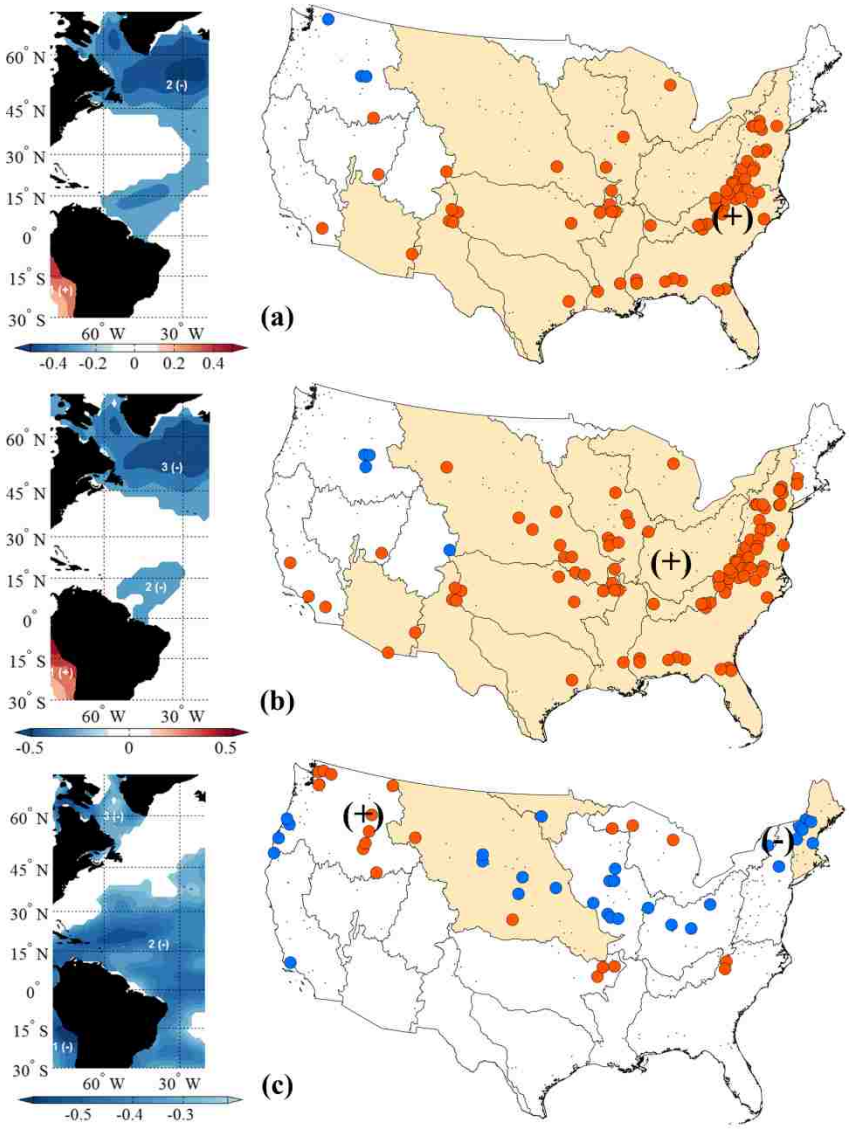

Figure 3.3. Heterogeneous correlation figures for SVD (first mode) for Atlantic (Dec-Feb) SST and (a) spring-summer (Mar-Aug) streamflow, (b) spring (Mar-May) streamflow, and (c) summer (Jun-Aug) streamflow generated through SVD. Significant (>90%) grid regions approximated as positive (negative) are represented as red (blue) colors. Significant (>90%) positive (negative) streamflow stations are represented by red (blue) circles. Colored regions in continental U.S. show field significance.

with the southern Atlantic Ocean. The spring season had significant correlation with mostly eastern and central U.S. streamflow regions namely Mid-Atlantic (2), South Atlantic-Gulf (3), the Great Lakes (4), Ohio (5), Tennessee (6), Upper Mississippi (7), Lower Mississippi (8), Missouri (10), Arkansas-White-Red (11), Texas-gulf (12), Rio Grande (13), and the Lower Colorado (15). In the summer season however New England (1), Souris-Red-rainy (9) and Missouri (10) had significant correlations.

The significantly correlated regions with the U.S. spring-summer, spring, and summer streamflow were identified in the fall SST. The SVD on the Atlantic fall SST and continental U.S. streamflows resulted in SCF of approx 45.1%, 49.2%, and 38.1% and a NSC value of 2.3%, 2.3%, and 2.06% for the first mode for the three streamflow seasons, respectively (Table 3.2). 66%, 65%, and 87% of the Atlantic SST regions were found to be correlated significantly with the streamflow at $p \leq 0.10$. Similarly, the second mode explained 18.8%, 17.2%, and 16.8%, respectively, of the variance for the three seasons. Most of the Atlantic Ocean SSTs showed significant correlation with the streamflows in the first mode. The higher correlated regions of the Atlantic Ocean tended to shift westwards from spring to summer, similar to the streamflow regions of the United States. The streamflow regions identified with strong correlations in spring were the Mid-Atlantic (2), South Atlantic-Gulf (3), the Great Lakes (4), Ohio (5), Tennessee (6), the Lower Mississippi (8), Souris-Red-Rainy (9), and the Lower Colorado (15). Streamflow regions identified in summer are New England (1), the Great Lakes (4), Souris-Red Rainy (9), and Missouri (10).

3.4.2. Streamflow and Geopotential Height

3.4.2.1. Pacific Z_{500} and U.S. Streamflows

The SVD analysis between the Pacific winter Z_{500} and spring-summer, spring, and summer streamflows resulted in an SCF of 67.8%, 68.6%, and 63.3%, respectively, for the first mode; 10.8% , 10.5%, and 9.6%, respectively, for the second mode; and a NSC value of 3.34%, 3.49%, and 2.81%, respectively. The heterogeneous correlation maps for the first mode are represented by Figure 3.4, displaying significant Pacific Z_{500} and streamflow regions. Around 2243 (75%) of Pacific Z_{500} grid cells showed significant correlations with the streamflows in the three seasons. The regions around the equatorial belt showed the most significant correlations. Additionally, the Pacific regions at the western coast of the United States as well as regions in northwest Canada and coast of Alaska showed high correlation with the streamflows (Figure 3.4). The spring season Z_{500} showed significant correlation with most of the streamflow regions, whereas the summer season Z_{500} showed significant correlations with the western United States (Figure 3.4). The SVD analysis of the relationship between the Pacific fall Z_{500} and spring-summer, spring, and summer streamflows resulted in a SCF of 49%, 50.3%, and 49.8%, respectively, for the first mode; 18.4%, 19.7%, and 14.9%, respectively, for the second mode; and an NSC value of 2.41%, 2.42%, and 2.57%, respectively. Out of 2988 cells considered in the Pacific Z_{500}, 61%, 59%, and 64%, respectively, showed significant correlations with the streamflows for the three seasons. As in winter Pacific Z_{500}, the regions around the equatorial belt showed the most significant correlations. The highly correlated spring Z_{500} regions tended to move westwards in the summer season. The

streamflow regions showed high correlation with Souris-Red-Rainy (9), Missouri (10), Rio Grande (13), Lower Colorado (15), Great Basin (16), and Pacific Northwest (17).

3.4.2.2. Atlantic Z_{500} and U.S. Streamflows

The Atlantic winter Z_{500} and the spring-summer, spring, and summer streamflow SVDs resulted in SCFs of 67%, 69.7%, and, 58.3%, respectively, in the first mode; with NSC values of 3.2%, 3.2%, and 2.69%, respectively. Out of 1025 cells considered in the Atlantic Z_{500}, 621 (61%), 631 (62%), and 629 (61%), respectively, were significantly correlated with the streamflow for the three seasons. Figure 3.5 shows the heterogeneous maps for significant correlations for first mode of SVD. The second mode gave a SCF of 14%, 12.3%, and 20.4%, respectively, for the three seasons. The region near the equatorial belt correlated mostly to the U.S. streamflow. In the spring season, most of the streamflow regions showed significant correlation with Z_{500} regions; however, in the summer seasons, the streamflow regions identified with significant correlation were New England (1), Missouri (10), Texas-Gulf (12), and Pacific Northwest (17).

The Atlantic fall Z_{500} and the spring-summer, spring, and summer streamflow SVDs resulted in SCF of 56%, 56.3%, and 59.4%, respectively, in the first mode with a NSC value of 2.41%, 2.6%, and 2.4%, respectively. Out of 1025 cells considered in the Atlantic Z_{500}, 63%, 64%, and 64%, respectively, were significantly correlated with the streamflow. The second mode gave a SCF of 15.4%, 20.4%, and 13.6%, respectively. The Atlantic Z_{500} regions showing significant correlations with U.S. streamflows were similar to that of the Atlantic winter Z_{500}, i.e., mostly in the equatorial belt. The streamflow regions identified are in the central United States.

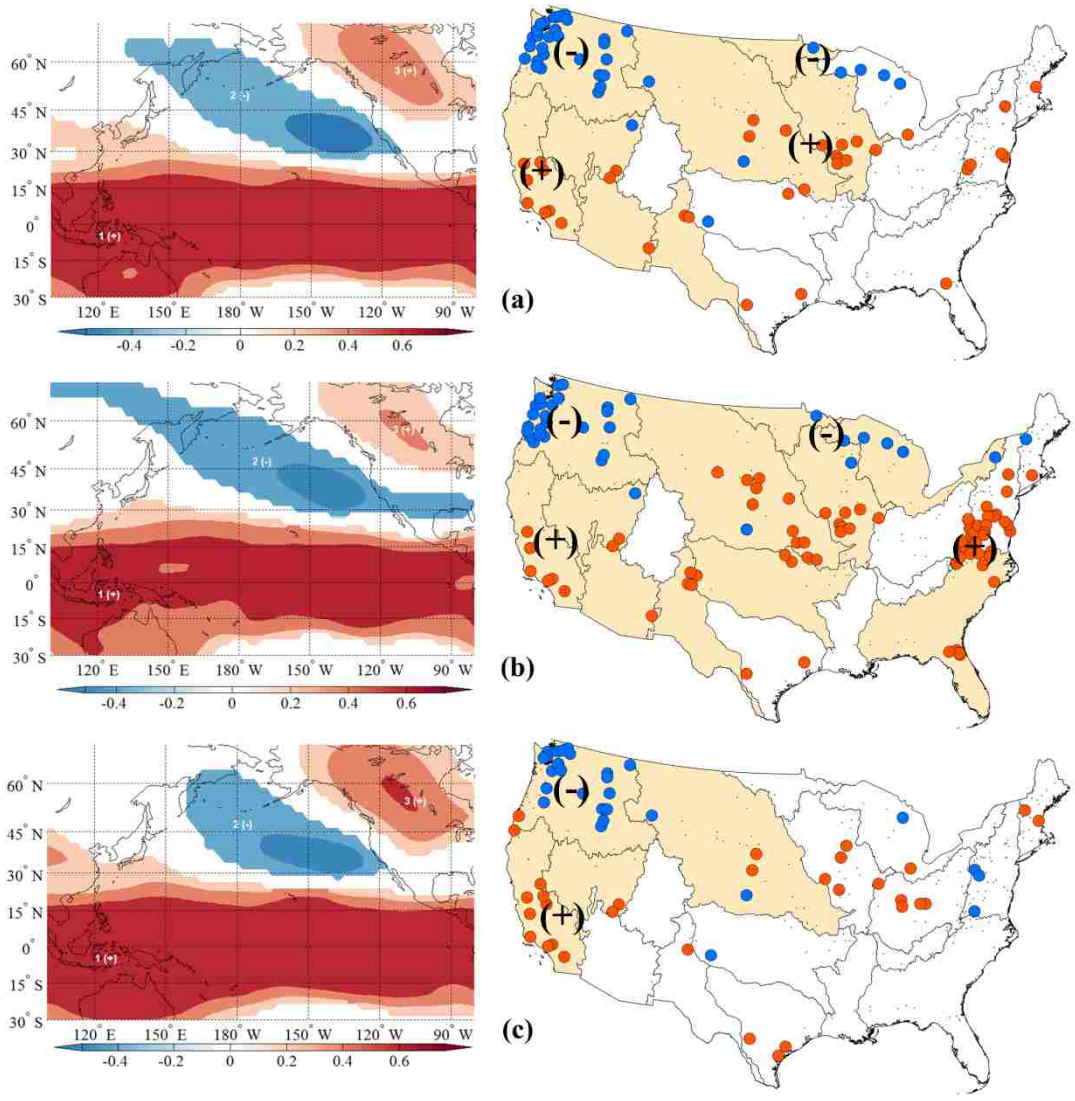

Figure 3.4. Heterogeneous correlation figures (first mode) for Pacific winter (Dec-Feb) Z_{500} and (a) spring-summer (Mar-Aug) streamflow, (b) spring (Mar-May) streamflow, and (c) summer (Jun-Aug) streamflow generated through SVD. Significant (>90%) grid regions approximated as positive (negative) are represented as red (blue) colors. Significant (>90%) positive (negative) streamflow stations are represented by red (blue) circles. Colored regions in continental U.S. show field significance.

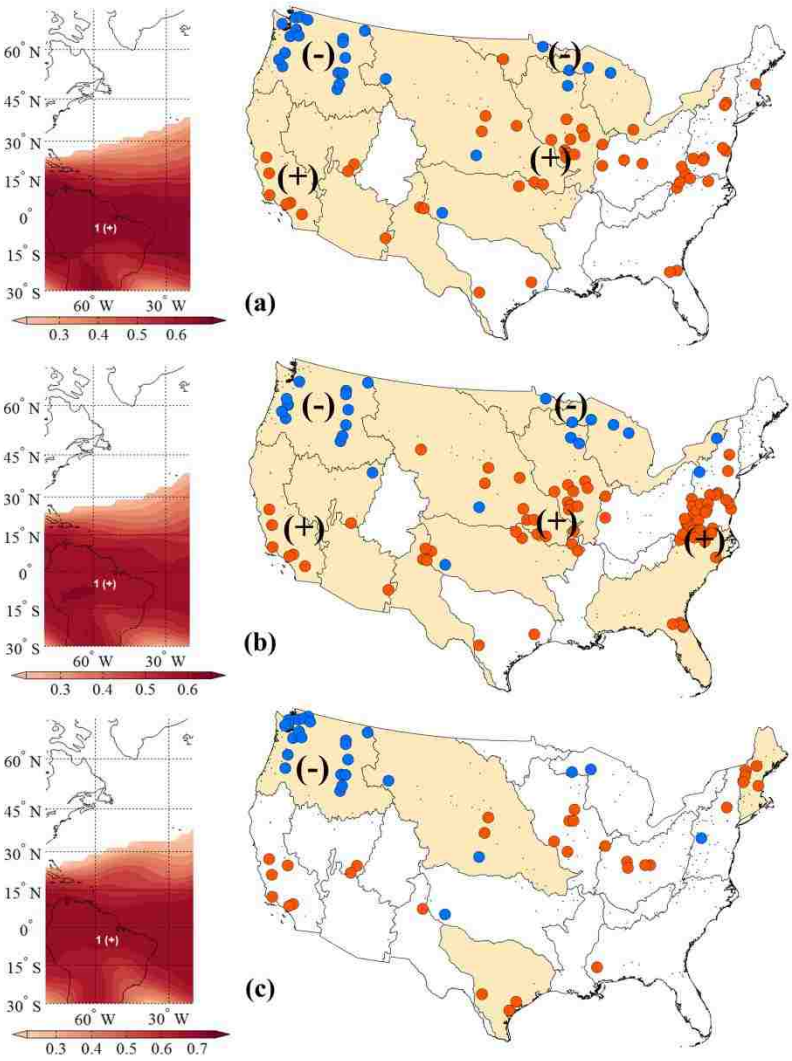

Figure 3.5. Heterogeneous correlation figures (first mode) for Atlantic winter (Dec-Feb) Z_{500} and (a) spring-summer (Mar-Aug) streamflow, (b) spring (Mar-May) streamflow, and (c) summer (Jun-Aug) streamflow generated through SVD. Significant (>90%) grid regions approximated as positive (negative) are represented as red (blue) colors. Significant (>90%) positive (negative) streamflow stations are represented by red (blue) circles. Colored regions in continental U.S. show field significance.

3.4.3. PDO Phase Relationship with Streamflow

3.4.3.1. PDO Cold and U.S. Streamflows

As shown in Figure 3.6, for the PDO cold phase analysis, the heterogeneous correlation maps display the significant Pacific Ocean winter SST and continental U.S.

spring-summer, spring, and summer streamflow for the first mode of SVD. The first mode resulted in SCF value of 44.5%, 46.2%, and 41.6%, respectively, and the second mode resulted in SCF of 21.4%, 17.1%, and 17.7%, respectively, at NSC values of 4.44%, 4.5%, and 4.12%, respectively. Out of 3432 cells in the Pacific SST, 48%, 47%, and 45%, respectively, were significantly correlated with the streamflows. The PDO Pacific SST had five significant clusters for spring-summer streamflows; however, the major cluster shown as 2(-ve), which was near the equatorial belt and ranged from 90W to 180W. In the spring season, the streamflow regions of the southern U.S. – namely South Atlantic-Gulf, Arkansas-White-Red (11), Texas-Gulf (12), Rio-Grande (13), Lower Colorado (15), and the Great Basin (16) – showed significant correlation with the Z_{500}; however, in summer, as the Z_{500}-correlated region moved northwards towards the western U.S. (Figure 3.6), the significant streamflow-correlated regions were the Mid-Atlantic (2), Missouri (10), the Great Basin (16) and the Pacific Northwest (17).

The heterogeneous correlation results for Pacific Ocean fall SST and continental U.S. spring-summer, spring, and summer streamflow SVDs for the PDO cold phase resulted in SCF values of 47.9%, 52.1%, and 45.9%, respectively, in the first mode and 19.4%, 15.1%, and 16.4%, respectively, in the second mode, with NSC values of 4.3%, 4.54%, and 4.21%, respectively. Approximately 56%, 54%, and 53%, respectively, of the Pacific SST grid cells correlated significantly with the streamflows in the three seasons. The spatial correlations for the PDO cold fall SST were similar to the PDO cold winter SST, with spring streamflows showing higher correlations than summer. The significant regions of streamflow tended to move northwards from spring to summer, similar to the results for the winter PDO cold streamflow.

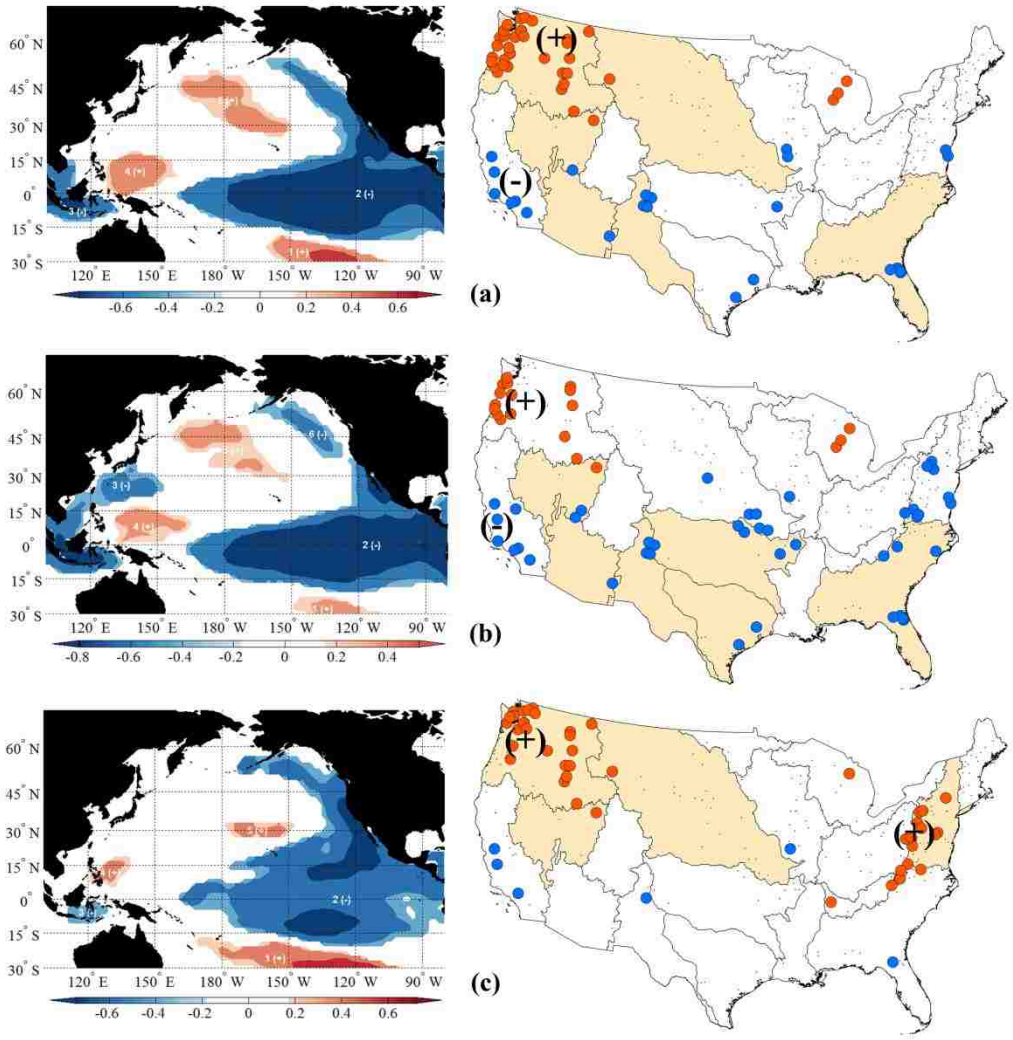

Figure 3.6. Heterogeneous correlation figures (first mode) for PDO cold Pacific winter (Dec-Feb) SST and (a) spring-summer (Mar-Aug) streamflow, (b) spring (Mar-May) streamflow, and (c) summer (Jun-Aug) streamflow generated through SVD. Significant (>90%) grid regions approximated as positive (negative) are represented as red (blue) colors. Significant (>90%) positive (negative) streamflow stations are represented by red (blue) circles. Colored regions in continental U.S. show field significance.

3.4.3.2. PDO Warm and U.S. Streamflows

In the analysis of PDO warm years, Pacific winter SST and continental U.S. spring-summer, spring, and summer streamflows resulted in SCF of 44.4%, 33.4%, and 54.8%, respectively, for first mode and NSC values of 3.6%, 3.26%, and 3.76%,

respectively. The heterogeneous correlation maps for the PDO warm year SVDs are presented in Figure 3.7, which show significantly correlated regions and stations. Out of 3432 grid cells for the Pacific SST, 47%, 43%, and 53%, respectively, were significantly correlated with the streamflow. The SCF values for the second mode were 19.9%, 20.8%, and 12.89% for the respective three seasons. The PDO warm winter Pacific SST regions showing significant correlations with the United States were confined within 30 degrees of the equatorial belt. However, the SST region showed two separate signs of correlation, i.e., negative from 120 E to 150 W (near the Asian and Australian continents) and positive from 180W to 90W (near the western coast of the Americas). The spring PDO related to the central U.S., whereas the summer PDO related to the eastern United States (Figure 3.7).

In the analysis of PDO warm years, Pacific fall SST and continental U.S. spring-summer, spring, and summer streamflow SVDs resulted in SCFs of 43.3%, 36.3%, and 55.4%, respectively, for the first mode and a NSC value of 3.21%, 2.96%, and 3.56%, respectively. Around 46%, 54%, and 55% of the Pacific SST grid cells were significantly correlated with the streamflow, and the SCF values for the second mode were 18.6 %, 18.6%, and10% for the respective three seasons. The PDO warm fall SST showed similarity with PDO warm winter SST regions; however, the region near the continents of Asia and Australia were more prominent than the positive region near the Americas. The U.S. streamflow regions showed same pattern as the winter PDO warm streamflows.

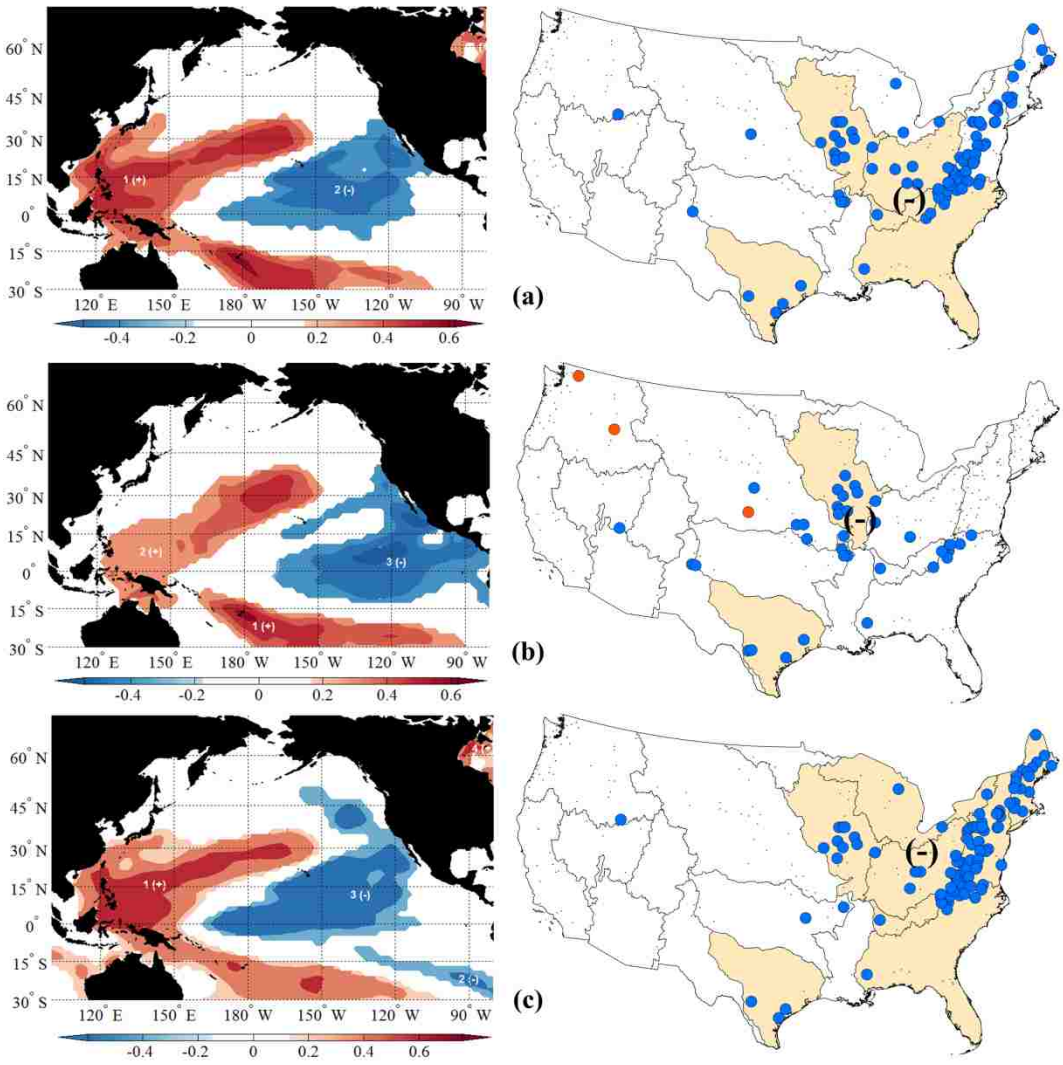

Figure 3.7. Heterogeneous correlation figures (first mode) for PDO warm Pacific winter (Dec-Feb) SST and (a) spring-summer (Mar-Aug) streamflow, (b) spring (Mar-May) streamflow, and (c) summer (Jun-Aug) streamflow generated through SVD. Significant (>90%) grid regions approximated as positive (negative) are represented as red (blue) colors. Significant (>90%) positive (negative) streamflow stations are represented by red (blue) circles. Colored regions in continental U.S. show field significance.

3.4.4. AMO Phase Relationship with Streamflow

3.4.4.1. AMO Cold and U.S. Streamflows

For AMO cold phase winter SST, SVD analysis of the heterogeneous correlation figures – representing significantly correlated regions of continental U.S. streamflow for

spring-summer, spring, and summer for the first mode – are presented in Figure 3.8. The SCF values for the first mode are 40.7%, 39%, and 35.2%, respectively, the second mode are 17.1%, 16.1%, and 17.6%, respectively, with NSC values of 3.83%, 3.74%, and 3.39%, respectively. Out of 1149 cells in the Atlantic SST, the three seasons had 39%, 38%, and 48% significantly correlated grid cells with the streamflow. The Atlantic SST during AMO cold winter months for spring-summer streamflows had two major SST regions, one positive correlated region between 10S to 30N and another negative correlated region between 20 N to 45N. The spring SST results were the same as the spring-summer; however, the summer SST regions showed a new positively correlated region from 45N to 70N (Figure 3.8). The streamflow regions identified with significant correlations were New England (1), Mid-Atlantic (2), the South Atlantic-Gulf (3), Ohio (5), Tennessee (6), the Upper Mississippi (7), Missouri (10), Arkansas-White Red (11), Texas-Gulf (12), Rio Grande (13), and the Lower Colorado (15). The Pacific Northwest (17) showed correlations for some of its stations in the summer season (Figure 3.8).

For AMO cold phase fall SST, SVD analysis of the heterogeneous correlation results provided significant correlated regions of continental U.S. streamflow for spring-summer, spring, and summer. SCF values were 27.6%, 25.1%, and 29.2%, respectively, for the first mode; 20.6%, 17.4%, and 19.3%, respectively, for the second mode; and had NSC values of 3.27%, 3.21%, and 3.26%, respectively. Out of 1149 cells in the Atlantic SST, 22%, 24%, and 21% were significantly correlated with the streamflows for the respective three seasons. The AMO cold fall SST showed smaller and fewer grids cells that were significantly correlated with the U.S. streamflows. The spring-summer

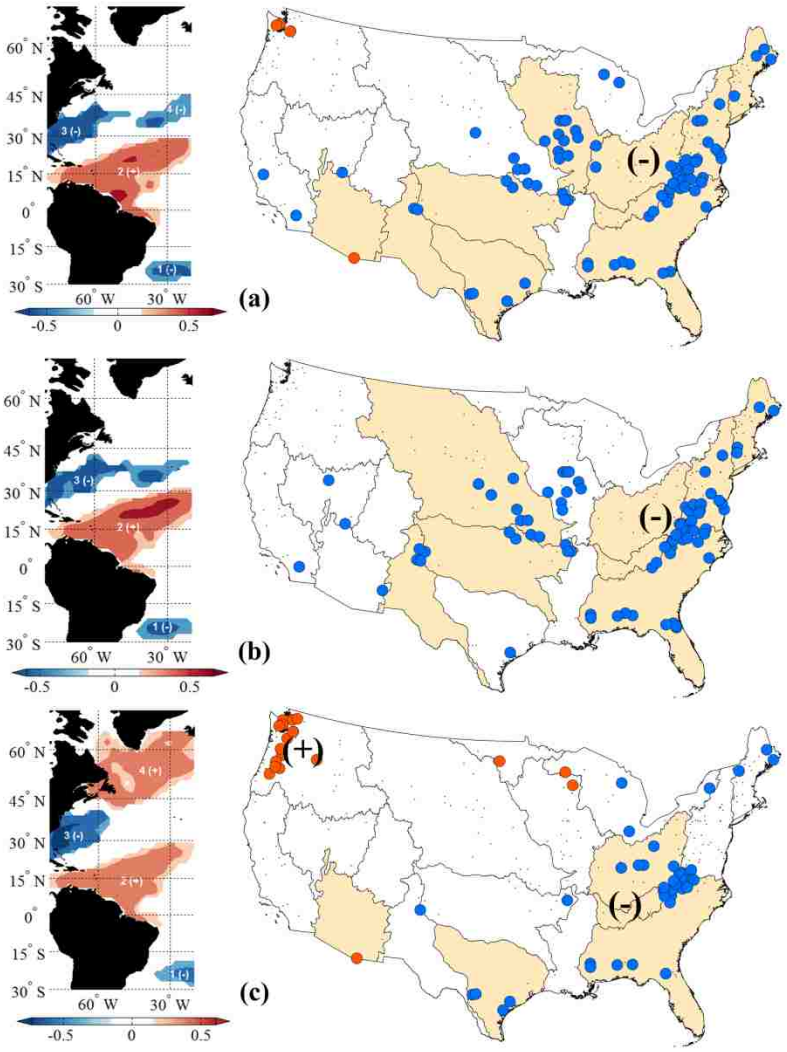

Figure 3.8. Heterogeneous correlation figures (first mode) for AMO cold Atlantic winter (Dec-Feb) SST and (a) spring-summer (Mar-Aug) streamflow, (b) spring (Mar-May) streamflow, and (c) summer (Jun-Aug) streamflow generated through SVD. Significant (>90%) grid regions approximated as positive (negative) are represented as red (blue) colors. Significant (>90%) positive (negative) streamflow stations are represented by red (blue) circles. Colored regions in continental U.S. show field significance.

streamflow regions showed significant correlation in Mid-Atlantic (2), the South-Atlantic-Gulf (3), Ohio (4), and Rio Grande (13). The spring SST regions mostly were correlated near 15N latitude, and the correspondingly significant streamflow regions were located in the central U.S., such as the Mid-Atlantic (2), Upper Mississippi (7), Missouri (10), Arkansas-White-Red (11), Rio-Grande (13), and Great Basin (16). The significant

SST region for summer was located at 45N and between 30W to 60W; the eastern U.S. streamflow regions from New England (1) to Lower Mississippi (8) were significantly correlated.

3.4.4.2. AMO Warm and U.S. Streamflows

Figure 3.9 depicts the heterogeneous correlation maps for the Atlantic winter SST and the spring-summer, spring, and summer streamflow in the warm phase of AMO, and shows 40.8%, 33.8%, and 47.4% , respectively, of the variance in the first mode of SVD. The second mode showed 15%, 18.2%, and 13.2%, respectively, of the variance at NSC values of 3.42%, 3.28, and 3.71%, respectively. 55%, 56%, and 56% of the Atlantic SST grid cells showed significant correlations with the streamflows. The AMO warm winter SST region had two significantly correlated regions, one at 30N and between 30W and 60W and the other at 60N. The significantly correlated U.S. streamflow regions were South-Atlantic-Gulf (3), the Great Lakes (4), Arkansas-White-Red (11), and Texas-Gulf (12). The spring and summer SST regions were similar to the spring-summer combined; however, the summer season showed more streamflow regions with significant correlations (Figure 3.9).

The heterogeneous correlation results for the Atlantic winter SST and the spring-summer, spring, and summer streamflow in the positive phase of AMO showed 51.9%, 46.1%, and 55.8%, respectively, of the variability in the first mode of SVD. The second mode showed 14.1%, 13.6%, and 10.5%, respectively, of the variability. These results were at NSC values of 3.96%, 3.90%, and 3.83% for the respective three seasons. Out of

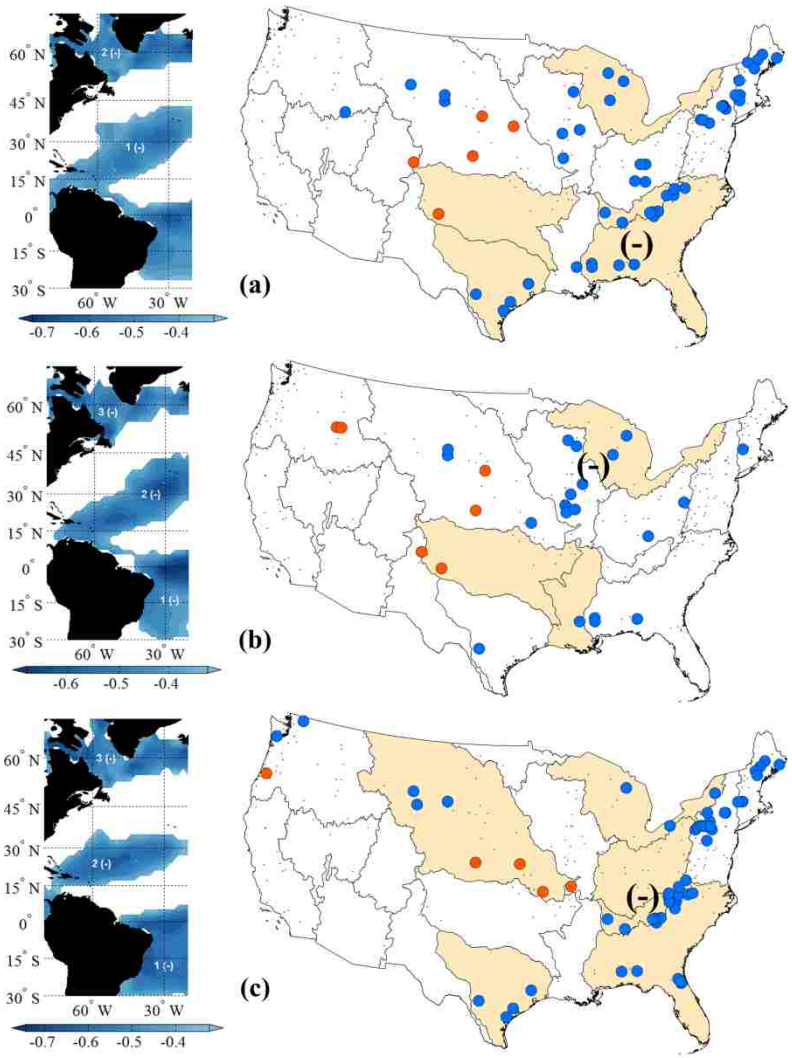

Figure 3.9. Heterogeneous correlation figures (first mode) of AMO warm Atlantic winter (Dec-Feb) SST and (a) spring-summer (Mar-Aug) streamflow, (b) spring (Mar-May) streamflow, and (c) summer (Jun-Aug) streamflow generated through SVD. Significant (>90%) grid regions approximated as positive (negative) are represented as red (blue) colors. Significant (>90%) positive (negative) streamflow stations are represented by red (blue) circles. Colored regions in continental U.S. show field significance.

1149 cells in the Atlantic SST, 74%, 64%, and 69%, respectively, showed significant correlations with the spring-summer, spring, and summer streamflows. The AMO warm fall SST did not favor any particular region; rather, most of the grid cells were correlated with the U.S. streamflows. Most of the eastern U.S. streamflow regions showed significant correlation with the Atlantic AMO warm phased fall SST.

3.4.5. SVD on detrended SST, Z_{500}, and U.S. streamflow

The detrended analysis indicted that 1754 (51%) of Pacific Ocean SST cells in winter season and 1461(43%) Pacific SST grid cells in fall season have trends, which influence more than 10% of the variability. In the Atlantic Ocean 494 (43%) SST grid cells in winter and 642(56%) SST cells in fall show trends to influence more than 10% of the variability. Similarly, 1828(61%) Pacific Z_{500} grid cells in winter and 1813(61%) grid cells in fall explain more than 10% of the variability and 653 (64%) Atlantic Z_{500} grid cells in winter and 649 (63%) grid cells in fall accounted for more than 10% of variability. The streamflows trends residuals show 14(6%) streamflow stations in spring-summer, 12(5%) in spring and 17(7%) in summer with more than 10% influence on the streamflow variability.

Figure 3.10 shows the results of the SVD analysis performed on detrended winter Pacific SST data and detrended streamflow data. The first mode of winter Pacific Ocean SST resulted in SCF of 60.6%, 67.5% and 54.5% in spring-summer, spring, and summer season streamflow, respectively. The fall Pacific SST resulted in SCF of 60.7%, 67.5%, and 52.2% for the three seasons. Spatially, the significant regions identified using the detrended winter Pacific SST and streamflow (Figure 3.10) were similar with regions identified using the non-detrended (Figure 3.2) data. The first mode of winter Atlantic Ocean SST resulted in SCF of 45.2%, 48.8%, and 32.7% for the three temporal time

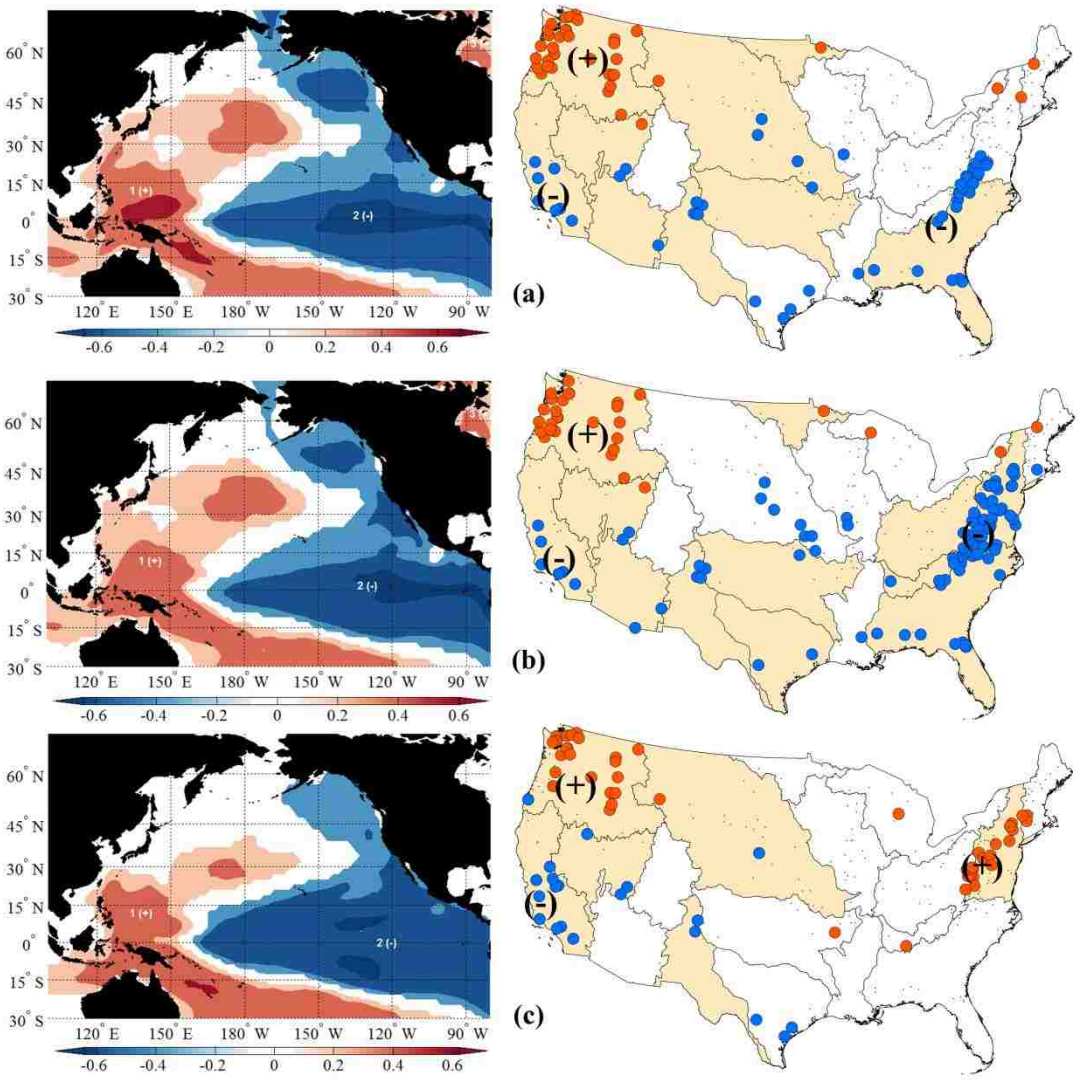

Figure 3.10: Heterogeneous correlation figures (first mode) for detrended Pacific winter (Dec-Feb) SST and (a) spring-summer (Mar-Aug) streamflow, (b) spring (Mar-May) streamflow, and (c) summer (Jun-Aug) streamflow generated through SVD. Significant (>90%) grid regions approximated as positive (negative) are represented as red (blue) colors. Significant (>90%) positive (negative) streamflow stations are represented by red (blue) circles. Colored regions in continental U.S. show field significance.

periods. The Atlantic Ocean fall SST and streamflow SVD resulted in SCF of 51.14%, 53%, and 36.42% for the first mode during the three seasons. The Pacific winter Z_{500} and streamflow SVD resulted in SCF of 59.3%, 67.2%, and 55.6% whereas, fall Z_{500} resulted in SCF of 37.6%, 43.3%, and 28.6% for the first mode during the three seasons. The first

mode of Atlantic winter Z_{500} and streamflow SVD resulted in SCF of 51.2%, 62.8%, and 47%, whereas fall Z_{500} resulted in 34.9%, 47.5%, and 28.9% during the three seasons.

The PDO cold winter SST and streamflow SVD resulted in SCF of 47.3%, 48.5%, and 41.5%, and fall SST resulted in SCF of 52.5%, 55.5%, and 43.9% for the first mode during the three seasons. The PDO warm winter and streamflow SVD resulted in SCF of 37.3%, 27.5%, and 44.2% for the three seasons and fall SST resulted in SCF of 38.7%, 27.5%, and 49.1% for the three seasons. The AMO cold phase winter SST and streamflow SVD resulted in SCF of 40.2%, 39%, and 32.3%, and fall SST resulted in SCF of 34.1%, 30.1%, and 33.1% for the three seasons in the first mode. The warm phase of AMO resulted in SCF of 25%, 25.1%, and 24.8% in the first mode for winter SST in the three seasons, and SCF of 28.8%, 27%, and 22.2% for fall SST for the three seasons.

3.5. Discussion

SVD analysis of SST, Z_{500}, and seasonal streamflow identified significant regions depicting the spatio-temporal variability in U.S. streamflow with the Pacific and Atlantic regions. The SST phase analysis for the Pacific and Atlantic Ocean, using PDO and AMO, indicated differences in spatial correlation patterns and signals with streamflows. The majority of variability in streamflow was represented by the temporal expansion series of first mode of SVD in SST and Z_{500}.

The first identified region in the east equatorial Pacific Ocean SST resided in the ENSO belt, confirms to the Niño index. The second region to be highly correlated in the Pacific SST was seen to be consistent in all the seasons, including the PDO cold and warm phases, and had been identified in previous studies to be associated with hydrological variability of streamflow, snow, and precipitation in different parts of the U.S. (Wang and

Ting, 2000; Rajgopalan et al., 2000; Tootle and Piechota, 2006; Soukup et al., 2009; and Aziz et al., 2011). The Pacific Northwest region is consistently teleconnected directly with the first SST region and inversely teleconnected with the second SST region identified in the Pacific Ocean.

The phases of the PDO influenced the spatial positioning of significant correlation of the SST regions with the streamflow. The PDO cold phase significantly correlated with the Pacific Northwest (17), the Great Basin (16) and the Missouri (10) regions. Significantly correlated SST regions for PDO cold years were concentrated near the equatorial belt around Niño 3.4 and Niño 3 regions. An SST region with significant negative correlation for PDO warm years was seen to have shifted towards the Niño 3.4 region; a positively correlated region near the coast of Japan and Australia was found to have a prominent horseshoe shape. The PDO warm years were more correlated with the eastern United States.

The north-central region of the Pacific SST, bounded around 150 E to 160 W and 24 N to 34 N, was shown to be significantly correlated with Pacific Northwest (17) and Souris-Red-Rainy (9) and directly and inversely with Mid-Atlantic (2), South-Atlantic-Gulf (3), and Midwest region of the U.S., and California (18) in almost all the seasons for the Pacific SST, including the PDO cold and warm phase. This region has been named the Hondo region, and has been found to influence the hydrology of several areas around Japan and Asia as well as basins in the western United States (Zhang et al., 1997; Wang and Ting, 2000; Rajgopalan et al., 2000; Tootle and Piechota, 2006; Aziz et al., 2010; Aziz et al., 2011; Soukup et al., 2009; Lamb et al., 2011; Kalra et al., 2013c). This region

Table 3.2: Seasonal singular valued decomposition results for sea surface temperature and 500 mbar geopotential height.

			SST					**Z_{500}**		
			SCF (%)		**NSC**	**Sig Cells**	**SCF (%)**		**NSC**	**Sig Cells**
Climate Variability	Anomaly Season	Streamflow Season	*Mode 1*	*Mode 2*			*Mode 1*	*Mode 2*		
Pacific	Winter	Spring-Summer	52.9	17.1	2.7	2390	67.8	10.8	3.34	2243
		Spring	56.9	18.1	3	2380	68.6	10.5	3.49	2181
		Summer	45.6	20.3	2.55	2297	63.3		2.81	2228
	Autumn	Spring-Summer	56.2	13.8	2.9	2294	49	18.4	2.41	1810
		Spring	59.9	13.6	3.2	2146	50.3	19.7	2.42	1753
		Summer	46	18.9	2.6	2312	49.8	14.9	2.57	1905
Atlantic	Winter	Spring-Summer	36.9	25.1	2.2	561	67	14	3.2	621
		Spring	41.7	21.6	2.2	485	69.7	12.3	3.2	631
		Summer	31	21.5	2.04	835	58.3	20.4	2.69	629
	Autumn	Spring-Summer	45.1	18.8	2.3	760	56	15.4	2.41	643
		Spring	49.2	17.2	2.3	744	56.3	20.4	2.6	653
		Summer	38.1	16.8	2.06	1005	59.4	13.6	2.4	661
			Cold				**Warm**			
PDO	Winter	Spring-Summer	44.5	21	4.44	1631	44.4	19.9	3.6	1602
		Spring	46.2	17.1	4.5	1606	33.4	20.8	3.26	1488
		Summer	41.6	17.7	4.12	1553	54.8	12.9	3.76	1825
	Autumn	Spring-Summer	47.9	19.4	4.3	1914	43.3	18.6	3.21	1580
		Spring	52.1	15.1	4.54	1184	36.3	18.6	2.96	1862
		Summer	45.9	16.4	4.21	1802	55.4	10	3.56	1885
AMO	Winter	Spring-Summer	40.7	17.1	3.83	452	40.8	15	3.42	635
		Spring	39	16.1	3.74	439	33.8	18.2	3.28	646
		Summer	35.2	17.6	3.39	557	47.4	13.2	3.71	639
	Autumn	Spring-Summer	27.6	20.6	3.27	256	51.9	14.1	3.96	852
		Spring	25.1	17.4	3.211	276	46.1	13.6	3.9	740
		Summer	29.2	19.3	3.26	241	55.8	10.5	3.83	792

has been found to improve predicting abilities when used in streamflow forecasting (Kalra et al., 2013c). The Hondo region acts as an important pathway for different air streams (e.g., the East Asian Jet Stream) to divide and move into particular directions, ultimately entering the western U.S. envelope (Zhang et al., 1997). Due to identified teleconnections of this region with the western U.S., pressure differences in this region when SST is cooler can cause a cyclonic cell near the western U.S., enhancing a subtropical jet and returning moist air from the subtropical Pacific Ocean. The SVD analysis in this study identified regions in the Pacific Ocean similar to work by Aziz et al. (2010), Soukup et al. (2009), and Grantz et al. (2005). The regions centered in the equatorial region, with ENSO-like dynamics involving the thermocline depth of the ocean and the atmosphere's trade winds. This could be responsible for the observed variability.

Atlantic SST regions correlated for all years were similar to those identified by Tootle and Piechota (2006), both spatially and in signs (positive or negative).The Atlantic SST resulted in higher correlations with the eastern U.S. than the western U.S., compared to the Pacific SST. The seasonal variations in winter and fall SST-significant regions showed the highly correlated north region moved southwards towards the tropic and equator. The streamflow regions were confined to the east coast for fall SST, and winter SST influenced the deeper Midwest regions. The differences in the AMO cold and warm phases were evident in the signs of their teleconnections with the U.S. streamflows; the sub-tropics on cold AMO showed opposite relationships with the eastern U.S. streamflow, and the AMO warm phase showed direct relationships. The AMO cold phase fall SST had the weakest signals in influencing the streamflows, with low SCF values in

the first mode. The Atlantic SST regions identified in AMO cold years as well as the correlation type differed from those identified by Tootle and Piechota (2006). Similar results were found by Chang et al. (1997), who pointed out that the equatorial region of the Atlantic SST was found, in many studies, to influence the variability of rainfall in Northeast Brazil and the Sahel region of Africa (Moura and Shukla, 1981; Hastenrath, 1984; Folland et al., 1986).

The first mode SVD on Pacific SST and seasonal streamflow at $p \leq 0.10$ gave a minimum correlation value of |0.21| and maximum correlation value of |0.65|; however, the maximum r value increased up to |0.80| in PDO cold phases. Likewise, the r value obtained from first mode Atlantic SST and 60-year streamflow gave a maximum r value of |0.55|; however, it increased to |0.74| in the AMO warm phase. The increase in correlation values while considering the multi-decadal oceanic oscillations only can be indicative to more regional teleconnections of the multidecadal oscillations with the streamflow. The Pacific Z_{500} regions remained concentrated in the equatorial region. Two other regions showed significant teleconnections with the U.S. streamflow from December to February; however, they showed very weak teleconnections with the streamflow from September to November. Interestingly, winter Pacific and Atlantic Z_{500} influenced the central and western U.S., whereas the fall Pacific and Atlantic Z_{500} tended to influence the central U.S. streamflow. Z_{500} explained variability better than other factors due to a higher SCF value.

Weather systems and atmospheric circulations are responses of uncertain boundary forcings between sea surface temperatures, land surface changes and other climate variables, many of which are yet to be fully understood. Z_{500} level on average

exists at around 5.5km above the sea level and the weather systems beneath it steer in the same direction as the winds at the Z_{500} level. A jet stream is created when the geopotential index level changes more rapidly i.e., the contours are close to each other. The contours of the Z_{500} present the troposphere waves with troughs representing cyclones and (ridges anticyclones, which vary rapidly in the mid-latitudes creating a circumpolar jet stream. The short-wave troughs lead to surface cyclones and precipitation. Z_{500} has a strong regulating effect on winter precipitation depending upon the depth of the short-wave troughs. Higher depth of the trough i.e., stronger jets leads to intense precipitation and cyclone. The movement of the precipitation over U.S. is driven by polar jet stream along the coast of Alaska and Canada and moves from west towards east in the northern United States. A southward movement of this polar jet towards southwestern and central U.S. will capture more moisture and bring higher than average precipitation leading to higher streamflow. The third positive significantly correlated region off the coast of Washington State (Figure 3.4) has been identified by Grantz et al. (2005) in high streamflow years to develop winter low-pressure jet streams. This jet stream brings moisture through the southerly winds towards the Sierra Nevada Mountains resulting in increased snowfall and spring streamflow. Low streamflow is followed by decreased snow when cold and dry air is brought by the northwesterly winds.

Precipitation in the southeast U.S. has shown to be influenced by an anomalous trough, which extends from the northern Pacific basin and induces southerly or southwesterly flow anomalies that provide a moisture supply from the eastern Pacific and the Gulf of Mexico. Regions of stable low-pressure anomalies in the North Pacific (Gulf of Alaska), South Central U.S., and North Atlantic (east of the Labrador Sea) have shown

to influence winter precipitation in the southeastern United States (Chen et al., 2014). Literature directs that the spring-summer flows in the U.S. are primarily modulated by location of the pressure gradients driving the wind directions (jet streams). Precipitation has shown to be an immediate response to movement of these jet streams arising from geopotential pressure level differences. Further, Z_{500} has shown to improve the forecasting skill for streamflow and the snow-water equivalent (Grantz et al., 2005; Soukup et al., 2009; Aziz et al., 2011). The Z_{500} anomalies have shown to be consistent with vector winds, and the SST patterns have shown to be a direct response to pressure and winds (Grantz et al., 2005).

SVD results on detrended SST and $Z_{500,}$ and streamflow data were similar when compared with the results using non-detrended data. The Pacific and Atlantic SST and streamflow analysis showed better explanation of variance on detrended data, but the Z_{500} showed decreases in the SCF values for the first mode. The PDO warm phase SCF values decreased when trends were removed, but no differences were observed in the cold phase. The AMO warm phase showed increases in the explanation of variance, but cold phase results were consistent with the non-detrended results. Overall there was no change in identification of regions. Identification of similar regions using raw and detrended data indicated that there was no bias in the analysis introduced due to not detrending the time series, and trends do not mask the underlying variability explained by SST and Z_{500} data.

The temporal expansion series of the first mode of SST and Z_{500} showed higher correlation values obtained from the expansion series, indicating the use of SST and Z_{500} data as important predictor variables for improving the forecasting of streamflows. Heterogeneous correlation maps and correlation values that were generated provided

information about the interactions of the various regions of the U.S. streamflows with significant SST and Z_{500} regions. This current study identified spatial SST and Z_{500} regions that explained the majority of this variability in continental U.S. streamflow.

The SVD of Z_{500} with streamflow and snowpack were in agreement with previous studies (Grantz et al., 2005; Soukup et al., 2009; Aziz et al., 2011). In comparison to hydrologic information only, the inclusion of climate information, particularly the Z_{500}, was shown to substantially improve the forecasts at longer lead times (Grantz et al., 2005; Soukup et al., 2009; Kalra et al., 2013c). Coupled effects of indices influencing each other have been reported in other studies. Moreover, the North Pacific oscillation has been observed to employ a modulating effect on ENSO teleconnections (Gershunov and Barnett 1998).

One limitation of this type of study is the absence of longer instrumental records. Potentially, the use of reconstructed data from tree rings can address this issue (Carrier et al., 2011; 2013); however, it has certain limitations. With land use changes, several unimpaired stations now are influenced by human activities, leading to the revision of the HCDN dataset. Overall, the identification of coupled regions of oceanic-atmospheric predictors and streamflow can help to understand the complex hydrologic response of watersheds to climate variability and potentially improve streamflow forecasts.

3.6. Conclusions

SVD analysis on the streamflows of the entire continental U.S. provides a comprehensive idea about the possible influences of climate variability on a broader spatial scale. The results showed a large incongruity regarding influencing streamflows in

different regions of the continental U.S., where two adjacent basins could have different associations with the oceanic-atmospheric indicators.

In this study, new regions of SST were identified that influence the streamflows in different hydrologic regions of the U.S.; moreover, regions of atmospheric Z_{500} were identified that might be correlated to continental U.S. streamflows. The understanding that the geopotential height index is associated with streamflow is relatively recent, and can improve the accuracy of correlations of the oceanic-atmospheric indicators that influence streamflows. This research contributes to comprehensively understanding the influence of SST and Z_{500} on the continental U.S. streamflow. The analysis led to the generation of a temporal expansion series of SST and Z_{500} (significant SVD mode), which can be used to improve the lead time for streamflow forecasts.

The inclusion of variable modes of the SST and Z_{500} was facilitated by using a long period of Pacific and Atlantic SST and $Z_{500,}$ which desegregated the various multi-decadal phenomena, i.e., PDO and AMO. By means of the temporal expansion series, the Pacific Ocean SVD showed a strong influence of the ENSO and PDO signals. The oceanic-atmospheric indicators showed significant correlations with streamflow.

The results in the current study suggest the persistent relationships of the climate variability and streamflow in different seasons. The teleconnections identified in the study offer possible improvements in forecasting techniques for peak streamflow seasons with one to four month ahead. The inclusion of entire SST and Z_{500} regions avoided the conservative tendency of using pre-defined indices. The major contributions of this work are:

(1) Inclusion of Z_{500} index for analysis of seasonal streamflow variability in the continental United States;

(2) The identification of the Pacific and Atlantic Ocean SST and Z_{500} regions that associate with a longer new improved dataset of unimpaired gauge streamflow stations in the continental United States.;

(3) Comparison of the influence of phases of PDO and AMO SST climate indices on the continental U.S. streamflow, and

(4) Comparison of teleconnections of SST and Z_{500} with the continental U.S. streamflow in the 18 hydrologic regions.

Although, the current study is very comprehensive, still there are some unexplained variances, which cannot be addressed using the approach adopted in the current study. Moreover, not all physical mechanisms of teleconnections are fully understood at this time. The underlying mechanisms resulting in the Atlantic Ocean relationships with streamflow should be further explored. Future research at the local/regional scale is also required to study the climate forcing in detail.

CHAPTER 4: PACIFIC OCEAN SST AND Z_{500} CLIMATE VARIABILITY AND WESTERN U.S. SEASONAL STREAMFLOW

Abstract

A study on the interactions between the Pacific Ocean climate variability and western U.S. streamflow investigated unimpaired streamflows of six major basins of the western U.S., as defined by United States Geological Survey: Rio Grande, Upper Colorado, Lower Colorado, Great Basin, Pacific Northwest, and California. The singular-valued decomposition (SVD) technique was applied on data from 50 years (1960-2010) of sea-surface temperatures (SST), geopotential height index of 500 mbar (Z500), and western U.S. streamflows; the results established a spatio-temporal association for each major hydrologic region in the western U.S. with Pacific oceanic variability. An approach using a three-to-nine month lead time was utilized, i.e., the previous year's July to August SST/Z500, the previous year's October to December SST/ Z500 to predict streamflow for current year spring-summer (April to September), spring (April to June), and summer (July to September) seasons. Significant regions of the Pacific were identified that influence hydrology of the western U.S. The traditional El Niño/Southern Oscillation (ENSO) and Pacific Decadal Oscillation (PDO) regions were identified along with regions over eastern Russia, Canadian British Columbia, and the Hondo region along the east coast of Japan. Most of the streamflow regions showed similar relationships with the Pacific region, except for the Pacific Northwest, which showed opposite relationships compared to other regions. The SVD results showed improvement in correlation values of smaller spatial regions over larger regions, and a lagged response of adjacent hydrologic regions to the same physical indicators; this could be due to topographic and

local factors. The results obtained in this study could be helpful in improving the current forecasting models for water management.

4.1. Introduction

Climate change and its effects on different water systems has been an important research topic for scientists and engineers for the sustainable management of water resources. Water resource managers are responsible for meeting water demands for municipal, irrigation, industries, fisheries, and hydroelectricity use. Furthermore, they need to diligently balance increasing water demands while dealing with the effects of climate variability (Schaake and Kaczmarek, 1979). Therefore, it is important for them to understand various types of climate variability and their potential effects on water resources. These growing requirements have led scientists and engineers to focus on understanding the relationship between climate variability and its hydrologic consequences (Walker and Bliss,1932). With limited inland freshwater sources to rely upon, various techniques have been studied to understand the future of water sources (Nemec and Schaake, 1982; Shrestha et al., 2011; 2012; Qaiser et al., 2011; 2013). Significant research regarding climate indicators and relating them with hydrologic variables has led to a better understanding of the changing water systems (Puri et al., 2011a; 2011b).

In particular, the western U.S. highlands are affected by orographic lifting that results from extreme precipitation and flooding during winter storms (Goodridge, 1994; Kalra et al., 2011). This precipitation is influenced by a widening tropical belt (Seidel et al., 2008) and the northward shift of westerly winds (Archer and Caldeira, 2008). Other changes include reduced snow-cover and earlier snowmelt leading to early spring runoff;

these issues have become a concern for hydrologic scientists as well as water managers. Moreover, forecasts from the Natural Resources Conservation Service and the National Weather Service on the current water supply is based on different statistical techniques, and this forecasts is not available to water managers until four to five days before the beginning of a month (Pagano and Garren, 2006). Although a growing body of literature has established relationships between climate variability and the hydroclimate, there still is a need to develop better models with sufficient lead time for decision making.

Periodic oceanic oscillations, such as the Southern Oscillation Index (SOI), El Niño, La Niña, Pacific Decadal Oscillation (PDO), North Atlantic Oscillation (NAO), Atlantic Multi-Decadal Oscillation (AMO), and other climate indices have been identified (Walker 1924; Philander, 1990; Mantua et al. 1997; Enfield et al., 2001) that have complex relationships with inland hydrology in terms of time and space (Ropelewski and Halpert, 1986,1987; Lamb and Peppler, 1987; Redmond and Koch, 1991; Cayan and Webb, 1992; Hurrel, 1995; Trenberth., 1997; Rodo et al 1997; Kiffney et al., 2002; Gordon and Giulivi, 2004; Ma, 2007). These oscillations have been established to have associations with U.S. hydrology, and affect, for example, precipitation (Gutzler et al., 2002; Goodrich, 2004; Kurtman and Scanion, 2007), snowpack (e.g., Aziz et al., 2010), streamflow (e.g., Barlow et al., 2001), droughts (e.g., Goodrich, 2007; Nigam et al., 2011), and fires (Hessl et al., 2004).

The sea-surface temperatures (SST) influence the air above them, developing pressure variability. The pressure differences at various zones drive wind dynamics and circulatory movements. The SST has been utilized to establish relationships with snowpack, precipitation, streamflow, etc., in western United States. The El Niño

Southern Oscillation (ENSO) is a dominant oceanic phenomenon in the Pacific that affects both sides of the tropics, and its effects on western U.S. hydrology has been prominent (Ropelweski and Halpert, 1986; Redmond and Cayan 1994). It affects the circulation of winds by increasing the winds over North Pacific Ocean; these winds can move further south and bring higher precipitation in the southwest region as well as lower in the northwest region of the western U.S. (Redmond and Koch, 1991; Cayan and Webb, 1992). During El Niño, the Southwest has shown to be wet and the northwest dry; this effect is reversed for La Niña.

The PDO has been identified to have relationships with snowmelt in California (Dettinger and Cayan, 1994), precipitation and streamflow of the Colorado River Basin (Hidalgo and Dracup, 2002; Canon et al., 2007), and the United States in general (Barlow et al., 2001; Tootle and Piechota, 2006). The traditional method of identifying these relationships has been established by using sea-surface temperature (SST) data of a particular index region – for example, the Niño 3.4 region lies in between 5 N–5 S and 120W–170W – and by using statistical methods for correlation with the hydroclimate. Despite the identification of the standard indices of the Pacific in influencing the hydrology (i.e., Niño 3, Niño 4, PDO, and others), these have not been efficient predictors for the hydrology of all the basins of western United States. These indexes mostly are confined to certain locations, and small changes in climate pattern can lead to erroneous correlations with the hydrology and fail to establish consistent relationships.

Aziz et al. (2010) used SST data and snowpack data for the Upper Colorado River Basin (UCRB) to discover a region around 34°N–24°N and 150°E–160°W that was a primary driver of UCRB snowpack and which was not included in the ENSO or PDO

region. Similarly, Lamb et al. (2011) found this region to be a driver of the Colorado River Basin streamflow. Moreover, considering only particular index regions masks the effect that other regions of the Pacific might have with seasonal hydrology of the western U.S. basins. McCabe and Dettinger (2002) studied the relationships among 323 snow water equivalent (SWE) stations in the western U.S., PDO, and ENSO SST; they found that PDO and ENSO represent variability in SWE, but they could not establish relationship successfully of central western U.S. snowpack with either PDO or ENSO. Additionally, the northern and southern subtropical jets both influence the central western U.S., which could be responsible for undermining the effects of other phenomena, such as ENSO or PDO, in these regions. Significantly influential regions of the Pacific vary for each basin in the western U.S., and need to be distinguished.

Geopotential height (HGT) is an atmospheric variable, and its anomalies have shown to be associated with climate variability. Geopotential height is defined as the height of a particular pressure surface above mean sea level in the atmosphere. Studies of the 500-mbar geopotential height (Z_{500}) show the Z_{500} index values to be identified with significant climate variability (Blackmon, 1976; Blackmon et al., 1977). The Z_{500} has been found to be associated with precipitation over Greece (Xoplaki et al., 2000), Europe (Casty et al., 2007), the eastern U.S., (Serreze et al., 1998), and southeastern U.S. (Chen et al., 2014). When used as a predictor in streamflow forecasting models, the Z_{500} has shown a substantially improved capability (Grantz et al., 2005). Mostly, the Z_{500} has shown to improve the short-lead time forecasts (three months) in comparison to SST (Soukup et al., 2009; Aziz et al., 2011). Thus, it is an important variable, representing climate variability, and is finding increasing application in climate-predicting models.

Hydrological variables show random variability, and statistical concepts have long been used to analyze natural phenomena. Statistical methods – such as canonical correlation analysis, principal component analysis, and singular value decomposition – have been used to establish relationships between two spatio-temporal datasets. Out of several methods available, singular value decomposition (SVD) has been tested to be better for identifying relationships between two spatio-temporal fields (Bretherton et al., 1992). Wallace et al. (1992) tested SVD over wintertime SST and Z_{500} anomalies, and found a coupling with regard to their similar patterns. Since then, SVD has been used in numerous applications to identify relationships and spatial patterns of climate variability with precipitation (Wang and Ting, 2000), droughts (Rajagopalan et al., 2000), and streamflow (Tootle and Piechota 2006, McCabe et al., 2014), on larger scale. On a smaller scale, Tootle et al. (2008) used SVD to establish relationships among the Colombian streamflow with the Pacific and Atlantic SSTs. Soukop et al. (2009) used SVD on streamflows of the North Plate River basin, oceanic SST, and atmospheric Z_{500} in order to develop their forecasting techniques. Aziz et al. (2010; 2011; 2012) used SVD to determine regions of significance in snow and streamflow data in the western U.S. and France. One limitation in using SVD on a large-resolution-spatial dataset is that the effect of smaller significant regions was diminished; otherwise, this would be significant at a smaller scale

Unimpaired streamflow as the integrator of various components of the hydrological cycle can be represented as an indicator of climate change. This study focused on evaluating the relationships between the spatio-temporal fields of Pacific ocean SST and atmospheric pressure (Z_{500}) with streamflow in the western U.S. This will

aid in identifying significant associated regions in the Pacific that are not covered under standard climate indices. In this study, SVD was performed on spring-summer streamflows for six major hydrologic regions in the western U.S.; the study used 3-, 6-, and 9-month lead SST and Z_{500} datasets of the Pacific Ocean. Additionally, SVD on each hydrologic region was performed individually, which might result in spatio-temporal relationships with the Pacific that are not evident when global or lower-spatial-resolution data is used. The temporal expansion series obtained from this analysis might be used for generating predictor variables for streamflow forecasting.

4.2. Study Area and Data

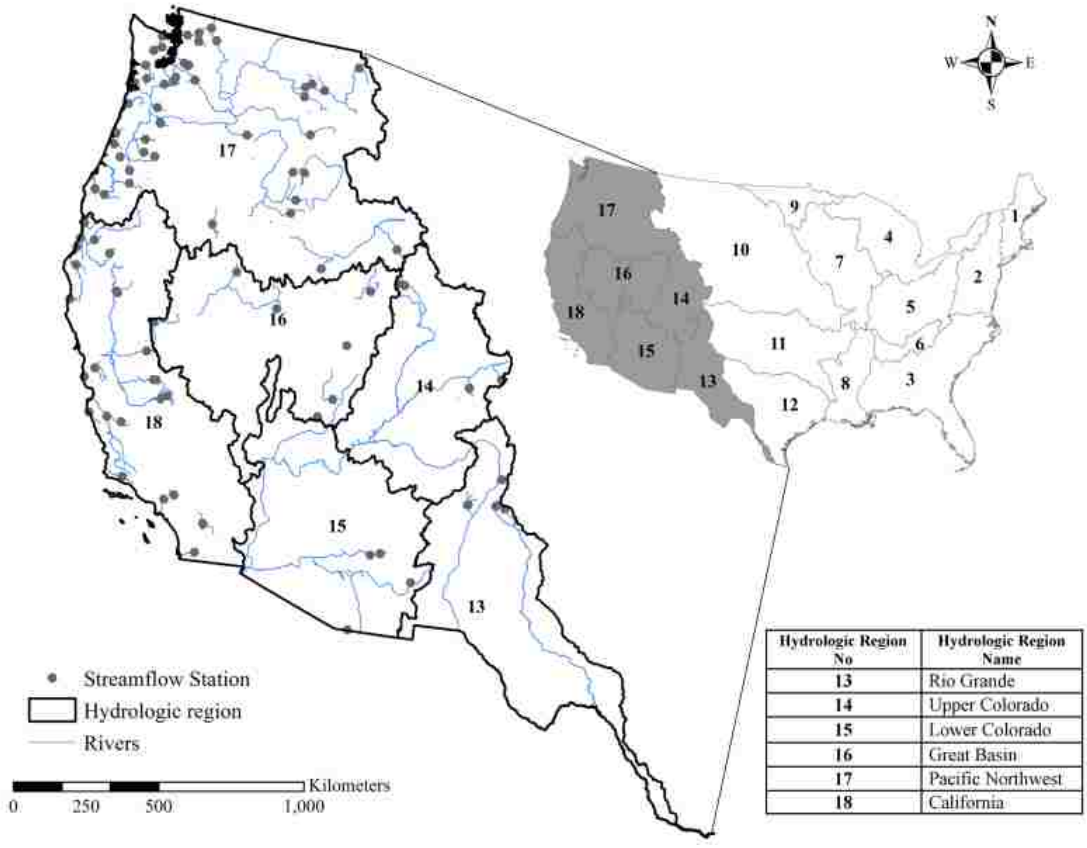

Figure 4.1: Western U.S. hydrologic regions and the unimpaired streamflow stations

U.S. hydrology has been divided into 21 hydrologic regions by United States Geological Survey (USGS). These regions are divided by taking into consideration their unique topography and a major river or a typical water system. The western U.S. is in close proximity to the Pacific Ocean, and is affected by the trade winds and the moisture brought in from the Pacific. The study area consists of six major hydrologic regions of the West, as defined by USGS, namely, Rio Grande (13), Upper Colorado (14), Lower Colorado (15), Great Basin (16), Pacific Northwest (17), and California (18), as illustrated in Figure 1. The Rocky Mountains in Upper Colorado gives this region an alpine-type climate, with maximum precipitation when winter snows feed the rivers in spring by snowmelt. The Rio Grande and Lower Colorado are fed by snowmelt from the Rockies as well, with mild precipitation due to winter and summer storms. The Great Basin mostly has a mid-latitude desert climate, and is bordered by the Sierra Nevada mountains to the west. California's Mediterranean climate results in cool, rainy winters and dry summers. The Pacific Northwest on the west coast has a marine oceanic climate in the west coast; further to the east, it has a semi-arid steppe type of climate. This region receives huge amounts of rainfall through the year except during summers, which are milder.

4.2.1. Streamflow data

Natural fluctuations in the hydroclimate are harder to measure because human interventions, such as reservoirs and other diversions, alter the routes of many river systems. The USGS maintains unimpaired streamflow stations under the Hydro-Climatic Data Network 2009 (HCDN-2009) (Lins, 2009; Falcone et al., 2012). The new HCDN-2009 dataset, which is a revision of the original USGS HCDN network (Slack et al.,

1992), includes the dataset for the revised Geospatial Attributes of Gages for Evaluating Streamflow, Version II (GAGES) (Falcone et al 2010).

The HCDN-2009 has 704 stations within 18 hydrologic regions in the continental United States. In this study, these 704 stations in the network were checked for their spatial attributes and data consistency. Out of the stations in the western U.S. hydrologic regions, only 90 stations had continuous monthly streamflow data for 50 years. Some regions had no stations with longer datasets; for example, the Upper Colorado had no stations with 60 years of data. Thus, the time period for the 90 unimpaired stations in the western United States was set as 50 years (1951 to 2010). The spatial distribution of these stations is shown in Figure 1, and the number of stations in each hydrologic region is given in Table 1. Data for average monthly streamflow for all the stations were obtained from the USGS online database (http://www.usgs.gov/)

Table 4.1: Number of Unimpaired Stations per Each Hydrologic Region in the Western United States

Hydrologic Region No	Hydrologic Region Name	Number of Unimpaired Stations
13	Rio Grande	4
14	Upper Colorado	4
15	Lower Colorado	4
16	Great Basin	7
17	Pacific Northwest	46
18	California	25
13-18	Total Western U.S.	90

4.2.2. Sea Surface Temperatures (SST)

The monthly data for sea-surface temperature used in this study was obtained from the Physical Sciences Division of the National Oceanic and Atmospheric Administration's Earth System Research Laboratory (NOAA ESRL) The oceanic SST

data consisted of average monthly values for a 2˚ X 2˚ grid cell (Smith and Reynolds, 2004). In this study, the region used for Pacific Ocean SST was 100E to 80W and 30S to 70N. This consisted of a gridded set of 3,432 SST cells in the Pacific Ocean.

4.2.3. 500-mbar Geopotential Height Index (Z_{500})

The monthly Z_{500} index data available from the NOAA Physical Sciences Center was used. The dataset is a product of the reanalysis project by the National Centers for Environmental Prediction and the National Center for Atmospheric Research, commonly known as NCEP/NCAR Reanalysis (Kalnay et al., 1996), a 40-year project. The Z_{500} data are available in 2.5˚ X 2.5˚ degree grid cells. The region used for gridded data of the Pacific Ocean Z_{500} was from 100E to 80 W and 70N to 30S. The Pacific region involved 2,988 grid cells.

4.3. Methods

4.3.1. Singular Valued Decomposition

For finding the spatial-temporal relationships between two fields, SVD has emerged as a suitable tool. This paper provides a brief description of this method; for a more detailed discussion, readers are referred to Bretherton et al. (1992) and Strang (1998). SVD is a factorization of a matrix that results in three matrices (i.e., $M = USV^T$). The orthogonal matrices, U and V, consist of generated singular vectors commonly referred to as the left and right matrices. The center diagonal matrix, S, consists of non-zero singular values of the original matrix. In general, the first three modes (i.e., the first three diagonal elements in S) must explain a significant portion of the variance for SVD in order to be statistically applicable (Newman and Sardeshmukh, 1995). Due to issues

related to statistical inference, caution must be observed when making assertions about the cause of the relationships based on the results of SVD, as is required when using most statistical tools. In order to apply SVD, the matrices of standardized anomalies for the variables should be generated. The temporal resolution and size must match among all matrices in order to apply SVD; however, the spatial characteristics do not need to be similar. Cross-covariance matrices are found among the matrices, and are decomposed using SVD.

A square covariance fraction (SCF), or percentage, was calculated by taking the square of each singular value and dividing it by the sum of all the squared singular values. The SCF value, which indicates how much variability can be explained by the model used, has been found to explain variability better than other models (Bretherton et al., 1992). The singular values that were generated – when squared and divided by the count of one variable data point times the count of a second variable data point – resulted in the normalized square covariance (NSC) (Wallace et al., 1992; Bretherton et al., 1992).

Similar to the SCF, the NSC value is a comparative measurement of the decomposition by SVD, with a lower value explaining a better fit. The column vectors contained in the left and right matrices are projected onto the original standardized anomaly matrices and vice versa. The i^{th} projected vector is the temporal expansion series for the i^{th} mode. Only the modes that correspond to a SCF of 10% or greater are retained. Finally, in order to find the relationship between the two fields, the temporal expansion series are correlated with the original standardized anomalies of variables.

4.3.2. Statistical approach

Flows for spring (April to June, AMJ), summer (July to September, JAS), and spring-summer (April to September, AMJJAS) were averaged for 50 years (1961 to 2010). The SST monthly data was averaged for 50 years for July to September (JAS) from 1960 to 2009, and October to December (OND) from 1960 to 2009. Over the streamflow, both a 6-to-9-month lead of JAS SST and Z_{500} and a 3-6-month lead of OND SST and Z_{500} was achieved, useful in evaluating a spatial lead-lagged effect on the streamflow.

SVD is used to evaluate the spatio-temporal relationships among the Pacific SST and Z_{500} and the western U.S. streamflow. First, SVD decomposed the JAS and OND Pacific SST and Z_{500} with spring-summer, spring, and summer streamflows for the entire western U.S. streamflow. This was repeated for the stations of each hydrologic region, using the Pacific SST and Z_{500}. Thus, a lag of 9, 6, and 3 months for SST and Z_{500} over the seasonal streamflows was used to develop the relationships. Heterogeneous correlation values were used to generate heterogeneous correlation maps, which were used to analyze the significant regions at $p \leq 0.10$. The temporal expansion series obtained from SVD was used to derive correlation values by means of typical correlation techniques that can establish the relationships between oceanic-atmospheric variability and streamflow variability. The correlation values were developed between seasonal SST/Z_{500} (JAS and OND) and the seasonal streamflows (AMJJAS, AMJ, and JAS). All the computations were performed using Matlab 2013a which has inbuilt SVD function. SVD, within Matlab, is implemented through geometric mechanism quantified through QR < 75 for convergence and identification of singular eigenvectors.

4.4. Results

Section 4.4.1 discusses the SVD results of the SST and Z_{500} with streamflow of entire western U.S. followed by Sections 4.4.2 to 4.4.7, which discuss the SVD results of the SST and Z_{500} with streamflows of individual hydrologic regions. The SST and Z_{500} heterogeneous correlation maps for JAS and OND variabilities (Figures 4.2 to 4.10), depicting significant correlated regions at $p \leq 0.10$, identify the spatio-temporal relationships for the first mode. The regions identified for positive (negative) SST/ Z_{500} had direct relationships with the positive (negative) streamflow regions such that increases (decreases) in streamflow were related to increases (decreases) in SST/Z_{500}, and vice versa. Table 4.2 gives the SCF values for the first mode from the SVD analysis for all the hydrologic regions. The number of Pacific grid cells (SST/ Z_{500}) showing significant relationships with the streamflow were for the first mode.

4.4.1. Western U.S. Regions

Figures 4.2, 4.3, and 4.4 present the heterogeneous correlation maps generated from spatially plotting the significant correlated streamflows and values of the Pacific region obtained from SVD results of all the 90 stations taken in combination. The SVD of Pacific Ocean SSTs and western U.S. streamflows resulted in squared covariance fractions (SCF) of 68.5% for the first mode and 10.44% for the second mode for JAS SST and AMJJAS streamflows. Fifty-four streamflow stations showed significant correlation with the Pacific JAS SST, and 2091 (61%) SST grid cells showed significant correlation with the streamflows. SVDs for the JAS SST and AMJ streamflows resulted in SCFs of 68% and 12.5%, respectively, for the first and second modes. Moreover, 2110 (61%) number of SST cells showed significant correlation, and 52 streamflow stations

showed significant correlation with the Pacific JAS SST. The JAS SST and JAS streamflow SVDs resulted in SCFs of 54.89% and 22.19% for first and second modes, with 44 stations showing significant correlation; 2068 (60%) grid cells showed significant correlation.

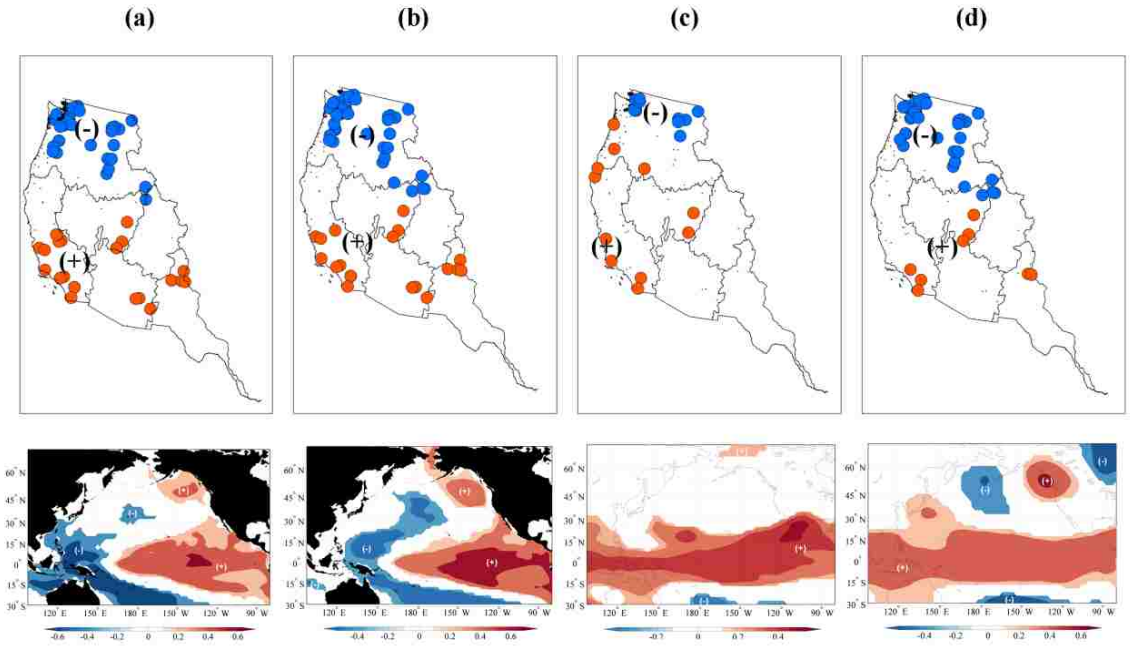

Figure 4.2: Heterogenous correlation maps representing the results of SVD of AMJJAS streamflows with (a) JAS SST, (b) OND SST, (c) JAS Z_{500}, and (d) OND Z_{500}

The correlation values obtained for the streamflow ranged from |0.002| to |0.62| for AMJJAS, |0.009| to |0.636| for AMJ, and |0.004| to |0.53| for JAS streamflows. The OND SST and AMJJAS SVD resulted in an SCF of 73.6% in the first mode; 56 stations showed significant correlation and 2120 (62%) stations showed significant correlation. The OND SST and AMJ streamflow SVD resulted in 73.6% for the first mode. 54 streamflow stations had significant correlation with SST, and 2111 (62%) Pacific SST grid cells showed significant correlation with the streamflow. The JAS streamflow and OND SST SVD resulted in an SCF of 60.12% in the first mode and 20.33% in the second

mode, with 47 stations showing significant correlation with SST and 2061 (60%) SST grid cells showing significant correlation with the streamflows. The correlation values obtained for the streamflows ranged from |0.01| to |0.66| for AMJJAS, |0.001| to |0.67| for AMJ, and |0.01| to |0.58| for JAS streamflows.

The SVD on Z_{500} and 90 streamflow stations resulted in an SCF of 54.74% for the first mode and 25.09% for the second mode for JAS Z_{500} and AMJJAS streamflows. Twenty-two stations showed significant correlation with Z_{500}. Out of 2988 Z_{500} grid cells in the Pacific, 1450 (49%) Z_{500} grid cells showed significant correlation with the streamflow. The JAS Z_{500} and AMJ streamflow SVD resulted in SCFs of 50.9% and 29%% for the first and second modes, respectively, with 38 stations showing significant correlation with Z_{500} and 1434 (48%) Z_{500} grid cells showing significant correlation with the streamflow.

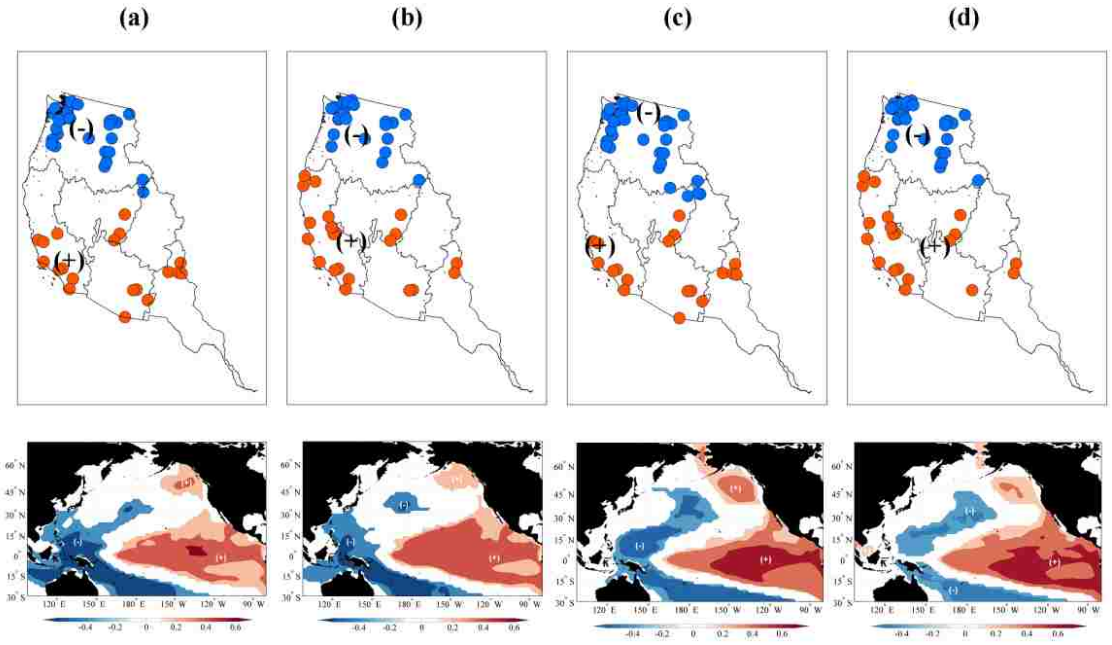

Figure 4.3: Heterogenous correlation maps representing the results of SVD of (a) JAS SST with AMJ streamflow, (b) JAS SST with JAS streamflow, (c) OND SST with AMJ streamflow, and (d) OND SST with JAS streamflow

The JAS Z_{500} and JAS streamflow SVD resulted in SCFs of 58.47% and 14.21% and 11.13%, respectively, for the first three modes. Twenty stations showed significant correlation with Z_{500} and 1648 (55%) Z_{500} grid cells showed significant correlation with the streamflow. The correlation values obtained for the streamflow ranged from |0.001| to |0.39| for AMJJAS, |0.004| to |0.36| for AMJ, and |0.007| to |0.38| for JAS streamflow. The OND Z_{500} and AMJJAS SVD resulted in an SCF of 66.7% for the first mode and 16.8% for the second mode. Forty-one stations showed significant correlation with Z_{500} grid cells and 1873 (63%) Z_{500} grid cells showed significant correlation with the

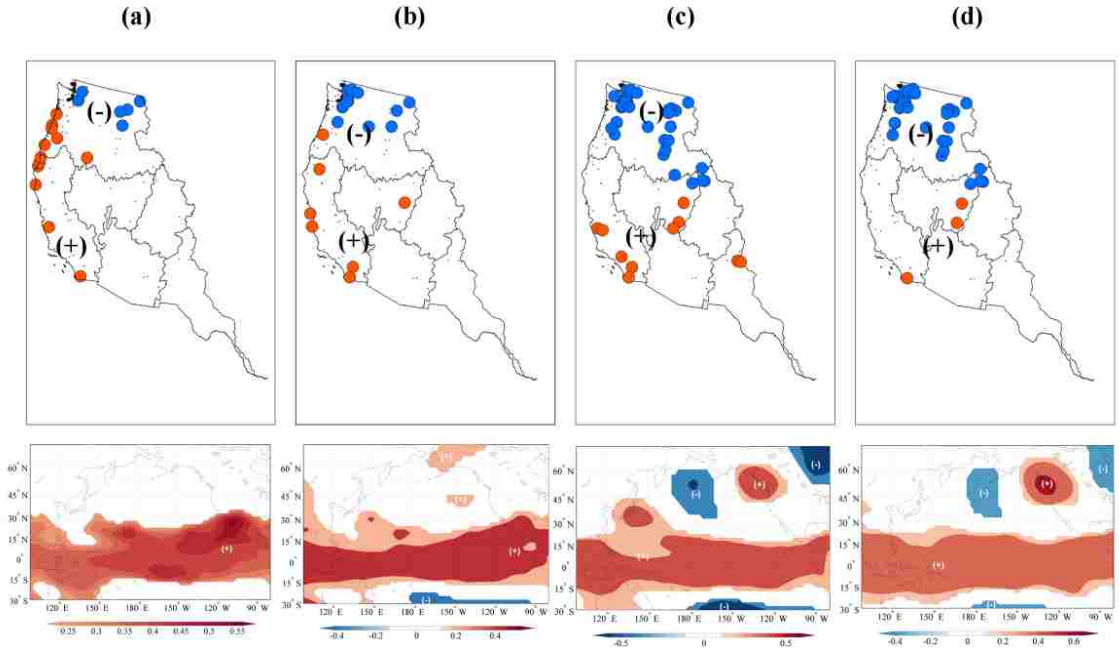

Figure 4.4: Heterogenous correlation maps representing the results of SVD of (a) JAS Z_{500} with AMJ streamflow, (b) JAS Z_{500} with JAS streamflow, (c) OND Z_{500} with AMJ streamflow, and (d) OND Z_{500} with JAS streamflow

streamflow. SVD on OND Z_{500} and the AMJ streamflow resulted in an SCF of 63.94% for the first mode and 17.17% for the second mode, with 42 stations showing significant correlation with Z_{500} and 1822 (61%) Z_{500} grid cells showing significant correlation with the streamflow. The JAS streamflow and OND Z_{500} SVD resulted in an SCF of 62.9% in

the first and 19.45% in the second mode for R13 to R18 regions. Thirty-four stations showed significant correlation with Z_{500} and 1766 (59%) Z_{500} grid cells showed significant correlation with the streamflow. The correlation values obtained for the streamflow ranged from |0.002| to |0.63| for AMJJAS, |0.002| to |0.65| for AMJ, and |0.006| to |0.54| for JAS streamflow.

Table 4.2: The Square Covariance Fraction (Percent) from First mode of SVD analysis.

Hydrologic Region			Streamflow seasons		
	Pacific Indices↓		Spring-Summer (AMJJAS)	Spring (AMJ)	Summer (JAS)
R13-18	SST	JAS	69	68	55
		OND	74	74	60
	Z_{500}	JAS	55	51	58
		OND	67	64	63
R13	SST	JAS	91	93	79
		OND	93	95	79
	Z_{500}	JAS	81	84	66
		OND	92	94	74
R14	SST	JAS	69	69	71
		OND	72	73	69
	Z_{500}	JAS	63	59	69
		OND	80	75	84
R15	SST	JAS	80	93	60
		OND	90	96	57
	Z_{500}	JAS	75	90	77
		OND	83	91	48
R16	SST	JAS	73	71	73
		OND	71	70	72
	Z_{500}	JAS	68	66	62
		OND	66	66	59
R17	SST	JAS	80	78	62
		OND	86	84	72
	Z_{500}	JAS	60	53	69
		OND	86	86	82
R18	SST	JAS	74	71	78
		OND	76	73	81
	Z_{500}	JAS	75	73	72
		OND	75	72	76

The SCF values and the heterogeneous correlation maps of the combined SVD analysis for six regions showed an overlay of the individual hydrologic-region SVDs with

the Pacific (Table 4.2). The significant SST regions in the Pacific Ocean that correspond to streamflow mostly were similar for both 6-month and 3-month time periods. The ENSO and PDO regions both were highlighted, and showed strong correlations with the streamflow. The northwest U.S. – i.e., the Pacific Northwest region – behaved differently from other regions, showing negative correlation with the ENSO region (highlighted in Figure 4.2 and 4.3) but directly proportional to the SST regions east of the Asian continent. The region close to the Gulf of Alaska was significantly related with the streamflows as well as to the individual basins.

4.4.2. Individual Regions

4.4.2.1. Region 13 (Rio Grande)

Figure 4.5 shows the heterogeneous correlation maps for the first mode for Rio-Grande stations and the Pacific region. The SVD analysis with JAS SST and AMJJAS streamflow for Region 13 resulted in an SCF of 90.9% for the first mode. Out of 3432 SST grid cells in the Pacific Ocean, 1016 (30%) SST grid cells showed significant correlation with the streamflows of Rio Grande. The JAS SST and AMJ streamflow SVD resulted in SCF of 93% for the first mode, with 860 (25%) SST grid cells showing significant correlation. The JAS SST and JAS streamflow resulted in SCF of 79.3% for the first mode and 14.2% for the second mode, with 901 (26%) SST grid cells showing significant correlation with the streamflow. The correlation values obtained for the streamflow were high in the range from |0.42| to |0.53| for AMJJAS, |0.39| to |0.51| for AMJ, and |0.12| to |0.49| for JAS.

The OND SST and AMJJAS streamflow SVD resulted in an SCF of 93.2% for the first mode, with 1676 (49%) SST grid cells showing significant correlation. The OND

SST and AMJ streamflow SVD resulted in an SCF of 94.6% for the first mode, with 1583 (46%) SST grid cells showing significant correlation. The OND SST and JAS streamflow SVD resulted in an SCF of 79.3% for the first mode and 14.23% for the second mode, with 1348 (39%) SST grid cells showing significant correlation. The streamflow correlation values ranged from |0.41| to |0.56| for AMJJAS, |0.45| to |0.55| for AMJ, and |0.08| to |0.48| for JAS.

The SVD analysis for JAS Pacific Z_{500} and AMJJAS streamflow resulted in an SCF of 80.84% for the first mode and 14.6% for the second mode. Out of the 2988 Z_{500} grid cells, 205 (7%) showed significant correlation with the streamflow for the first mode. The JAS Z_{500} and AMJ streamflow SVD resulted in SCF of 83.5% for the first mode and 12.53% for the second mode, with 203 (7%) grid cells showing significant correlation. The JAS Z_{500} and JAS streamflow SVD resulted in SCF of 65.9% for the first mode and 22.8% for the second mode, with only 45 (2%) grid cells showing significant correlation (Figure 5 c). The correlation values obtained for the JAS Z_{500} on the streamflow ranged from |0.40| to |0.56| for AMJJAS, |0.38| to |0.56| for AMJ, and |0.26| to |0.48| for JAS.

The SVD analysis between OND Z_{500} and AMJJAS streamflow resulted in SCF of 92.3% for the first mode, with 1126 (38%) Z_{500} grid cells showing significant correlation. The OND Z_{500} and AMJ streamflow SVD resulted in an SCF of 94.32% for the first mode, with 1040 (35%) Z_{500} grid cells showing significant correlation. The OND Z_{500} and JAS streamflow SVD resulted in an SCF of 73.6% for the first mode and 17.38% for the second mode, with 494 (17%) cells showing significant correlation. The

correlation values for 3 to 6 month lead of OND Z_{500} on streamflow ranged from |0.44| to |0.58| for AMJJAS, |0.44| to |0.56| for AMJ, and |0.27| to |0.46| for JAS streamflow.

In Rio Grande region, all four stations showed significant correlation with the SST and Z_{500} indicators. The 6-9 months' lead of the JAS SST with AMJ and JAS streamflows showed the streamflow to be positively correlated with the SST in the eastern Pacific region and negatively correlated with the western Pacific region above the equator, also known as the Hondo region. The 3-month to 6-month lead of OND SST with AMJ and JAS streamflow showed a variation in the SST regions. The negatively correlated region grew wider from JAS to OND SST seasons, and a region closer to the northwestern U.S. moved farther west towards 45N and 150W from AMJ to JAS streamflow seasons.

The ENSO region continued to show significant correlations, and moved westward from Niño 3 to Niño 3.4 in OND, compared with JAS SST (Figure 4.5b). The Z_{500} correlation maps, however, showed two significant regions for the 6- to 9-month lead time from JAS Z_{500} with respect to AMJ and JAS streamflows. There was one positively-correlated region from 30N to 45N and 180W and another negatively-correlated region above 60N and in-between 150W to 180W. However, the 3- to 6-month lead time of OND Z_{500} and AMJ and JAS streamflow showed five significant regions in the Pacific region. These regions mostly were confined to the northern part above 30N; in between 120E to 150E, 150E, and 150W; and in-between 120W to 90W (Figure 4.5d).

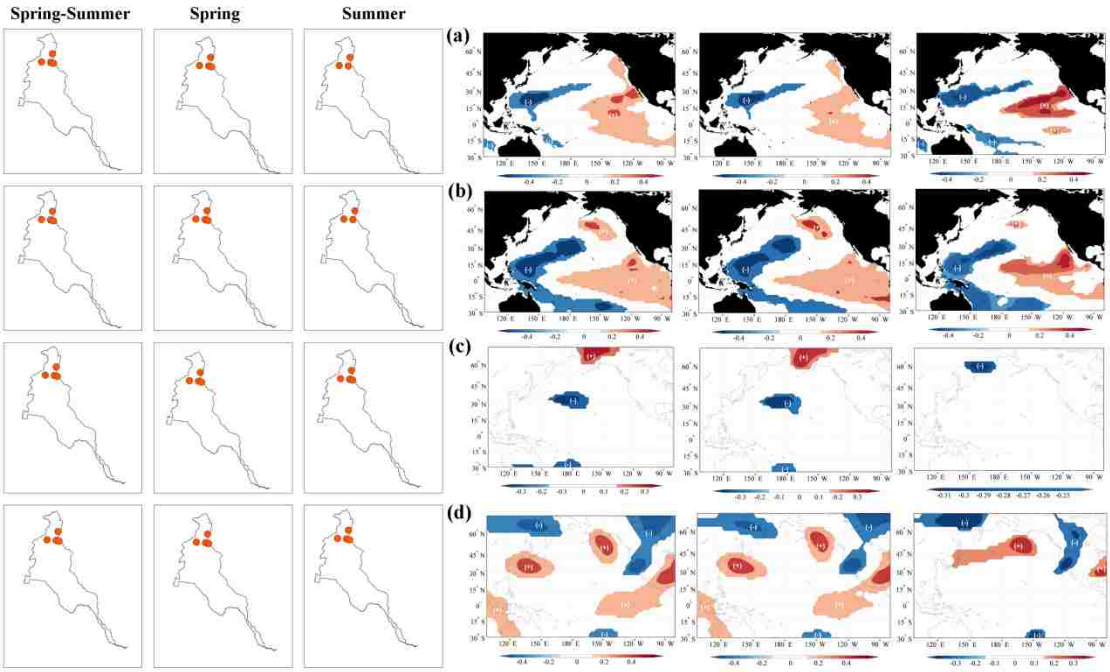

Figure 4.5: Heterogenous correlation maps of spring-summer (AMJJAS), spring (AMJ), and summer(JAS) streamflow of Rio Grande (Region 13) with (a) JAS SST, (b) OND SST (c) JAS Z_{500}, (d) OND Z_{500} for first mode of SVD

4.4.2.2. Region 14 (Upper Colorado)

The heterogeneous correlation maps for the first mode of the SVD results are represented in Figure 6. The SVD analysis between JAS SST and AMJJAS streamflow of Upper Colorado resulted in an SCF of 68.7% for the first mode and 21.7% for the second mode, with 566 (16%) SST grid cells showing significant correlation. The SVD between JAS SST and AMJ streamflow resulted in an SCF of 69.4% for the first mode and 21.7% for the second mode, with 676 (20%) SST grid cells showing significant correlation. The JAS streamflow SVD resulted in an SCF of 70.6% for the first mode and 21.1% for the second mode, with 320 (9%) grid cells showing significant correlation. The 6- to 9-month lead time of JAS SST with the streamflow resulted in correlation values that ranged from |0.07| to |0.48| for AMJJAS, |0.005| to |0.47| for AMJ, and |0.29| to |0.48| for JAS. The OND SST and AMJJAS streamflow SVD resulted in an SCF of 71.9% for the first mode

and 21.1% for the second mode, with 760 (22%) grid cells showing significant correlation. The OND SST and AMJ streamflow SVD resulted in an SCF of 72.6% for the first mode and 19.9% for the second mode, with 839 (24%) SST grid cells showing significant correlations. The OND SST and JAS streamflow SVD resulted in an SCF of 68.7% for the first mode and 25.9% for the second mode, with 360 (10%) SST grid cells with significant correlation. The correlation values obtained for the 3- to 6-month lead OND SST on the streamflow ranged from |0.10| to |0.53| for AMJJAS, |0.09| to |0.53| for AMJ, and |0.26| to |0.49| for JAS.

The SVD analysis between JAS Pacific Z_{500} and AMJJAS streamflow resulted in an SCF of 62.9% for the first mode and 29.6% for the second mode, with 572 (19%) Z_{500} grid cells with significant correlation. The SVD analysis between JAS Z_{500} and AMJ streamflow resulted in an SCF of 58.8% and 35.25% for the first and second modes, respectively, with 1101 (37%) Z_{500} grid cells with significant correlation. The SVD between JAS SST and JAS streamflow resulted in an SCF 69.4% and 20.5% in the first and second modes, respectively, with only 43 (1%) of cells significantly correlated with the streamflow for the first mode. The 6- to 9-month lead time resulted in correlation values ranging from |0.05| to |0.26| for AMJJAS, |0.04| to |0.23| for AMJ, and |0.05| to |0.24| for JAS streamflow. The SVD analysis of OND Z_{500} and AMJJAS streamflow resulted in an SCF of 80.2% and 14.9% for the first mode, with 582 (19%) cells with significant correlation. The SVD analysis of OND Z_{500} and AMJ streamflow resulted in an SCF of 75.37% and 19.98% for the first and second modes, respectively, with 650 (22%) cells with significant correlation. The SVD analysis with OND Z_{500} and JAS streamflow resulted in an SCF of 84.02% and 11.06% for the first and second modes,

respectively, with 308 (10%) Z_{500} cells with significant correlation. The 3- to 6-month lead of OND Z_{500} resulted in correlation values of the streamflows, which ranged from |0.09| to |0.49| for AMJJAS, |0.06| to |0.50| for AMJ, and |0.16| to |0.40| for JAS.

In the Upper Colorado region, the correlation values for JAS streamflow compared to AMJ streamflow for SST with better results. The El Niño region was negatively correlated with the streamflow (Figures 4.6a and b). The SST regions showing connections with spring and summer streamflow differed, however. The summer (JAS) streamflow showed relationships with the Hondo region. However, the OND SST region indicated a new region that was positively correlated with the streamflows at around 45N and in between 150W to 180W; another was negatively associated region near the west coast of Canada at around 45N and 130W to 140W. The results for the Z_{500} and streamflows did not identify streamflow stations that had significant relationships with JAS Z_{500}; however, OND Z_{500} showed significant influence. The Z_{500} regions identified in OND were similar to the SST regions identified in OND for the Upper Colorado Basin, with the negatively-correlated region over western Canada and the positively-correlated, newly identified region below the coast of Alaska.

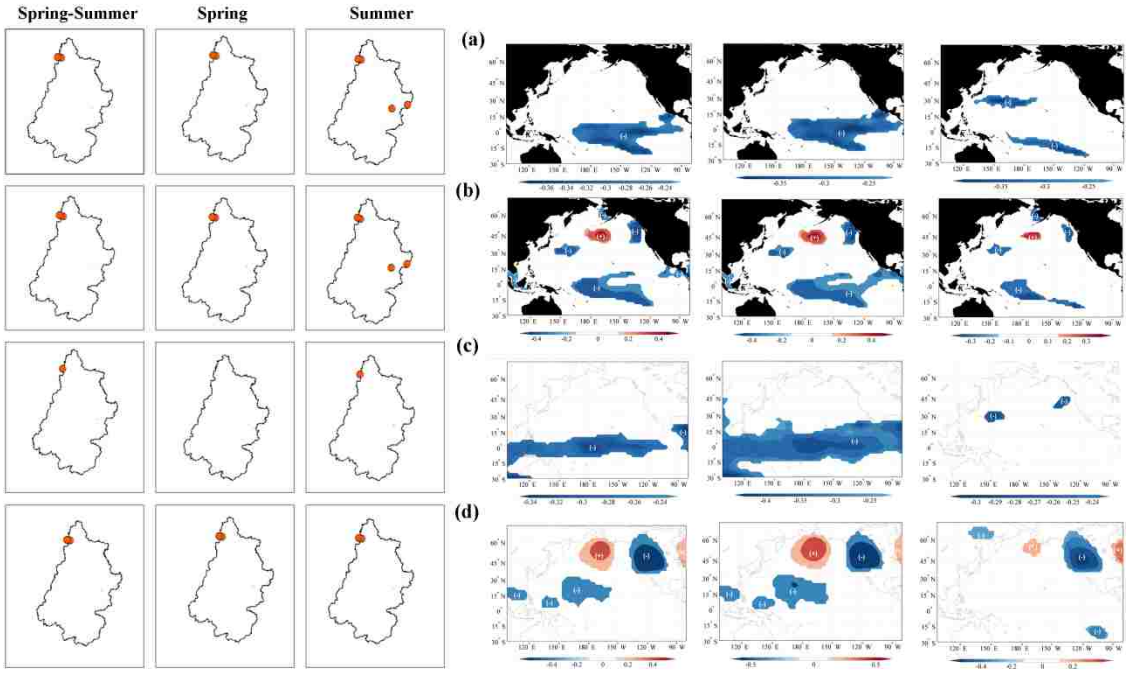

Figure 4.6: Heterogenous correlation maps of spring-summer (AMJJAS), spring (AMJ), and summer(JAS) streamflow of Upper Colorado (Region 14) with (a) JAS SST, (b) OND SST (c) JAS Z_{500}, (d) OND Z_{500} for first mode of SVD

4.4.2.3. Region 15 (Lower Colorado)

Figure 4.7 shows the heterogenous correlation maps for the first mode of the Lower Colorado and the significant Pacific SST and Z_{500} regions. The SVD analysis with JAS Pacific SST and AMJJAS streamflow resulted in an SCF of 80.46% and 15.41% for the first and second modes, respectively, with 1653 (48%) SST grid cells showing significant correlation. The JAS SST and AMJ streamflow SVD explained 92.98% of the variability for the first mode, with 1547 (45%) SST grid cells with significant correlation. The SVD for JAS SST and JAS streamflow resulted in an SCF of 60.39% , 27.75%, and 10.87% for first , second, and third modes, respectively, with only 513 (15%) SST grid cells with significant correlation for the first mode. The correlation values obtained using the temporal expansion series for JAS SST ranged from |0.005| to |0.59| for AMJJAS,

|0.35| to |0.59| for AMJ, and |0.12| to |0.45| for JAS streamflow. The SVD analysis of OND SST and AMJJAS streamflow resulted in SCF of 90.15% for the first mode; 1750 (51%) SST grid cells showed significant correlation. The OND SST and AMJ streamflow resulted in an SCF of 95.73% for the first mode, with 1820 (53%) grid cells showing significant correlation. The OND SST and JAS streamflow SVD analysis resulted in an SCF of 57.19% for first mode , 23.53% for second mode, and 18.02% for the third mode, with 650 (19%) grid cells showing significant correlation. The correlation values of the 3- to 6-month lead time for OND SST and the streamflow ranged in between |0.09| to |0.64| for AMJJAS, |0.39| to |0.64| for AMJ, |0.09| to |0.33| for JAS streamflow.

The SVD on JAS Pacific Z_{500} and AMJJAS streamflow resulted in SCF of 74.60% and 18.81% for the first and second modes, respectively, with 666 (22%) grid cells showing significant correlation. The SVD analysis for AMJ streamflow with JAS Pacific Z_{500} resulted in an SCF of 90.3% for the first mode; 675 (23%) Z_{500} grid cells had significant correlation. The JAS Z_{500} and JAS streamflow SVD resulted in SCF of 77.14% for the first mode and 15.58% for the second mode, with 408 (14%) Z_{500} grid cells showing significant correlation. The correlation values for the streamflow ranged from |0.20| to |0.49| for AMJJAS, |0.30| to |0.45| for AMJ, and |0.17| to |0.28| for JAS. The OND Z_{500} and AMJJAS streamflow SVD resulted in SCF of 83.47% and 10.45% for the first and second modes, with 542 (18%) Z_{500} grid cells showing significant correlation. The OND Z_{500} and AMJ streamflow SVD resulted in SCF of 91.21% for the first mode, with 629 (21%) Z_{500} grid cells showing significant correlation. The OND Z_{500} and JAS streamflow SVD resulted in SCF of 48.43% for the first mode and 31.12% for the second mode, with only 32 (1%) grid cells showing significant correlation. The 3- to

6-months lead time SVD for Z_{500} resulted in streamflow correlation values that ranged from |0.20| to |0.63| for AMJJAS, |0.47| to |0.70| for AMJ, and |0.13| to |0.29| for JAS.

The Lower Colorado region showed strong correlations with both SST and Z_{500} regions; moreover, the spring (AMJ) streamflow explained around 90% of its spring variability. The strong relationships between the spring streamflow and Pacific variability were validated from the high correlation values. The JAS and OND SST showed similar influence on the streamflow, indicating that a 6-month lead was capable of explaining the streamflow variability. The SST regions identified with significant relationships showed the prominence of ENSO and PDO signals. However, for summer (JAS) streamflow, these signals were poor. The streamflow had a positive correlation with the El Niño region and negative correlation with the region east of the Asian continent (Figures 7a and b). The significant JAS Z_{500} regions identified with the spring (AMJ) streamflow showed negative correlation, and the JAS Z_{500} region identified with summer streamflow showed positive correlation (Figure 4.7c). The OND Z_{500} regions identified with spring (AMJ) streamflow mostly involved five major clusters with two positively correlated clusters, a negative region over eastern Russia, another over Central Canada, and the third negative region over the southwestern U.S. (Figure 4.7d). However, the summer streamflow showed only one station that had a direct correlation with a small region over 15N and in-between 150W to 120W (Figure 4.7d).

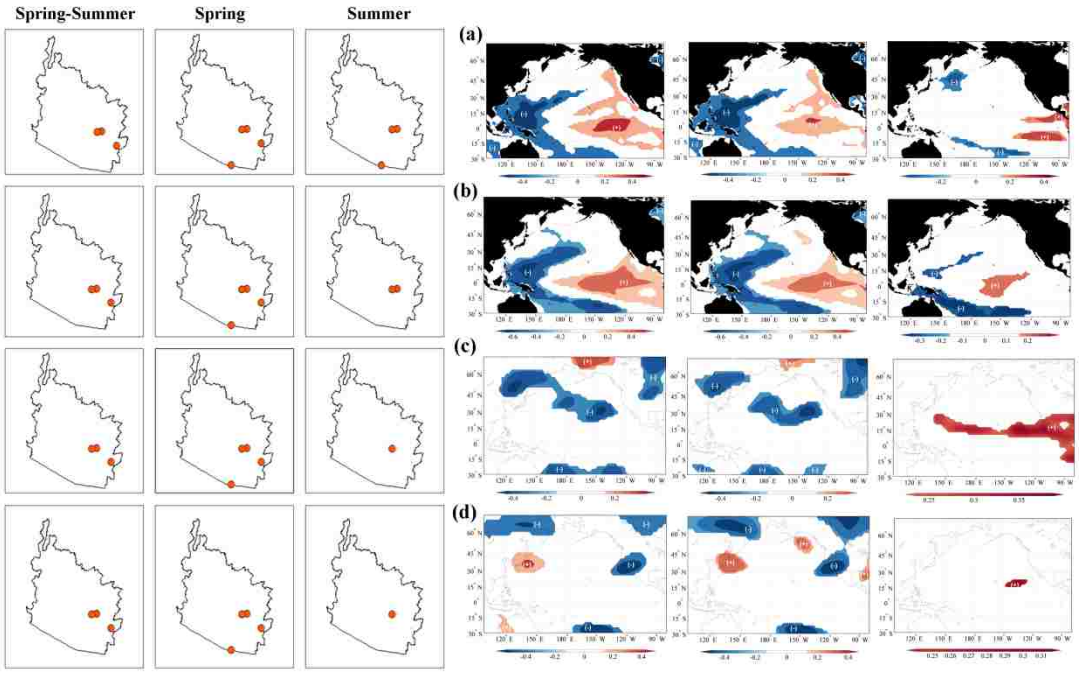

Figure 4.7: Heterogenous correlation maps of spring-summer (AMJJAS), spring (AMJ), and summer (JAS) streamflow of Lower Colorado (Region 15) with (a) JAS SST, (b) OND SST (c) JAS Z_{500}, (d) OND Z_{500} for first mode of SVD

4.4.2.4. Region 16 (Great Basin)

The heterogeneous maps derived from the first mode of the SVD results for Great Basin are shown in Figure 4.8. The SVD analysis between JAS Pacific SST and AMJJAS streamflow resulted in an SCF of 73.07% for the first mode and 16.09% for the second mode, with 1362 (40%) SST grid cells showing significant correlation. The SVD analysis between JAS Pacific SST and AMJ streamflow resulted in an SCF of 71.14% for the first mod and 16.84% for the second mode, with 1448 (42%) SST grid cells showing significant correlation. The SVD analysis between JAS SST and JAS streamflow resulted in an SCF of 72.98% for the first mode and 13.60% for the second mode, with 1104 (32%) SST grid cells showing significant correlation for the first mode. The correlation values for streamflow, obtained by using the temporal expansion series, ranged from

|0.06| to |0.55| for AMJJAS, |0.02| to |0.52| for AMJ, and |0.05| to |0.56| for JAS. The OND SST and AMJJAS streamflow SVD resulted in an SCF of 71.47% for the first mode and 20.82% for the second mode; 1465 (43%) SST grid cells showed significant correlation with the Great Basin streamflows. The OND SST and AMJ SVD resulted in an SCF of 69.71% and 21.40% for the first and second modes, respectively; 1597 (47%) SST grid cells showed significant correlation. The SVD between OND SST and JAS SVD resulted in an SCF of 72.34% for the first mode and 17.07% for the second mode, with 1096 (32%) SST grid cells showing significant correlation. The 3- to 6-month lead time resulted in streamflow correlation values that ranged from |0.01| to |0.51| for AMJJAS, |0.06| to |0.50| for AMJ, and |0.05| to |0.53| for JAS.

The SVD between Pacific JAS Z_{500} and AMJJAS streamflow resulted in an SCF of 67.58% for the first mode and 19.86% for the second mode, with 307 (10%) Z_{500} cells showing significant correlation. The JAS Z_{500} and AMJ streamflow SVD resulted in an SCF of 65.98% and 22.96% for the first and second modes, respectively, with 303 (10%) Z_{500} grid cells showing significant correlation. The JAS Z_{500} and JAS SVD analysis resulted in an SCF of 62.46% and 22.03% for the first and second modes, respectively, with 442 (15%) Z_{500} grid cells showing significant correlation. The correlation values obtained using the JAS Z_{500} temporal expansion series and the Great Basin streamflow ranged from |0.01| to |0.35| for AMJJAS, |0.01| to |0.32| for AMJ, and |0.04| to |0.38| for JAS streamflow. The SVD analysis for OND Z_{500} and AMJJAS streamflow resulted in an SCF of 65.89% for the first mode and 25.97% for the second mode, with 1214 (41%) Z_{500} grid cells showing significant correlation. The SVD analysis for OND Z_{500} and AMJ streamflow resulted in an SCF of 65.96% and 24.93% for the first and second modes,

respectively, with 1224 (41%) Z_{500} grid cells showing significant correlation. The OND Z_{500} and JAS streamflow resulted in an SCF of 58.94% and 31.44% for the first and second modes, respectively, with 1203 (40%) Z_{500} grid cells showing significant correlation. The correlation values obtained for OND Z_{500} and streamflows, using the temporal expansion series from the SVD results, ranged from |0.04| to |0.45| for AMJJAS, |0.04| to |0.44| for AMJ, and |0.003| to |0.44| for JAS.

The results of SVD for the Great Basin were consistent in all seasons. The significant SST regions for the 6-month JAS lead and 3-month OND lead were similar to spring (AMJ) streamflow (Figures 4.8a and 4.b). Similarly, the 9-month JAS SST lead and 6-month OND SST lead for summer (JAS) streamflow in the Great Basin identified similar regions (Figure 8a and b). The SVD for Z_{500} as well as spring and summer streamflow showed consistent results with JAS and OND Z_{500}, indicating that a 9-month lead over streamflows for JAS SST will produce similar results to a 6-month lead; a 6-month lead over streamflow for OND Z_{500} will produce results similar to a 3-month lead. The regions around the equator showed a positive correlation with the streamflow for JAS and OND Z_{500}. Two clusters of negative correlation with the streamflows were seen over northeastern Russia and the northwest U.S. The correlation values obtained from the SST were better than Z_{500} for the Great Basin.

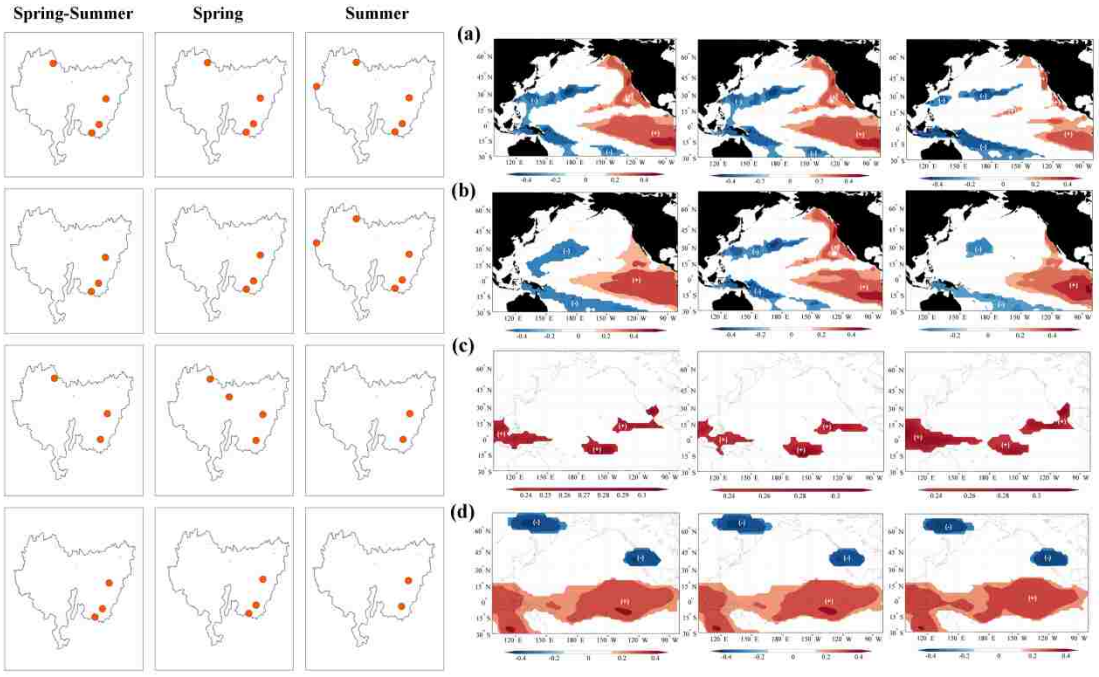

Figure 4.8: Heterogenous correlation maps of spring-summer (AMJJAS), spring (AMJ), and summer(JAS) streamflow of Great Basin (Region 16) with (a) JAS SST, (b) OND SST (c) JAS Z_{500}, (d) OND Z_{500} for first mode of SVD.

4.4.2.5. Region 17 (Pacific Northwest)

The results of the SVD analysis of the Pacific region (SST and Z_{500}) with Pacific Northwest region are represented in Figure 4.9 as heterogeneous correlation maps. The SVD analysis between Pacific JAS SST and AMJJAS streamflow resulted in an SCF of 79.81% for the first mode, with 1617 (47%) SST grid cells showing significant correlation. The JAS SST and AMJ streamflow resulted in an SCF of 78.09% for the first mode and 10.35% for the second mode, with 1623 (47%) SST grid cells showing significant correlation. The SVD for JAS SST and JAS streamflows resulted in an SCF of 61.74% and 20.86% for the first and second modes, respectively, with 1185 (35%) SST grid cells showing significant correlation. The correlation values obtained for the streamflow through the SVD ranged from |0.01| to |0.65| for AMJJAS, |0.02| to |0.65| for

AMJ, and |0.002| to |0.59| for JAS. The OND SST and AMJJAS streamflow resulted in an SCF of 85.81% for the first mode, with 1908 (56%) SST grid cells showing significant correlation. The OND SST and AMJ streamflow resulted in an SCF of 84.31% for the first mode, with 1972 (57%) SST grid cells showing significant correlation. The OND SST and JAS streamflow resulted in an SCF of 72.05% and 15.73% for the first and second modes, with 1546 (45%) SST grid cells showing significant correlation. The correlation values of SST information, obtained for streamflows with 3- to 6-month lead times, ranged from |0.04| to |0.70| for AMJJAS, |0.03| to |0.69| for AMJ, and |0.001| to |0.62| for JAS.

The SVD analysis between Pacific JAS Z_{500} and AMJJAS streamflow resulted in an SCF of 60.36% and 27.89% for the first and second modes, respectively, with 1331 (45%) Z_{500} grid cells showing significant correlation. The SVD for JAS Z_{500} and AMJ streamflow resulted in an SCF of 53.16% and 34.35% for the first and second modes, respectively, with 1372 (46%) Z_{500} grid cells showing significant correlation. The SVD for JAS Z_{500} and JAS streamflow resulted in an SCF of 68.94% and 14.56% for the first and second modes, respectively, with 1283 (43%) Z_{500} grid cells showing significant correlation. The 6- to 9-month lead times resulted in correlation values ranging from |0.01| to |0.43| for AMJJAS, |0.003| to |0.42| for AMJ, and |0.01| to |0.40| for JAS. The SVD for OND Z_{500} and AMJJAS streamflow resulted in an SCF of 85.78% for the first mode, with 1811 (61%) grid cells showing significant correlation. The SVD between OND Z_{500} and AMJ streamflows resulted in an SCF of 85.52% for first mode, with 1762 (59%) Z_{500} grid cells showing significant correlation. The SVD between OND Z_{500} and JAS streamflows resulted in SCF of 82.48% for the first mode with 1740 (58%) Z_{500} grid

cells showing significant correlation. The 3- to 6-month lead Z_{500} gave correlation values ranging from |0.01| to |0.65| for AMJAAS, |0.002| to |0.67| for AMJ, and |0| to |0.56| for JAS.

The Pacific Northwest showed significant relationships with the Pacific SST. The significant SST regions identified in the Pacific Ocean showed strong ENSO and PDO signals. The El Niño region showed opposite correlation with the streamflow, whereas the PDO regions showed positive correlations with the streamflow. The region near the Gulf of Alaska – at around 150W and 45N to 60N – showed opposite correlations with the streamflow of Pacific Northwest (Figure 4.9a). However, the OND SST showed the well-identified Hondo region to correlate directly with the Pacific Northwest streamflows (Figure 9b). The effect of the PDO signals on summer streamflow was faint. The Z_{500} regions that showed that the most significant relationships with the Pacific Northwest streamflow were located in the equatorial belt. Stations of the Pacific Northwest streamflow in the northern part of the region showed a direct correlation with the equatorial JAS Z_{500}; the southern part of the region showed an opposite correlation with the equatorial JAS Z_{500}. On the other hand, the OND Z_{500} showed an opposite correlation to the streamflows of Pacific Northwest. Two other significant regions were identified in the OND Z_{500}, one with a direct correlation with the streamflows at 180W and in between 30N and 60N and another over the coast of western Canada in British Colombia. Notable variations for JAS and OND in the influence over the Pacific Northwest streamflows were important when considering lead times.

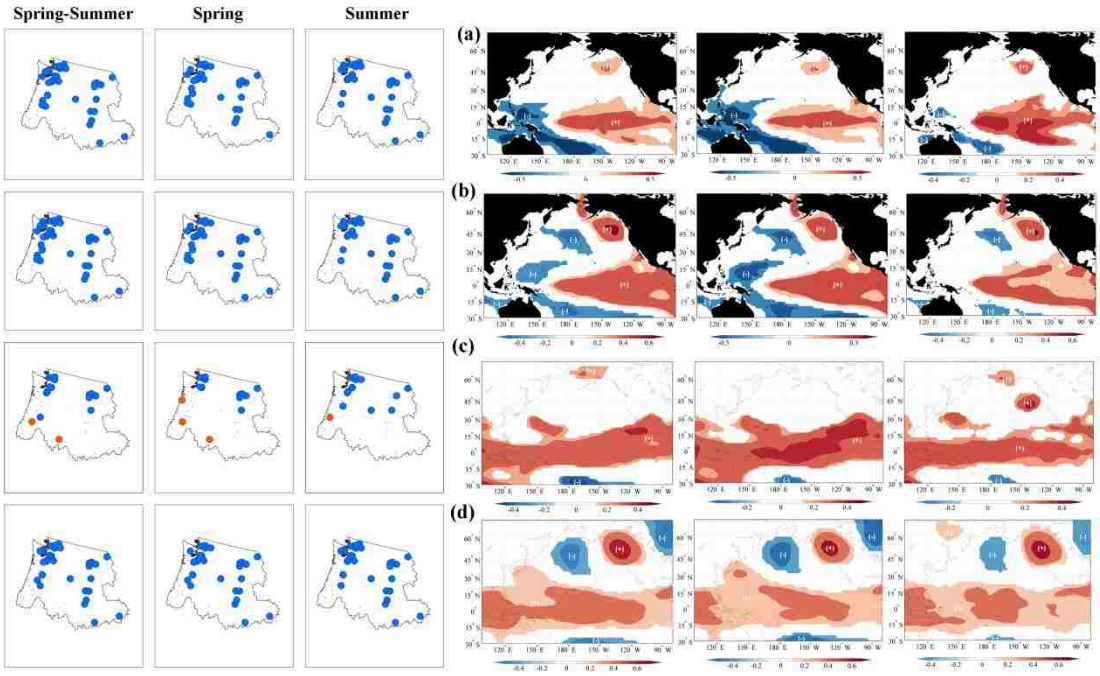

Figure 4.9: Heterogenous correlation maps of spring-summer (AMJJAS), spring (AMJ), and summer(JAS) streamflow of Pacific Northwest (Region 17) with (a) JAS SST, (b) OND SST (c) JAS Z_{500}, (d) OND Z_{500} for first mode of SVD

4.4.2.6. Region 18 (California)

The heterogeneous correlation maps generated from the SVD results for California streamflow are shown in Figure 4.10.The SVD analysis of Pacific JAS SST and AMJJAS streamflow resulted in an SCF of 74.17% for the first mode and 16.73% for the second mode, with 1167 (34%) grid cells showing significant correlation. The SVD of AMJ streamflow with JAS SST resulted in an SCF of 70.98% and 19.65% in the first and second modes, respectively, with 1218 (35%) SST grid cells showing significant correlation. The JAS streamflow with JAS SST resulted in an SCF of 78.07% for the first mode; 1307 (38%) SST grid cells showed significant correlation. The correlation values obtained for California streamflow from a lead time of 6 to 9 months for JAS SST ranged between |0.07| to |0.58| for AMJJAS, |0.08| to |0.58| for AMJ, and |0.12| to |0.56| for JAS.

The SVD for OND SST and AMJJAS streamflow resulted in an SCF of 76.13% and 14.44% for the first and second modes, with 1188 (35%) grid cells showing significant correlation. The SVD for OND SST and AMJ streamflow resulted in an SCF of 72.67% for the first mode and 17.41% for the second mode, with 1302 (38%) SST grid cells showing significant correlation with the streamflows in the first mode. The SVD analysis for OND SST and JAS streamflow resulted in an SCF of 81.02% for the first mode; 1284 (37%) SST grid cells showed significant correlation with the streamflow. The 3- to 6-month lead time for the OND SST temporal expansion series resulted in generating streamflow correlation values ranging from |0.05| to |0.58| for AMJJAS, |0.02| to |0.58| for AMJ, and |0.12| to |0.56| for JAS.

The SVD analysis between Pacific JAS Z_{500} and AMJJAS streamflow resulted in an SCF of 75.14% for the first mode and 16.95% for the second mode, with 610 (20%) Z_{500} grid cells with significant correlation. The SVD analysis for JAS Z_{500} and AMJ streamflow resulted in an SCF of 73.45% and 17.26% for the first and second modes, respectively, with 698 (23%) Z_{500} grid cells showing significant correlation. The SVD analysis for JAS Z_{500} and JAS streamflow resulted in an SCF of 72.29% and 13.08% for the first and second modes, respectively, with 293 (10%) Z_{500} grid cells having significant correlation with the streamflows. The correlation values resulting from the temporal expansion series ranged from |0.14| to |0.33| for AMJJAS, |0.13| to |0.33| for AMJ, and |0.10| to |0.38| for JAS. The SVD for OND Z_{500} and AMJJAS streamflow resulted in an SCF of 74.51% and 13.53% for the first and second modes, with 577 (19%) Z_{500} grid cells showing significant correlation. The SVD for OND Z_{500} and AMJ streamflow resulted in an SCF of 72.21% and 15.41% for the first and second modes,

with 663 (22%) grid cells showing significant correlation. The SVD analysis of OND Z_{500} and JAS streamflow resulted in an SCF of 75.58% for the first mode, with 564 (19%) Z_{500} grid cells showing significant correlation. The correlation values for streamflow obtained using the temporal expansion series ranged from |0.14| to |0.49| for AMJJAS, |0.10| to |0.48| for AMJ, and |0.17| to |0.50| for JAS.

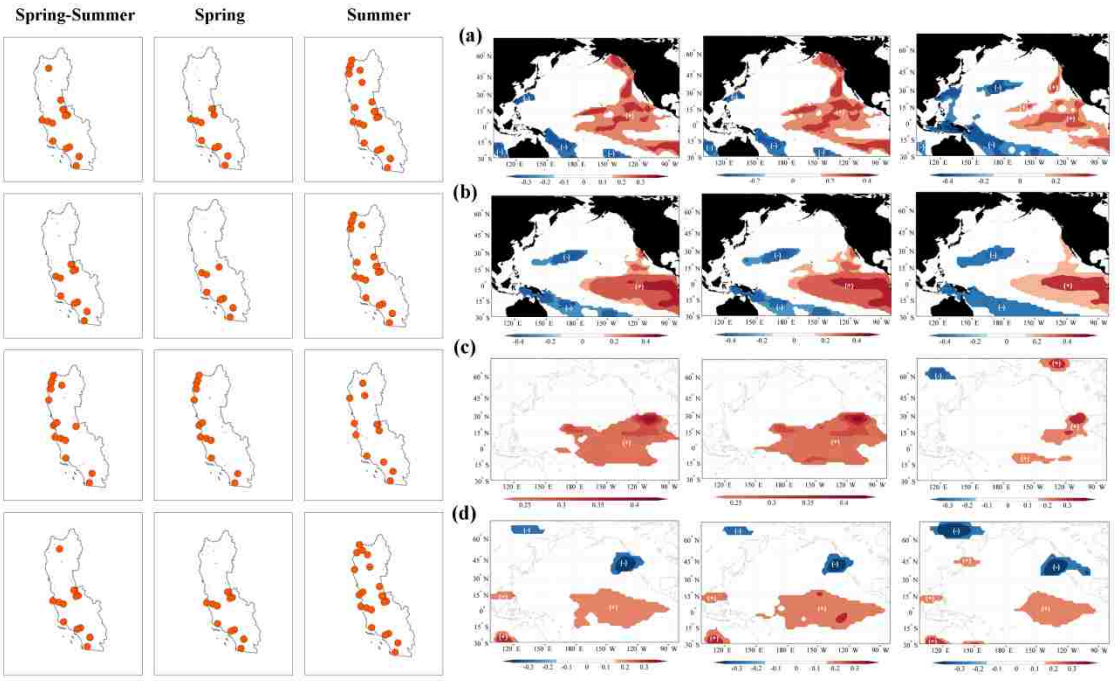

Figure 4.10: Heterogenous correlation maps of spring-summer (AMJJAS), spring (AMJ), and summer(JAS) streamflow of California (Region 18) with (a) JAS SST, (b) OND SST (c) JAS Z_{500}, (d) OND Z_{500} for first mode of SVD

The Californian streamflows were positively influenced by the SST of the El Niño region and negatively influenced by the PDO region and the Hondo regions. The Z_{500} regions that showed significant correlation were located in the equatorial belt towards the American continents. However, the JAS Z_{500} and summer (JAS) streamflow resulted in three SST regions that could influence the streamflows. A negatively-correlated region at

120E and 60 N was observed. Furthermore, the OND Z_{500} around the equator and the El Niño region showed to be positively correlated with the streamflow. Two negatively-correlated regions with the Californian streamflow were identified, 1) one was over the eastern Russian region that was similar to the JAS Z_{500} and summer (JAS) streamflow region and 2) another over the western Canadian coast of British Columbia. The correlation values for JAS streamflow were higher, compared to the ones for the AMJ streamflow of California.

4.5. Discussion

The results of the SVD analysis helped to identify the spatio-temporal relationships between the different basins of the western U.S. and the Pacific Ocean. Among the six basins, the SVD of the Rio Grande showed one of the highest SCFs (Table 4.2). The correlation values obtained for summer (JAS) streamflow were lower than spring (AMJ) and spring-summer AMJJAS) streamflows. The streamflow in the Rio Grande during spring was shown to be influenced mostly by the Pacific Ocean by means of ENSO and PDO, both in terms of spatial and temporal variations (Khedun et al., 2012).

The Upper Colorado showed the least SCF among the basins (Table 4.2). The ENSO had little effect on Upper Colorado hydrology (McCabe and Dettinger, 2002; Aziz et al., 2010; Lamb et al., 2011). On the other hand, the Lower Colorado showed very good SCF (Table 4.2) and correlation values for spring (AMJ) streamflows. Winter precipitation as snowfall is the major water source of Upper Colorado; as snowmelt, it flows into the Lower Colorado Basin. This might be a reason for the lagged response of the streamflow of the Upper Colorado to Pacific variability. The SST regions identified to

have significant relationships for the Lower Colorado were identified in Rio Grande as well (Section 4.4.2.1).

The significant regions identified in the Pacific for the Great Basin were consistent for the streamflow seasons over up to a 9-month lead time of information, which could be used for long-lead forecasting in this region. The Pacific Northwest showed an opposite correlation with the Pacific, except for theZ_{500} in the equatorial region for the JAS season. The Niño 3.4 (Trenberth, 1997) SST region, located along the equatorial Pacific Ocean (5°S–5°N, 170°–120°W), showed to have strong relationships with the individual basins. In addition, the PDO, which is bounded in northern Pacific Ocean (poleward of 20° north) (Mantua et al., 1997), was a strong indicator of hydrologic variability.

The Hondo region – identified in various studies as located at around 150 E to 160 W and 24N to 34N; and which influences the hydrology of Japan, Asia, and the western U.S. (Zhang et al., 1997; Wang and Ting, 2000; Rajgopalan et al., 2000; Tootle and Piechota, 2006; Aziz et al., 2010; Aziz et al., 2011; Soukup et al., 2009; Lamb et al., 2011; Kalra et al., 2013c) – was identified to influence each of the basins in terms of seasonal SST or Z_{500}. The lead times associated with this region and each basin were an important factor while considering streamflow forecasting.

Physical explanations for this region is that it is an important pathway for different air streams (e.g., the East Asian Jet Stream) to divide and move into particular directions, ultimately entering the western U.S. envelope (Zhang et al., 1997). Due to teleconnections of this region that are identified with the western U.S., pressure differences in this region when SST is cooler can cause a cyclonic cell near the western

U.S., enhancing subtropical jet and returning moist air from the subtropical Pacific Ocean. Another region identified over northeastern Russia and eastern Asia, as explained Zhang et al. (1997), is a region of storm tracking that enters the East Asian Jet Stream.

The movement of the winds and the pathways they take has been the main cause of precipitation in various forms, from low to intensified rain or snow. A jet stream is created when the geopotential index level changes more rapidly, i.e., the contours are close to each other. The contours of the Z_{500} represent the troposphere waves, with troughs representing cyclones and ridges that indicate anticyclones, which vary rapidly in the mid-latitudes and create a circumpolar jet stream. Z_{500} has a strong regulating effect on winter precipitation, depending upon the depth of the short-wave troughs.

The movement of the precipitation over U.S. is driven by a polar jet stream along the coast of Alaska and Canada. Precipitation has shown to be an immediate response to movement of these jet streams, arising from differences is the level of geopotential pressure. A southward movement of this polar jet towards the southwestern and central U.S. captures more moisture, creating higher than average precipitation, which leads to higher streamflow. The Cascade Range, the Sierra Nevadas, and the Rocky Mountains pick up most of the moisture from these jet streams by orographic effects, resulting in most of the precipitation in the American West.

In this study, the region over the Gulf of Alaska and British Columbia, Canada, has shown prominence for a 3-month lead of Z_{500} for all the basins. This region is also identified by Grantz et al. (2005), and winter low-pressure jet streams developed in this region results in high streamflow years. By means of southerly winds, these jet streams bring moisture towards the Sierra Nevada mountains, resulting in increased snowfall and

spring streamflow (Grantz et al., 2005). Low streamflow is followed by decreased snow when cold and dry air is brought by northwesterly winds. Z_{500} for this region has shown to improve the forecasting skill for streamflow and the snow-water equivalent (Grantz et al., 2005; Soukup et al., 2009; Aziz et al., 2011).

The results of the combined analysis were mostly similar to the results of the individual analysis in most aspects, but also differed in some aspects. For example, the region around eastern Russia, which was prominent for each region individually, was not shown as significant in the combined analysis. This directs the research team to use individual basins for SVD analysis in order to find relationships, since a comprehensive analysis would dampen the effect one grid region might have on other hydrological regions having different spatial attributes. The SCF values for individual regional analyses at a smaller scale improved in the combined analysis at a larger scale (Table 4.2).

This study acknowledges the bias that is produced when global datasets are used to find relationships between climate signals and hydrologic variables, such as streamflow (Rajgopalan et al., 2000; McCabe and Wolock, 2014). This work shows improvement over studies that were based on a larger spatial scale (Tootle et al., 2006; Aziz et al., 2010), thus addressing the bias that is generated by using global datasets. Using the correlation values developed in this study, future research may focus on the use of a streamflow forecast model that is non-parametric or regression-based and having long-lead times (Hastenrath et al. 1984, Tootle and Piechota 2001, Kalra et al., 2013).

4.6. Conclusions

The SVD analysis between the Pacific SST/ Z_{500} and the western U.S. streamflow helped in understanding the inter-relationships in the various; furthermore, it allowed comparison of the anomalies. The combined SVD of the six regions provided a comprehensive understanding of the complex teleconnections; moreover, the SVDs for the individual hydrologic region highlighted the inter-basin differences of responses to climate variability. The loss of noise (i.e., counterfeit regions) in the predictand dataset was possible by using smaller spatial regions as well as the inclusion of the entire Pacific region. Most importantly, the use of entire SST/ Z_{500} datasets of the Pacific over predefined regions of other indices (e.g., Niño 3.4) removed the biases or errors that are associated with small spatial change over the time period being considered.

The mapped spatial pattern identified in this study showed that the traditional ENSO-like and PDO-like patterns – along with other regions in the North Pacific – to be important factors. The overall contributions of this work are:

1) Inclusion of the new HCDN-2009 dataset, which has updated information of the unimpaired streamflow stations.
2) Identification of regions in the Pacific that were included in the ENSO or PDO regions but which are significantly related to the basins in the western United States.
3) Comparison of SVD analyse of larger spatial scale to those of smaller spatial scale, which indicated that the analysis of smaller regions should be preferred over larger regions for purposes of decision making.
4) Comparison of relationships of adjacent basins of the western U.S. with the Pacific region showed lagged response of certain basins to the same physical areas of

atmosphere and ocean; this could be due to differences in wind movements resulting from topography or local factors.

This work is important to determine improved results over global patterns and to avoid randomness in SVD results. Although several relationships are explained through this approach, future research efforts may focus on providing a physical explanation of the results by examining Z_{500} geopotential height, winds, and global circulation phenomena.

CHAPTER 5: CONTRIBUTIONS AND RECOMMENDATIONS

5.1. Summary

With rapid development and limiting resources, climate variability increases the uncertainty of available resources, of which water is a vital component. For the U.S. which has a diverse climate and many river systems, water resources are stressed by increasing demands of agriculture, industries, energy, and domestic needs; it becomes necessary to understand the factors contributing to streamflow variability. Oceanic-atmospheric indices have complex relationships with the hydrological cycle. Making better water management decisions depends on our understanding of the future of which climate change is an indispensable variable. Predicting the future starts from understanding the past changes and interactions of hydroclimatic variables. This study provides better understanding of the streamflow variability and factors affecting it in the continental United States.

In this study, statistical approaches were mostly used to address the three research questions. The study successfully identified the types of changes in the past years in the continental U.S. streamflows and their relationships with oceanic-atmospheric variability. A comprehensive study of the continental U.S. was conducted, followed by a focus on the western U.S., which is mostly influenced by Pacific Ocean variability. Unimpaired streamflow volumes and comparisons of different basins were key elements in this study. Three tasks were performed to address the research questions and their hypotheses posed in the study.

The first task investigated Research Question #1: What were the changes in the hydrology of the continental U.S. in the past years and how do they compare temporally

and spatially? It was hypothesized that unimpaired streamflows, which have the least anthropogenic interference, can best represent climate variability, and the phase changes of the multidecadal climate indices should be captured by streamflow. It was also hypothesized that as streamflow distributions did not have a definite pattern, using non-parametric tests would best represent streamflow variability. Research Question#1 was addressed by using two non-parametric statistical tests, Mann-Kendall and Pettitt, for 240 unimpaired streamflow stations in the continental United States. Streamflow volumes for 60 years starting from 1951 to 2010 were obtained from the USGS. The stations obtained were categorized into 18 major watershed regions as defined by the USGS. The persistence characteristic present in streamflows was addressed while analyzing the changes by incorporating variations accounting for short term and long-term persistence in the Mann-Kendall test. The change in terms of quantity was calculated through a Thiel-Sen trend-slope of the time series. The Pettitt test was able to identify the streamflow shifts, which had a major change point, as well as identifying the shift year. Grouping the stations according to the regions and using a global field significance Walker test helped in generalizing the results for each hydrologic region. A comparison of results among the regions helped in identifying the regions that had experienced significant higher, lower, or no changes.

The second task addressed Research Question #2: How do the oceanic-atmospheric indices affect (associate with) the streamflows of the continental United States? It was hypothesized that the oceanic-atmospheric indices affect the hydrologic cycle by influencing the winds, moisture, and ultimately the precipitation. It was also hypothesized that using a lead-time methodology, the interaction between the oceanic-

atmospheric indices and streamflow variability can be explored. In addition, it was hypothesized that different basins of the continental U.S. streamflow had significant associations with the oceanic-atmospheric indices, but geography would determine the differences. Research Question #2 was addressed by using the factorization technique known as singular valued decomposition to provide a 1-4 month lagged relationship between fall and winter (SST/Z_{500}) with the spring-summer streamflow volumes of 60 years in the continental United States. Further, SVD was applied to Pacific and Atlantic SST of the warm and cold phases of the multidecadal PDO and AMO, and heterogeneous correlations with the streamflows was obtained. The SVD analysis provided information about regions in the Pacific and Atlantic Oceans that are highly correlated to the continental U.S. streamflows and vice versa. The temporal expansion series obtained from the SVD may be used as input for forecasting models. The inclusion of the warm and cold phases of the PDO and AMO helped in identifying the possible coupled effects of the particular climate indices on streamflows. The identified oceanic regions showed signals of the ENSO and PDO regions. AMO, however was not seen as a significant influencing factor. The Walker test for global significance was used to determine the significant basins, which showed that geopotential height influenced the central U.S. streamflow more. The Z_{500} was showed better relationships with the streamflow variability than SST.

The final Research Question #3 How do the oceanic-atmospheric indices play a role in affecting streamflow in adjacent basins, and, can the lead time of streamflow forecasting be improved? It was hypothesized that western U.S. streamflow is strongly affected by Pacific Ocean variability, and depending on the precipitation of the region,

the association of the oceanic-atmospheric indices and streamflow has a lagged relationship. This study addressed research Question #3 by using singular valued decomposition on 3-9 month lead time Pacific sea surface temperature and pressures with western U.S. streamflow. Fifty years of 90 unimpaired spring-summer streamflow data for six hydrologic regions of the western U.S. were used. Additional SVDs were performed on each hydrologic region individually. It was observed that the relationships improve when analysis of individual basins was performed. The Z_{500} was shown to have better relationships to streamflow than sea-surface temperature at shorter lead times. Different basins showed strong relationships with similar regions in the Pacific but at different lag times. These results confirmed the third hypothesis.

5.2. Contributions

While previous authors have performed substantial work in these areas, the major contributions of this research are as follows. First, this research is the first of its kind that uses the HCDN-2009 stations, a new dataset of unimpaired streamflows for the continental United States. This work **identifies the significant changes that the continental U.S. streamflows have experienced in the past 60 years considering long term and short term persistence,** which has not been accounted for in previous studies. This is also the first use of the Pettit test to identify step changes and periods for streamflow at the continental U.S. scale.

Second this work presents **a comprehensive study that uses SVD on the Pacific and Atlantic SST and Z_{500} with the continental U.S. seasonal streamflow**. Use of 1-4 month lead time explains the significant anomalies between streamflow and oceanic-atmospheric variability.

The third contribution is in the use of geopotential height as an indicator for streamflow variability. **This is the first study to use the gridded Z_{500} data with continental U.S. streamflow variability.** Several studies have used correlation techniques to identify relationships between sea surface temperatures and streamflows. Finally, this study helps in improving our **understanding of the lagged effects of climate indices over seasonal streamflow**. The use of several lag times helps in removing the noisy regions and identifying some new regions in the Pacific Ocean, that have significant influences.

5.3. Limitations

Though this study makes a comprehensive attempt to answer the above described research questions listed, certain limitations are inevitable. The major dataset used was unimpaired streamflow. Due to anthropogenic influences, the major river systems have been controlled through diversions. This study tries to capture the lowermost streamflow station in a river, but some heavily regulated rivers could be missed due to non-availability of unimpaired data for some subwatersheds. This study started with 704 unimpaired stations initially, but due to unavailability of continuous data for longer timescales, many stations were removed. In order to capture the multidecadal oscillations properly, longer time periods provide better results. The limitation of hydrologic time series is that the results are dependent on the temporal window for which data are available. The time window being studied could be part of a longer periodic phenomenon that is not yet completely identified.

Singular valued decomposition is a technique that will nearly always find a relationship between two datasets, even if it is by pure chance. Therefore, one must be

cautious about the noise that arises in the results. Though statistical tests provide an understanding of the changes and relationships, the underlying physical mechanisms should be understood to interpret the results.

5.4. Recommendations for future work

The study presented is able to evaluate the significant changes in the continental U.S. streamflow and successfully identify the spatio-temporal relationships between streamflow variability and oceanic-atmospheric indices. However, many aspects that this work has brought to attention can be improved in terms of accuracy or future applications. Future researchers working on similar aspects of hydroclimate should consider the following:

1) This study analyzed the types of changes in streamflow over past years and explored the association of streamflow variability with climate variability. Future research should focus on understanding the underlying dynamics of these systems that explain the physical mechanisms.

2) Though a seasonal approach was used in this study for identifying the streamflow and climate relationships, only the peak streamflow seasons of spring and summer were used. Future research should include the low flow seasons, which are also important from a water management perspective.

3) One limitation of this study was unavailability of data for longer periods. Using tree ring or paleo reconstruction could extend the available time series. Future research should explore this option.

4) The statistical approaches implemented used in this study for hydrologic analysis have been long used. Other newer methods such as wavelet analysis or boot-strapping should be explored to get insights into time series analysis of hydroclimatic variables.

5) The study explores the oceanic-atmospheric variability of sea surface temperatures and 500mbar geopotential height. It is recommended that future research include the climate indices of ENSO, PDO, AMO, NAO, etc. and provide a comparison with entire gridded datasets. Geopotential height brings atmospheric jet streams into the picture, which should be explored further.

6) Various non-parametric modeling techniques can be employed to use the results obtained from the SVD analysis as predictors for streamflow forecasting. This should be tested with different lead times to determine the best possible approach for each basin.

REFERENCES

Adam, J. C., Hamlet, A. F, Lettenmaier, D. P., 2009. Implications of global climate change for snowmelt hydrology in the twenty-first century. Hydrological Processes. 23(7): 962-972. doi:10.1002/hyp.7201

Aguado, E., Cayan, D., Riddle, L., Roos, M., 1992. Climatic fluctuations and the timing of west coast streamflow. Journal of Climate 5(12). 1468-1483.

Ahmad, M. M., Ghumman, A. R., Ahmad, S., 2009. Estimation of Clark's Instantaneous Unit Hydrograph Parameters and Development of Direct Surface Runoff Hydrograph, Water Resources Management, 23(12):2417-2435.

Ahmad, M. M., Ghumman, A. R., Ahmad, S., Hashmi, H. N. 2010a. Estimation of a unique pair of Nash model parameters: An optimization approach. Water Resources Management, 24(12), 2971–2989.

Ahmad, S., Kalra, A., Stephen, H., 2010b. Estimating soil moisture using remote sensing data: a machine learning approach. Advances in Water Resources 33. (1), 69–80.

Ahmad, S., Prashar, D., 2010. Evaluating municipal water conservation policies using a dynamic simulation model. Water Resources Management. 24 (13), 3371–3395.

Ahmad, S., Simonovic, S. P., 2000a. Dynamic modeling of flood management policies, Proceedings of the 18th International Conference of the System Dynamics Society: Sustainability in the Third Millennium, Bergen, Norway.

Ahmad, S., Simonovic, S. P., 2000b. System dynamics modeling of reservoir operations for flood management. Journal of Computing in Civil Engineering. 14 (3), 190–198.

Ahmad, S., Simonovic, S. P., 2001a. Developing Runoff Hydrograph using Artificial Neural Networks. In Bridging the Gap: Meeting the World's Water and Environmental Resources Challenges, ASCE, pp 1-17 doi: 10.1061/40569(2001)54

Ahmad, S., Simonovic, S. P., 2001b. Integration of heuristic knowledge with analytical tools for selection of flood control measures. Canadian Journal of Civil Engineering. 28 (2), 208–221.

Ahmad, S., Simonovic, S. P., 2001c. Modeling Human Behavior for Evacuation Planning: A System Dynamics Approach. In Bridging the Gap: Meeting the World's Water and Environmental Resources Challenges, ASCE, pp 1-10. doi: 10.1061/40569(2001)462

Ahmad, S., Simonovic, S. P., 2001d. Modeling Dynamic Processes in Space and Time--A Spatial System Dynamics Approach. In Bridging the Gap: Meeting the World's Water and Environmental Resources Challenges, ASCE, pp 1-20, doi: 10.1061/40569(2001)88

Ahmad, S., Simonovic, S. P., 2004. Spatial system dynamics: new approach for simulation of water resources systems. Journal of Computing in Civil Engineering 18(4):331–340.

Ahmad, S., Simonovic, S. P., 2005. An Artificial Neural Network model for generating hydrograph from hydro-meteorological parameters. Journal of Hydrology 315(1-4): 236-251.

Ahmad, S., Simonovic, S. P., 2006. An intelligent decision support system for management of floods. Water Resources Management. 20 (3), 391–410.

Andreadis, K. M., Clark, E. A., Wood, A. W., Hamlet, A. F., Lettenmaier, D. P., 2005. Twentieth-Century Drought in the Conterminous United States. Journal of Hydrometeorology. 6(6), 985-1001.

Archer, C. L., Caldeira, K., 2008. Historical trends in the jet streams, Geophys. Res. Lett., 35, L08803, doi:10.1029/2008GL033614.

Arora,V. K., Boer, G. J., 2001. Effects of simulated climate change on the hydrology of major river basins. Journal of Geophysical Research. 106, D4, 3335-3348.

Aziz, O. A., Tootle, G. A., Gray, S. T., Piechota, T. C., 2010. Identification of Pacific Ocean sea surface temperature influences of Upper Colorado River Basin snowpack. Water Resources Research, 46(7), doi:10.1029/2009WR008053

Aziz, O. A., Tootle, G. A., Moser, C., Piechota, T., Lamb, K., 2011. Upper Colorado River and Great Basin streamflow and snowpack forecasting using Pacific oceanic–atmospheric variability. Journal of Hydrology, 410(3), 169-177. doi:10.1016/j.jhydrol.2011.09.030

Aziz, O. A., Tootle, G. A., Anderson, S., 2012. Atlantic Ocean sea-surface temperatures and regional streamflow variability in the Adour-Garonne basin, France. Hydrological Sciences Journal, 57(3), 496-506. doi:10.1080/02626667.2012.659250

Barlow. M, Nigam, S., Berbery, E., 2001. ENSO, Pacific Decadal Variability, and U.S. Summertime Precipitation, Drought, and Stream Flow. Journal of Climate, 14(9),

Bawden, A. J., Linton, H. C., Burn, D. H., Prowse, T. D., 2013. A spatiotemporal analysis of hydrological trends and variability in the Athabasca River Region, Canada. Journal of Hydrology. doi: http:// dx.doi.org/10.1016/j.jhydrol.2013.11.051.

Beamish, R. J., Neville, C. M., Cass, A. J., 1997. Production of Fraser River sockeye salmon (Oncorhynchus nerka) in relation to decadal-scale changes in the climate and the ocean, Canadian Journal of Fisheries and Aquatic Sciences. 54, 543–554.

Blackmon, M. L., 1976. A Climatological Spectral Study of the 500 mb Geopotential Height of the Northern Hemisphere. Journal of the Atmospheric Sciences, 33(8), 1607-1623. doi:10.1175/15200469(1976)033<1607:ACSSOT>2.0.CO;2

Blackmon, M. L., Wallace, J. M., Lau, N., Mullen, S. L., 1977. An Observational Study of the Northern Hemisphere Wintertime Circulation. Journal of the Atmospheric Sciences, 34(7), 1040-1053. doi:10.1175/1520-0469(1977)034<1040:AOSOTN>2.0.CO;2

Bukhary, S., Chen, C., Kalra, A., Ahmad, S., 2014. Improving Streamflow Reconstructions Using Oceanic-Atmospheric Climate Variability. World Environmental and Water Resources Congress: pp. 846-855. doi: 10.1061/9780784413548.088

Bretherton, C. S., Smith, C., Wallace, J. M., 1992. An Intercomparison of Methods for Finding Coupled Patterns in Climate Data. Journal of Climate, 5(6), 541-560. doi:10.1175/15200442(1992)005<0541:AIOMFF>2.0.CO;2

Burn, D. H., 2008. Climatic influences on streamflow timing in the headwaters of the Mackenzie River Basin. Journal of Hydrology, 352(1–2), 225-238. doi:10.1016/j.jhydrol.2008.01.019

Burn, D. H., Elnur, M. A. H., 2002. Detection of hydrologic trends and variability. Journal of hydrology. 255(1), 107-122.

Cañón, J., González, J., Valdés, J., 2007. Precipitation in the Colorado River Basin and its low frequency associations with PDO and ENSO signals. Journal of hydrology, 333(2), 252-264. DOI:10.1016/j.jhydrol.2006.08.015

Carrier, C., Kalra, A., Ahmad, S., 2011. Using Proxy Reconstructions for Streamflow Forecasting. World Environmental and Water Resources Congress :. 3124-3133. doi: 10.1061/41173(414)326

Carrier, C., Kalra, A., Ahmad, S., 2013. Using Paleo Reconstructions to Improve Streamflow Forecast Lead Time in the Western United States. Journal of the American Water Resources Association. 49(6): 1351-1366. doi:10.1111/jawra.12088.

Casty, C., Raible, C. C., Stocker, T. F., Wanner, H., Luterbacher, J., 2007. A European pattern climatology 1766–2000. Climate Dynamics, 29(7-8), 791-805. DOI:10.1007/s00382-007-0257-6

Cayan, D. R., 1996. Interannual Climate Variability and Snowpack in the Western United States. Journal of Climate, 9(5), 928-948. doi:10.1175/1520-0442(1996)009<0928:ICVASI>2.0.CO;2

Cayan, D. R., Peterson, D. H., 1989. The influence of north pacific atmospheric circulation on streamflow in the west. Geophysical Monograph Series, 55, 375-397.

Cayan, D. R., Redmond, K. T., Riddle, L. G., 1999. ENSO and Hydrologic Extremes in the Western United States. Journal of Climate, 12(9), (1999)

Cayan, D. R., Webb, R. H., 1992. El Niño/southern oscillation and streamflow in the western United States: Historical and Paleoclimatic Aspects of the Southern Oscillation, 29-68.

Chandimala, J., Zubair, L., 2007. Predictability of stream flow and rainfall based on ENSO for water resources management in Sri Lanka Journal of Hydrology, 335(3), 303-312. doi:10.1016/j.jhydrol.2006.11.024

Chang, P., Ji, L., Li, H., 1997. A decadal climate variation in the tropical atlantic ocean from thermodynamic air-sea interactions. Nature, 385(6616), 516-518.

Chen, C. J., Georgakakos, A.P., 2014. Hydro-climatic forecasting using sea surface temperatures: methodology and application for the southeast US. Climate Dynamics, 42(11-12), 2955-2982. doi: 10.1007/s00382-013-1908-4

Chiew, F. H.,McMahon, T. A., Dracup, J. A. Piechota, T. C., 1994. El-Nino/Southern Oscillation and streamflow patterns in South-east Australia. Civil Engineering Transactions/the Institution of Engineers, Australia, 36(4), 285.

Choubin, B., Sigaroodi, S. K., Malekian, A., Ahmad, S., Attarod, P., 2014. Drought forecasting in a semi-arid watershed using climate signals: a neuro-fuzzy modeling approach. Journal of Mountain Science 11(5). DOI: 10.1007/s11629-014-3020-6

Cohn, T. A., Lins, H. F., 2005. Nature's style: Naturally trendy. Geophysical Research Letters, 32, L23402, doi:10.1029/2005GL024476.

Dawadi, S., Ahmad, S., 2012. Changing climatic conditions in the Colorado River Basin: Implications for water resources management. Journal of Hydrology, 430, 127-141. doi:10.1016/j.jhydrol.2012.02.010

Dawadi, S., Ahmad, S., 2013. Evaluating the impact of demand-side management on water resources under changing climatic conditions and increasing population. Journal of Environmental Management. 114: 261-275.

Dettinger, M. D., Cayan, D. R., 1995. Large-Scale Atmospheric Forcing of Recent Trends toward early snowmelt runoff in California. Journal of Climate,8(3), 606-623. doi: http://dx.doi.org/10.1175/1520-0442(1995)008<0606:LSAFOR>2.0.CO;2

Dettinger, M. D., Cayan, D. R., McCabe, G. J., Marengo, J. A., 2000b. Multiscale Streamflow Variability Associated with El Niño/Southern Oscillation Cambridge University Press Cambridge

Dettinger, M. D.,Diaz, H. F., 2000a. Global Characteristics of Stream Flow Seasonality and Variability. Journal of Hydrometeorology, 1(4), 289-310.

Easterling, D. R., Evans, J., Groisman, P. Y., Karl, T., Kunkel, K., Ambenje, P., 2000. Observed Variability and Trends in Extreme Climate Events: A Brief Review. Bulletin-American Meteorological Society. 81(3), 417-426.

Easterling, D. R., Karl, T. R., Gallo, K. P., Robinson, D. A., Trenberth, K. E. Dai, A., 2000. Observed climate variability and change of relevance to the biosphere. Journal of Geophysical Research: Atmospheres (1984–2012), 105(D15), 20101-20114. doi:10.1029/2000JD900166

Ehsanzadeh, E., Adamowski, K., 2010. Trends in timing of low stream flows in Canada: impact of autocorrelation and long-term persistence. Hydrological Processes. 24: 970–980, doi: 10.1002/hyp.7533.

Ehsanzadeh, E., Ouarda, T. B., Saley, H. M., 2011. A simultaneous analysis of gradual and abrupt changes in Canadian low streamflows. Hydrological Processes. 25(5), 727-739, doi: 10.1002/hyp.7861.

Enfield, D. B., Alfaro, E. J., 2000. The Dependence of Caribbean Rainfall on the Interaction of the Tropical Atlantic and Pacific Oceans. Journal of Climate, 12(7).

Enfield, D. B., Mestas-Nuñez, A. M., Trimble, P. J., 2001. The Atlantic multidecadal oscillation and its relation to rainfall and river flows in the continental US. Geophysical Research Letters, 28(10), 2077-2080. doi : 10.1029/2000GL012745

Falcone, J. A., 2011. GAGES–II, Geospatial Attributes of Gages for Evaluating Streamflow [digital spatial dataset], http://water.usgs.gov/GIS/metadata/usgswrd/XML/gagesII_Sept2011.xml.

Falcone, J. A., Carlisle, D. M., Wolock, D. M., Meador, M.R., 2010. GAGES: A stream gage database for evaluating natural and altered flow conditions in the conterminous United States. Ecology. 91(2),621.

Folland, C.,Palmer, T., Parker, D., 1986. Sahel rainfall and worldwide sea temperatures, 1901–85. Nature, 320(6063), 602-607.

Fonseca, B. R., Castro, M. de., 2002. On the connection between winter anomalous precipitation in the Iberian Peninsula and North West Africa and the summer subtropical Atlantic sea surface temperature. Geophysical Research Letters, 29(18), 10-1-10-4. doi:10.1029/2001GL014421

Forsee, W. J., Ahmad, S., 2011a. Evaluating Urban Storm-Water Infrastructure Design in Response to Projected Climate Change. Journal of Hydrologic Engineering, 16(11), 865-873. doi:10.1061/(ASCE)HE.1943-5584.0000383

Forsee, W., Ahmad, S., 2011b. Using HEC-HMS for Stormwater Infrastructure Assessment in Response to Changes in Design Storm Depths Calculated from Climate Projections. World Environmental and Water Resources Congress, Bearing Knowledge for Sustainability, ASCE, pp. 1318-1327. doi: 10.1061/41173(414)137

Frederick, K.D., Major, D.C., 1997. Climate Change and Water Resources. Climate Change 37:7-23.

Gebert, W.A., Krug, W.R., 1996. Streamflow trends in Wisconsin's driftless area. Journal of the American Water Resources Association. 32(4): 733-744, doi: 10.1111/j.1752-1688.1996.tb03470.x.

Gershunov, A., 1998. ENSO Influence on Intraseasonal Extreme Rainfall and Temperature Frequencies in the Contiguous United States: Implications for Long-Range Predictability. Journal of Climate, 11(12)

Gershunov, A., Barnett, T. P., 1998. Interdecadal Modulation of ENSO Teleconnections. Bulletin of the American Meteorological Society, 79(12), 2715-2725. doi:10.1175/15200477(1998)079<2715:IMOET>2.0.CO;2

Ghumman, A. R., Ahmad, S., Hashmi, H. N., Khan, R. A., 2014. Comparative evaluation of implementing participatory irrigation management in Punjab, Pakistan, Irrigation and Drainage., 63(3): 315-327. doi: 10.1002/ird.1809

Giannini, A.,Kushnir, Y., Cane, M. A., 2000. Interannual Variability of Caribbean Rainfall, ENSO, and the Atlantic Ocean. Journal of Climate, 13(2), 297-311. doi:10.1175/15200442(2000)013<0297:IVOCRE>2.0.CO;2

Gill, M.K., Asefa, T., Kaheil, Y., McKee, M., 2007. Effect of missing data on performance of learning algorithms for hydrologic predictions: Implications to an imputation technique. Water Resources Research. 43(7), W07416, doi:10.1029/2006WR005298.

Gobena, A. K., Gan, T. Y., 2006. Low-frequency variability in Southwestern Canadian stream flow: links with large-scale climate anomalies. International Journal of Climatology, 26(13), 1843-1869. doi:10.1002/joc.1336

Goodrich, G. B., 2004. Influence of the Pacific decadal oscillation on Arizona winter precipitation during years of neutral ENSO. Weather and forecasting,19(5), 950-953. doi:http://dx.doi.org/10.1175/1520-0434(2004)019<0950:IOTPDO>2.0.CO;2

Goodrich, G. B., 2007. Influence of the Pacific decadal oscillation on winter precipitation and drought during years of neutral ENSO in the western United States. Weather and forecasting, 22(1), 116-124. doi: http://dx.doi.org/10.1175/WAF983.1

Goodridge, J. D., 1994. A study of 1000 year storms in California. In Predicting Heavy Rainfall Events in California: A Symposium to Share Weather Pattern Knowledge (3-72).

Gordon, A. L., Giulivi, C. F., 2004. Pacific decadal oscillation and sea level in the Japan/East Sea. Deep Sea Research Part I: Oceanographic Research Papers, 51(5), 653-663. DOI: 10.1016/j.dsr.2004.02.005

Grantz, K., Rajagopalan, B., Clark, M., Zagona, E., 2005. A technique for incorporating large-scale climate information in basin-scale ensemble streamflow forecasts. Water Resources Research, 41(10). doi:10.1029/2004WR003467

Groisman, P. Y., Knight, R. W., Karl, T. R., 2001. Heavy Precipitation and High Streamflow in the Contiguous United States: Trends in the Twentieth Century. Bulletin of the American Meteorological Society. 82(2), 219-246.

Gutzler, D. S., Kann, D. M., Thornbrugh, C., 2002. Modulation of ENSO-based long-lead outlooks of southwestern US winter precipitation by the Pacific decadal oscillation. Weather and Forecasting, 17(6), 1163-1172. doi: http://dx.doi.org/10.1175/1520-0434(2002)017<1163:MOEBLL>2.0.CO;2

Haan, C. T., 1977. Statistical Methods in Hydrology, The Iowa State University Press, Ames. http://hdl.handle.net/1969.3/24532

Hamed, K. H., 2008. Trend detection in hydrologic data: The Mann–Kendall trend test under the scaling hypothesis. Journal of Hydrology. 349(3–4), 350-363, doi:10.1016/j.jhydrol.2007.11.009.

Hamed, K. H., Ramachandra Rao, A., 1998. A modified Mann-Kendall trend test for autocorrelated data. Journal of Hydrology. 204(1), 182-196.

Hamlet, A. F., Lettenmaier, D. P., 1999. Columbia river streamflow forecasting based on ENSO and PDO climate signals. Journal of Water Resources Planning and Management. 125(6): 333-341.

Hamlet, A. F., Lettenmaier, D. P., 2007. Effects of 20th century warming and climate variability on flood risk in the western US. Water Resources Research. 43(6), W06427, doi:10.1029/2006WR005099.

Hamlet, A. F., Mote, P. W., Clark, M. P., Lettenmaier, D. P., 2005. Effects of Temperature and Precipitation Variability on Snowpack Trends in the Western United States. Journal of Climate. 18(21), 4545-4561.

Hamlet, A. F., Mote, P. W., Clark, M. P., Lettenmaier, D. P., 2007. Twentieth-Century Trends in Runoff, Evapotranspiration, and Soil Moisture in the Western United States. Journal of Climate. 20(8), 1468-1486.

Hare, S. R., Mantua, N. J., 2000. Empirical evidence for North Pacific regime shifts in 1977 and 1989. Progress in Oceanography. 4,7 103–145.

Hastenrath, S., Wu, M., Chu, P., 1984. Towards the monitoring and prediction of north-east Brazil droughts. Quarterly Journal of the Royal Meteorological Society, 110(464), 411-425. doi:10.1002/qj.49711046407

Hayhoe, K., Wake, C. P., Huntington, T.G., Luo, L., Schwartz, M.D., Sheffield, J., Wood, E., Anderson, B., Bradbury, J.,DeGaetano, A., Troy, T.J.,Wolfe, D., 2007. Past and future changes in climate and hydrological indicators in the US Northeast. Climate Dynamics. 28:381–407, doi 10.1007/s00382-006-0187-8.

Helsel, D. R., Hirsch, R. M., 1992. Statistical methods in water resources. Elsevier Science.

Hessl, A. E., McKenzie, D., Schellhaas, R., 2004. Drought and Pacific Decadal Oscillation linked to fire occurrence in the inland Pacific Northwest.Ecological Applications,14(2), 425-442. Doi: http://dx.doi.org/10.1890/03-5019

Hidalgo, H. G., Dracup, J. A., 2003. ENSO and PDO effects on hydroclimatic variations of the Upper Colorado River Basin. Journal of Hydrometeorology. 4, 5–23.

Hodgkins, G.A., Dudley, R.W., 2006. Changes in the timing of winter—spring streamflows in eastern North America, 1913—2002. Geophysical Research Letters. 33, L06402, doi:10.1029/2005GL025593.

Holbrook, S. J., Schmitt, R. J., Stephens, J. S., 1997. Changes in an assemblage of temperature reef fishes with climate shift. Ecological Applications. 7(4), 1299– 1310.

Hunter, T., Tootle, G., Piechota, T., 2006. Oceanic-atmospheric variability and western U.S. snowfall. Geophysical Research Letters, 33(13). doi:10.1029/2006GL026600

Huntington, T. G., 2006. Evidence for intensification of the global water cycle: Review and synthesis, Journal of Hydrology, 319, 83-95.

Hurrell, J. W., 1995 Decadal trends in the North Atlantic Oscillation-Regional temperatures and precipitation. Science 269:676-679

Hurst, H., 1951. Long-term storage capacity of reservoirs. Transactions of the American Society of Civil Engineers. 116, 770-799.

Impoinvil, D. E., Keating, J., Chowdhury, R. R., Duncan, R., Cardenas, G., Ahmad, S., Beier, J. C., 2007a. The association between distance to water pipes and water bodies positive for anopheline mosquitoes (Diptera: Culicidae) in the urban community of Malindi, Kenya. Journal of Vector Ecology, 32(2), 319-327.

Impoinvil, D. E., Ahmad, S., Troyo, A., Keating, J., Githeko, A. K., Mbogo, C. M., Beier, J. C. 2007b. Comparison of mosquito control programs in seven urban sites in Africa, the Middle East, and the Americas. Health Policy, 83(2), 196-212.

Kahya, E., Dracup, J. A., 1993. U.S. streamflow patterns in relation to the El Niño/Southern Oscillation. Water Resources Research, 29(8), 2491-2503. doi:10.1029/93WR00744

Kahya, E., Dracup, J.A., 1994. The Influences of Type 1 El Niño and La Niña Events on Streamflows in the Pacific Southwest of the United States. Journal of Climate, 7(6), 965-976. doi:10.1175/15200442(1994)007<0965:TIOTEN>2.0.CO;2

Kalnay, E., Kanamitsu, M., Kistler, R., Collins, W., Deaven, D., Gandin, L., Woollen, J., 1996. The NCEP/NCAR 40-Year Reanalysis Project. Bulletin of the American Meteorological Society, 77(3), 437-471. doi: 10.1175/15200477(1996)077<0437:TNYRP>2.0.CO;2

Kalra, A., Piechota, T. C., Davies, R., Tootle G. A., 2006. Is Climate Change Evident in U. S. Streamflow? World Environmental and Water Resource Congress, 1-9. doi: 10.1061/40856(200)44

Kalra, A., Ahmad, S., 2009. Using oceanic-atmospheric oscillations for long lead time streamflow forecasting. Water Resources Research, 45(3), doi:10.1029/2008WR006855

Kalra, A., Ahmad, S., 2011. Evaluating changes and estimating seasonal precipitation for the Colorado River Basin using a stochastic nonparametric disaggregation technique. Water Resources Research. 47, W05555, doi:10.1029/2010WR009118.

Kalra, A., Ahmad, S., 2012. Estimating annual precipitation for the Colorado River Basin using oceanic-atmospheric oscillations. Water Resources Research. 48, W06527, doi:10.1029/2011WR010667, 2012.

Kalra, A., Ahmad, S., Nayak, A., 2013a. Increasing streamflow forecast lead time for snowmelt-driven catchment based on large-scale climate patterns. Advances in Water Resources, 53, 150-162. doi:10.1016/j.advwatres.2012.11.003

Kalra, A., 2012. Association of oceanic–atmospheric oscillations and hydroclimatic variables in the Colorado River Basin. Ph.D. Dissertation, University of Nevada Las Vegas, Las Vegas, NV.

Kalra, A., Li, L., Li, X., Ahmad, S., 2013b. Improving Streamflow Forecast Lead Time Using Oceanic-Atmospheric Oscillations for Kaidu River Basin, Xinjiang, China . Journal of Hydrologic Engineering, 18(8), 1031-1040. doi:10.1061/(ASCE)HE.1943-5584.0000707

Kalra, A., Miller, W. P., Lamb, K. W., Ahmad, S., Piechota, T., 2013c. Using large-scale climatic patterns for improving long lead time streamflow forecasts for Gunnison and San Juan River Basins. Hydrological Processes, 27(11), 1543-1559. doi: 10.1002/hyp.9236

Kalra, A., Piechota, T. C., Davies, R., Tootle, G. A., 2008. Changes in U.S. Streamflow and Western U.S. Snowpack. Journal of Hydrologic Engineering. 13(3), 156-163.

Kalra, A., Sagarika, S., Ahmad, S., 2014a. Investigation of the Linkages between Oceanic Atmospheric Variability and Continental U.S. Streamflow. World Environmental and Water Resources Congress, 636-645. doi: 10.1061/9780784413548.068

Kalra, A., Ahmad, S., 2014b. Incorporating Climate Variability in a Nonparametric Modeling Framework for Improving Hydrologic Predictions. World Environmental and Water Resources Congress, 626-635. doi: 10.1061/9780784413548.067

Kendall, M. G., 1975. Rank correlation methods: Charles Griffin. London, UK.

Kerr, R. A., 1992. Unmasking a shifty climate system. Science, 255, 1508– 1510.

Khaliq MN, Ouarda TBMJ, Gachon P, Sushama L. 2008. Temporal evolution of lowflow regimes in Canadian rivers. Water Resources Research. 44: W08436. doi:10.1029/2007WR006132.

Khaliq, M., Ouarda, T., Gachon, P., 2009. Identification of temporal trends in annual and seasonal low flows occurring in Canadian rivers: The effect of short- and long-term persistence. Journal of Hydrology. 369(1-2), 183-197.

Khaliq, M.N., Gachon, P., 2010. Pacific Decadal Oscillation Climate Variability and Temporal Pattern of Winter Flows in Northwestern North America. American Meteorological Society. 11,917-933, doi: 10.1175/2010JHM1254.1.

Khedun, C. P., Mishra, A. K., Bolten, J. D., Beaudoing, H. K., Kaiser, R. A., Giardino, J. R., and Singh, V. P., 2012. Understanding changes in water availability in the Rio Grande/Río Bravo del Norte basin under the influence of large-scale circulation indices using the Noah land surface model. Journal of Geophysical Research: Atmospheres (1984–2012), 117(D5). doi:10.1029/2011JD016590.

Kiffney, P. M., Bull, J. P., Feller, M. C., 2002, Climatic and hydrologic variability in a coastal watershed of southwestern british columbia. Journal of the American Water Resources Association, 38:1437–1451. doi:10.1111/j.1752-1688.2002.tb04357.x

Koczot, K., Dettinger, M., 2003. Climate effects of Pacific decadal oscillation on streamflow of the Feather River, California. Paper presented at the Proc. 71st Western Snow Conf, (2003),139-142.

Koutsoyiannis, D., 2003. Climate change, the Hurst phenomenon, and hydrological statistics. Hydrological Sciences Journal. 48(1), 3-24.

Koutsoyiannis, D., 2006. Nonstationarity versus scaling in hydrology. Journal of Hydrology. 324(1-4), 239-254.

Koutsoyiannis, D., Montanari, A., 2007. Statistical analysis of hydroclimatic time series: Uncertainty and insights. Water Resources Research. 43(5), W05429, doi:10.1029/2006WR005592.

Koutsoyiannis. D., 2002. The Hurst phenomenon and fractional Gaussiannoise made easy. Hydrological Sciences Journal. 47(4): 573–595.

Kumar, S., Merwade, V., Kam, J., Thurner, K., 2009. Streamflow trends in Indiana: Effects of long term persistence, precipitation and subsurface drains. Journal of Hydrology. 374(1-2), 171-183.

Kurtzman, D., Scanlon, B. R., 2007. El Niño–Southern Oscillation and Pacific Decadal Oscillation impacts on precipitation in the southern and central United States: Evaluation of spatial distribution and predictions. Water Resources Research, 43(10). 43, W10427, doi:10.1029/2007WR005863.

Lamb, K. W., Piechota, T. C., Aziz,. O. A., Tootle, G. A., 2011. A basis for extending long-term streamflow forecasts in the Colorado River Basin. Journal of Hydrologic Engineering, doi:10.1061/(ASCE)HE. 1943-5584.0000153.

Lamb, P. J., Peppler, R. A., 1987. North Atlantic Oscillation: concept and an application. Bulletin of the American Meteorological Society, 68(10), 1218-1225. doi: http://dx.doi.org/10.1175/1520-0477(1987)068<1218:NAOCAA>2.0.CO;2

Lettenmaier, D. P., Wood, E. F., Wallis, J. R., 1994. Hydro-Climatological Trends in the Continental United States, 1948-88. Journal of Climate. 7(4), 586-607.

Lins, H. F., 2012. USGS Hydro-Climatic Data Network 2009 (HCDN–2009): U.S. Geological Survey Fact Sheet 2012–3047, 4 p., available only at http://pubs.usgs.gov/fs/2012/3047/.

Lins, H. F., Slack, J. R., 1999. Streamflow trends in the United States. Geophysical Research Letters. 26, 227-230, doi: 10.1029/1998GL900291.

Livezey, R. E., Masutani, M., Leetmaa, A., Rui, H., Ji, M., Kumar, A., 1997. Teleconnective Response of the Pacific–North American Region Atmosphere to Large Central Equatorial Pacific SST Anomalies. Journal of Climate, 10(8), 1787-1820. doi:10.1175/1520-0442(1997)010<1787:TROTPN>2.0.CO;2

Ma, Z., 2007. The interdecadal trend and shift of dry/wet over the central part of North China and their relationship to the Pacific Decadal Oscillation (PDO). Chinese Science Bulletin, 52(15), 2130-2139. doi:10.1007/s11434-007-0284-z

Ma, Z., 2007. The interdecadal trend and shift of dry/wet over the central part of North China and their relationship to the Pacific Decadal Oscillation (PDO). Chinese Science Bulletin, 52(15), 2130-2139. doi:10.1007/s11434-007-0284-z

Mann, H. B., 1945. Nonparametric tests against trend. Econometrica: Journal of the Econometric Society. 13(3), 245-259.

Mantua , N. J., Hare, S. R., 2002. The Pacific Decadal Oscillation. Journal of Oceanography. 58, 35-44.

Mantua, N. J., 2004. An overview of Pacific Decadal (climate) Variability impacts on hydroclimate and water resources management in the western US, Eos Transactions, American Geophysical Union, 85(47), Fall Meet. Supplementary., Abstract H24B-01.

Martín, M., Luna, M., Morata, A., Valero, F., 2004. North Atlantic teleconnection patterns of low-frequency variability and their links with springtime precipitation in the western Mediterranean. International Journal of Climatology, 24(2), 213-230. doi:10.1002/joc.993

Martino, G., Fontana, N., Marini, G., and Singh, V., 2013, Variability and Trend in Seasonal Precipitation in the Continental United States, Journal of Hydrologic Engineering, 18(6), 630–640.

McCabe, G. J., Betancourt, J. L., Hidalgo, H.G., 2007. Associations of decadal to multidecadal sea-surface temperature variability with Upper Colorado river flow. 43(1),183-192.

McCabe, G. J., Dettinger, M. D., 2002. Primary Modes and Predictability of Year-to-Year Snowpack Variations in the Western United States from Teleconnections with Pacific Ocean Climate. Journal of Hydrometeorology. 3(1), 13-25.

McCabe, G. J., Palecki, M. A.,Betancourt, J. L., 2004. Pacific and Atlantic Ocean influences on multidecadal drought frequency in the United States. Proceedings of the National Academy of Sciences of the United States of America, 101(12), 4136-4141. doi:10.1073/pnas.0306738101

McCabe, G. J., Wolock, D. M., 2002. A step increase in streamflow in the conterminous United States. Geophysical Research Letters. 29(24), 2185, doi:10.1029/2002GL015999

McCabe, G. J., Wolock, D. M., 2014. Variability Common to Global Sea Surface Temperatures and Runoff in the Conterminous United States. Journal of Hydrometeorology, 15(2), 714-725. doi: http://dx.doi.org/10.1175/JHM-D-13-097.1

Melesse, A.M., Ahmad, S., McClain, M.E., Wang, X., Lim, Y.H., 2011. Suspended sediment load prediction of river systems: an artificial neural networks approach. Agricultural Water Management. 98 (5), 855–866.

Middelkoop, H., Daamen, K., Gellens, D., Grabs, W., Kwadijk, J. C. J., Lang, H., Wilke, K., 2001. Impact of Climate Change on Hydrological Regimes and Water Resources Management in the Rhine Basin. Climatic Change, 49(1-2), 105-128.

Miller, W. P., Piechota, T. C., 2008. Regional Analysis of Trend and Step Changes Observed in Hydroclimatic Variables around the Colorado River Basin. Journal of Hydrometeorology. 9(5), 1020-1034.

Milly, P. C. D.,Wetherald, R. T., Dunnel, K. A., Delworth, T. L., 2002. Increasing risk of great floods in a changing climate. Nature, 415(6871), 514-517. doi:10.1038/415514a

Milly, P. C.,Dunne, K. A.,, Vecchia, A. V., 2005. Global pattern of trends in streamflow and water availability in a changing climate. Nature, 438(7066), 347-350. doi:10.1038/nature04312

Milly, P., Julio, B., Malin, F., Robert, M., Zbigniew, W., Dennis, P., Ronald, J., 2008. Stationarity is dead. Ground Water News & Views. 4(1), 6-8.

Milly, P., Wetherald, R., Dunne, K., Delworth, T., 2002. Increasing risk of great floods in a changing climate. Nature. 415(6871), 514-517.

Mirchi, A., Madani, K., Watkins Jr, D., and Ahmad, S., 2012. Synthesis of system dynamics tools for holistic conceptualization of water resources problems. Water Resources Management, 26(9), 2421-2442.

Mosquera, S-Machado., Ahmad, S., 2007. Flood hazard assessment of Atrato River in Colombia. Water Resources Management, 21(3), 591-609. doi:10.1007/s11269-006-9032-4

Moura, A. D., Shukla, J., 1981. On the Dynamics of Droughts in Northeast Brazil: Observations, Theory and Numerical Experiments with a General Circulation Model. Journal of the Atmospheric Sciences, 38(12), 2653-2675. doi:10.1175/15200469(1981)038<2653:OTDODI>2.0.CO;2

National Oceanic and Atmospheric Administration’s Earth System Research Laboratory . 2014 (http://www.esrl.noaa.gov/psd/data/gridded/data.nmc.marine.html/sst.mnmean.nc).Last obtained May 2014

National Oceanic and Atmospheric Administration's Earth System Research Laboratory. 2014 NOAA Physical Sciences Center (http://www.esrl.noaa.gov/psd/data/gridded/data.ncep.reanalysis.pressure.html/hgt.mon.mean.nc) Last obtained May 2014

Neal, E., Walter, M. T., Coffeen, C., 2002. Linking the pacific decadal oscillation to seasonal stream discharge patterns in Southeast Alaska. Journal of Hydrology, 263(1), 188-197. doi:10.1016/S0022-1694(02)00058-6

Němec, J., Schaake, J., 1982. Sensitivity of water resource systems to climate variation. Hydrological Sciences Journal, 27(3), 327-343. doi:10.1080/02626668209491113

Newman, M., Sardeshmukh, P. D., 1995. A Caveat Concerning Singular Value Decomposition. Journal of Climate, 8(2), 352-360. doi:10.1175/1520-0442(1995)008<0352:ACCSVD>2.0.CO;2

Nigam, S., Barlow, M., Berbery, E. H., 1999. Analysis links Pacific decadal variability to drought and streamflow in United States. EOS, Transactions American Geophysical Union, 80(51), 621-625. DOI: 10.1029/99EO00412

Nijssen, B., O'Donnell, O', G. M., Hamlet, A. F., Lettenmaier, D. P., 2001. Hydrologic Sensitivity of Global Rivers to Climate Change. Climatic Change. 50(1-2), 143-175.

Onoz, B., Bayazit, M., 2003. The Power of Statistical Tests for Trend Detection. Turkish Journal of Engineering and Environmental Sciences. 27(4), 247-251.

Owens, A. J., 1978. On detrending and smoothing random data. Journal of Geophysical Research: Space Physics (1978–2012) 83.A1: 221-224.

Pagano, T., Garen, D., 2006. Climate Variations, Climate Change, and Water Resources Engineering. Climate Variations, Climate Change, and Water Resources Engineering, 86. doi:10.5555/books10.1061/9780784408247

Pettitt, A., 1979. A Non-Parametric Approach to the Change-Point Problem. Applied Statistics. 28(2) , 126-135.

Philander, S. G., 1990. El Niño, La Niña and the Southern Oscillation. Academic Press Inc., San Diego, CA.

Piechota, T. C., Dracup, J. A., 1999. Long-Range Streamflow Forecasting Using El Niño-Southern Oscillation Indicators. Journal of Hydrologic Engineering, 4(2), 144-151. doi:10.1061/(ASCE)1084-0699(1999)4:2(144)

Piechota, T.C., Chiew, F.H.S., Dracup, J.A., McMahon, T.A., 2001. Development of exceedance probability streamflow forecast. Journal of Hydrologic Engineering 6 (1), 20–28.

Praskievicz, S., Chang, H., 2009. A review of hydrological modelling of basin-scale climate change and urban development impacts. Progress in Physical Geography, 33(5), 650-671. doi:10.1177/0309133309348098

Puri, S, Stephen, H., Ahmad, S., 2011a. Relating TRMM Precipitation Radar backscatter to water stage in wetlands. Journal of Hydrology, 401(3), 240-249. doi:10.1016/j.jhydrol.2011.02.026

Puri, S., Stephen, H., Ahmad, S., 2011b. Relating TRMM Precipitation Radar Land Surface Backscatter Response to Soil Moisture in the Southern United States, Journal of Hydrology, 402(1-2): 115-125.

Qaiser, K, Ahmad, S., Johnson, W., Batista, J. R., 2013. Evaluating Water Conservation and Reuse Policies Using a Dynamic Water Balance Model. Environmental Management, 51(2), 449-458. doi:10.1007/s00267-012-9965-8

Qaiser, K, Ahmad, S., Johnson, W., Batista, J., 2011. Evaluating the impact of water conservation on fate of outdoor water use: A study in an arid region. Journal of Environmental Management, 92(8), 2061-2068. doi:10.1016/j.jenvman.2011.03.031

Rajagopalan, B., Cook, E., Lall, U., Ray, B. K., 2000. Spatiotemporal Variability of ENSO and SST Teleconnections to Summer Drought over the United States during the Twentieth Century. Journal of Climate, 13(24), 4244-4255. doi:10.1175/1520-0442(2000)013<4244:SVOEAS>2.0.CO;2

Redmond, K. T, Koch, R. W., 1991. Surface Climate and Streamflow Variability in the Western United States and Their Relationship to Large-Scale Circulation Indices. Water Resources Research, 27(9), 2381-2399. doi:10.1029/91WR00690

Regonda, S. K., Rajagopalan, B., Clark, M., Pitlick, J., 2005. Seasonal Cycle Shifts in Hydroclimatology over the Western United States. Journal of Climate. 18(2), 372-384.

Rodó, X., Baert, E., Comin, F. A., 1997. Variations in seasonal rainfall in Southern Europe during the present century: relationships with the North Atlantic Oscillation and the El Niño-Southern Oscillation. Climate Dynamics, 13(4), 275-284. doi: 10.1007/s003820050165

Rogers, J. C., Coleman, J. S., 2003. Interactions between the Atlantic Multidecadal Oscillation, El Nino/La Nina, and the PNA in winter Mississippi valley stream flow. Geophysical Research Letters, 30(10)

Ropelewski, C. F., Halpert, M. S., 1986: North American precipitation and temperature patterns associated with El Ni~no/ Southern Oscillation (ENSO).Mon.Wea. Rev., 114, 2352–2362, doi:10.1175/1520-0493(1986)114,2352:NAPATP.2.0.CO;2.

Sagarika, S., Kalra, A., Ahmad, S., 2014 Evaluating the effect of persistence on long-term trends and analyzing step changes in streamflows of the continental United States. Journal of Hydrology. 517, 36-53. doi:10.1016/j.jhydrol.2014.05.002.

Schaake, J. S. Jr, Kaczmarek, Z., 1979. "Climate variability and the design and operation of water resource systems.". In Proc. World Climate Conference 290–312. Geneva: WMO.

Seidel, D. J., Fu, Q., Randel, W. J., Reichler, T. J., 2007). Widening of the tropical belt in a changing climate. Nature geoscience, 1(1), 21-24. doi:10.1038/ngeo.2007.38

Sen, P. K., 1968. Estimates of the Regression Coefficient Based on Kendall's Tau. Journal of the American Statistical Association. 63(324), 1379-1389, doi:10.1080/01621459.1968.10480934.

Serreze, M. C., Clark, M. P., McGinnis, D. L., 1998. Characteristics of Snowfall over the Eastern Half of the United States and Relationships with Principal Modes of Low-Frequency Atmospheric Variability. Journal of Climate, 11(2)

Shabbar, A., Skinner, W., 2004. Summer Drought Patterns in Canada and the Relationship to Global Sea Surface Temperatures. Journal of Climate, 17(14)

Shrestha, E, Ahmad, S., Johnson, W., Batista, J. R., 2012. The carbon footprint of water management policy options. Energy Policy, 42, 201-212, doi:10.1016/j.enpol.2011.11.074.

Shrestha, E., Ahmad, S., Johnson, W., Shrestha, P., Batista, J.R., 2011. Carbon footprint of water conveyance verses desalination as alternatives to expand water supply. Desalination. 280 (1–3), 33–43.

Simonovic, S. P., Ahmad, S., 2005. Computer-based model for flood evacuation emergency planning. Natural Hazards 34(1): 25-51.

Singhrattna, N.,Rajagopalan, B., Kumar, K. K., Clark, M., 2005. Interannual and Interdecadal Variability of Thailand Summer Monsoon Season. Journal of Climate, 18(11)

Slack, J., Landwehr, J., 1992. Hydro-climatic data network: A US geological survey streamflow data set for the United States for the study of climate variations, 1874–1988. USGS open-file report 92-129. US Geological Survey, Washington, DC Available from http://wwwrvares.Er.Usgs.gov/hcdnreport/abstract.Html.

Small, D., Islam, D., Vogel, R. M., 2006. Trends in precipitation and streamflow in the eastern U.S.: Paradox or perception? Geophysical Research Letters. 33, L03403, doi:10.1029/2005GL024995.

Smith, T. M., Reynolds, R. W., 2004. Improved Extended Reconstruction of SST (1854–1997). Journal of Climate, 17(12).

Soukup, T. L., Aziz, O. A., Tootle, G.A., Piechota, T. C., Wulff, S. S., 2009. Long lead-time streamflow forecasting of the North Platte River incorporating oceanic–atmospheric climate variability. Journal of Hydrology, 368(1), 131-142. doi:10.1016/j.jhydrol.2008.11.047

Stephen, H., Ahmad, S., Piechota, T. C., Tang, C., 2010. Relating surface backscatter response from TRMM precipitation radar to soil moisture: results over a semiarid region. Hydrology and Earth System Sciences. 14, 193–204.

Stewart, I. T., Cayan, D. R., Dettinger, M. D., 2005. Changes toward Earlier Streamflow Timing across Western North America. Journal of Climate. 18(8), 1136-1155.

Strang, G., 1998. Introduction to linear algebra 2nd ed., Addison-Wesley, SIAM.

Thiel, H., 1950. A Rank-Invariant Method of Linear and Polynomial Regression Analysis, Advanced Studies in Theoretical and Applied Econometrics. ,23, 345-381.

Tootle, G. A, Piechota, T. C., 2006. Relationships between Pacific and Atlantic ocean sea surface temperatures and U.S. streamflow variability. Water Resources Research, 42(7), W07411. doi:10.1029/2005WR004184

Tootle, G. A., Piechota, T. C., 2004. Suwannee River Long Range Streamflow Forecasts Based on Seasonal Climate Predictors. Journal of the American Water Resources Association, 40(2), 523-532., doi:10.1111/j.1752-1688.2004.tb01047

Tootle, G. A., Piechota, T. C., Gutiérrez, F., 2008. The relationships between Pacific and Atlantic Ocean sea surface temperatures and Colombian streamflow variability. Journal of Hydrology, 349(3), 268-276. doi:10.1016/j.jhydrol.2007.10.058

Tootle, G. A., Piechota, T. C., Singh, A., 2005. Coupled oceanic-atmospheric variability and U.S. streamflow. Water Resources Research. 41(12), W12408,. doi:10.1029/2005WR004381.

Tootle, G. A., Singh, A. K. Piechota, T. C. Farnham, I., 2007. Long Lead-Time Forecasting of U.S. Streamflow Using Partial Least Squares Regression. Journal of Hydrologic Engineering, 12(5), 442-451.doi:10.1061/(ASCE)1084-0699(2007)12:5(442)

Trenberth, K. E., 1997. The definition of El Niño, Bull. Am. Meteorol. Soc., 78, 2771–2777, doi:10.1175/1520-0477(1997)078<2771:TDOENO>2.0.CO;2.

United States.Environmental Protection Agency, 2012. Streamflow, Society and Ecosystems, Climate Change Indicators in the United States http://www.epa.gov/climatechange/science/indicators/society-eco/streamflow.html.

Uvo, C. B., Repelli, C. A., Zebiak, S. E. Kushnir, Y., 1998. The Relationships between Tropical Pacific and Atlantic SST and Northeast Brazil Monthly Precipitation. Journal of Climate, 11(4)

Uvo, C. B., 2003. Analysis and regionalization of northern European winter precipitation based on its relationship with the North Atlantic oscillation. International Journal of Climatology, 23(10), 1185-1194. doi:10.1002/joc.930

Vedwan, N., Ahmad, S., Miralles-Wilhelm, F., Broad, K., Letson, D., Podesta, G., 2008. Institutional evolution in Lake Okeechobee Management in Florida: characteristics. Impacts, and Limitations. Water Resources Management. 22, 699–718.

Venkatesan, A. K., Ahmad, S., Johnson, W., Batista, J. R., 2011a. Salinity reduction and energy conservation in direct and indirect potable water reuse. Desalination. 272 (1–3), 120–127.

Venkatesan, A. K., Ahmad, S., Johnson, W., Batista, J. R., 2011b. System dynamics model to forecast salinity load to the Colorado River due to urbanization within the Las Vegas valley. Science of the Total Environment. 409 (13), 2616–2625.

Villarini, G., Serinaldi, F., Smith, J. A., Krajewski, W.F., 2009. On the stationarity of annual flood peaks in the continental United States during the 20th century. Water Resources Research. 45(8), W08417, doi:10.1029/2008WR007645.

Villarini, G., Smith, J. A., 2010. Flood peak distributions for the eastern United States. Water Resources Research. 46(6), W06504, doi:10.1029/2009WR008395.

Vogel, R. M., Tsai, Y., Limbrunner, J. F., 1998. The regional persistence and variability of annual streamflow in the United States. Water Resources Research. 34(12), 3445-3459, doi:10.1029/98WR02523.

Voss, R., May, A.W., Roeckner, E., 2002. Enhanced Resolution Modelling Study on Anthropogenic Climate Change: Changes in extremes of the hydrological cycle. International Journal of Climatology. 22: 755-777, doi:10.1002/joc.757.

Walker, G. T., 1925. Correlation in Seasonal Variations of WEATHER---A Further Study of World WEATHER1.Monthly Weather Review,53, 252. doi:10.1175/1520-0493(1925)53<252:CISVOW>2.0.CO;2

Walker, G. T., Bliss, E. W., 1932. World weather. V. Mem. Roy. Meteor. Soc., 4, 53-84.

Wallace, J. M., Smith, C., Bretherton, C. S., 1992. Singular Value Decomposition of Wintertime Sea Surface Temperature and 500-mb Height Anomalies. Journal of Climate, 5(6), 561-576. doi:10.1175/1520-0442(1992)005<0561:SVDOWS>2.0.CO;2

Wang, H., Ting, M., 2000. Covariabilities of Winter U.S. Precipitation and Pacific Sea Surface Temperatures. Journal of Climate, 13(20)

Wang, S. Y., Gillies, R. R, Hipps, L. E., Jin, J., 2011. A transition-phase teleconnection of the Pacific quasi-decadal oscillation. Climate Dynamics 36, 681–693. doi:10.1007/s00382-009-0722-5

Wilks, D. S., 2006. On “Field Significance” and the False Discovery Rate. Journal of Applied Meteorology and Climatology. 45, 1181-1189.

Wu, G., Li, L., Ahmad, S., Chen, X., Pan, X., 2013. A Dynamic Model for Vulnerability Assessment of Regional Water Resources in Arid Areas: A Case Study of Bayingolin, China, Water Resources Management, 27(8), 3085-3101. doi: 10.1007/s11269-013-0334-z

Xoplaki, E., Luterbacher, J., Burkard, R., Patrikas, I., Maheras, P., 2000. Connection between the large-scale 500 hPa geopotential height fields and precipitation over Greece during wintertime. Climate Research, 14(2), 129-146.

Yue, S., Pilon, P., 2004. A comparison of the power of the t test, Mann-Kendall and bootstrap tests for trend detection. Hydrological Sciences Journal. 49(1), 21-37, doi:10.1623/hysj.49.1.21.53996.

Yue, S., Pilon, P., Phinney, B., Cavadias, G., 2002. The influence of autocorrelation on the ability to detect trend in hydrological series. Hydrological Processes. 16(9), 1807-1829, doi:10.1002/hyp.1095.

Zhang, X., Wang, J., Zwiers, F. W., Groisman, P. Y., 2010. The Influence of Large-Scale Climate Variability on Winter Maximum Daily Precipitation over North America. J. Climate, 23., 2902–2915. doi:10.1175/2010JCLI3249.1

Zhang, F., Li, L., Ahmad, S., Li, X., 2014. Using Path Analysis to Identify the Influence of Climatic Factors on Spring Peak Flow Dominated by Snowmelt in an Alpine Watershed, Journal of Mountain Science. 11(4): 990-1000. DOI: 10.1007/s11629-013-2789-z.

Zhang, Y., Sperber, K. R., Boyle, J. S., 1997. Climatology and interannual variation of the East Asian winter monsoon: Results from the 1979–95 NCEP/NCAR reanalysis. Monthly Weather Review, 125: 2605–2619.

Zhu, Y., Day, R., 2005. Analysis of streamflow trends and the effects of climate in Pennsylvania, 1971 TO 2001. Journal of the American Water Resources Association. 41(6), 1393-1405, doi: 10.1111/j.1752-1688.2005.tb03807.x.

VITA

Graduate College
University of Nevada, Las Vegas

Soumya Sagarika

Degrees:

Bachelor of Technology Civil Engineering, 2010, Biju Pattnaik University of Technology, India

Publications:

Sagarika, S., Kalra, A., Ahmad, S., 2014 Evaluating the effect of persistence on long-term trends and analyzing step changes in streamflows of the continental United States. Journal of Hydrology. 517, 36-53. doi:10.1016/j.jhydrol.2014.05.002.

Thesis Title: Identification of long-term changes and evaluation of the relationships among streamflow variability and oceanic-atmospheric indices.

Thesis Examination Committee:
Chairperson, Sajjad Ahmad, Ph.D.,
Committee Member, David E. James, Ph.D.
Committee Member, Haroon Stephen, Ph.D.
Graduate Faculty Representative, Ashok Singh, Ph.D.